AN ELECTRON PARAMAGNETIC RESONANCE STUDY OF SURFACTANT PROTEIN B MIMIC KL_4

By

AUSTIN LISLE TURNER

A DISSERTATION PRESENTED TO THE GRADUATE SCHOOL
OF THE UNIVERSITY OF FLORIDA IN PARTIAL FULFILLMENT
OF THE REQUIREMENTS FOR THE DEGREE OF
DOCTOR OF PHILOSOPHY

UNIVERSITY OF FLORIDA

2012

To my parents Randall and Kathleen Turner and my brothers Sean and Ashton Turner with special thanks to my grandmother Virginia Hawley, my godparents Jim and Sue Lamie, and my friends along the way

ACKNOWLEDGMENTS

First and foremost, I would like to thank my parents Kathleen and Randall Turner and my brothers Sean and Ashton for their sacrifices, support, patience and love. Without them, none of this work would have been possible.

Secondly, I want to express my deepest gratitude to my advisor and mentor, Doctor Gail E. Fanucci for her patience and encouragement, for countless opportunities to present my research at national conferences, and for her guidance and support. I would also like to offer my sincere gratitude to Doctor Joanna Long for her collaboration and insight on the surfactant project, in addition to welcoming me into her group as one of her own. I would also like to thank all the other members of my doctoral committee, Doctors Alex Angerhofer, Nicole Horenstein, and Ben Smith. I would like to thank Ben Smith for his acceptance and guidance throughout this Ph.D. process, Alex Angerhofer for his EPR expertise along the way, Nicole Horenstein for her help at seeing the big picture of my Ph.D. project along with giving me the opportunity to teach alongside her in Biochemistry Lab.

I would like to thank all past and present members of the Fanucci and Long groups for their friendship, help, and support, particularly Jeffrey Carter, Adam Smith, Suzanne Farver, Anna Kuznetsova and former members Doctors Jamie Kear, Luis Galiano, Jordan Mathias, Mandy Blackburn, and Natasha Pirman. Each of you played an important part in making graduate school more enjoyable and providing me with the memories that will last forever. In addition, thanks goes to former undergraduate Phil Goff who studied in the Fanucci group and helped keep me sane during the long EPR hours.

I would like to thank the Department of Chemistry at Bradley University, where I obtained my passion and love for chemistry. In particular I want to express my deepest gratitude to Doctor Max Taylor who without knowing it turned an electrical engineering student into a lifelong chemist by showing him his love and passion for chemistry. I would also like to thank the Department of Chemistry at the University of Wisconsin at Whitewater, where I finished my pursuit to obtain my Bachelor of Science (B.S.) degree in chemistry. In particular, I want to express my sincere gratitude to Doctor Kathy Asala for her mentoring and guidance along the way.

I would like to thank Doctor Ken Matuszak for his endless mentoring and countless scientific discussions while working at Abbott Laboratories and his continued friendship beyond. If it wasn't for him I would not be pursuing my Ph.D. at the University of Florida. In addition, I would like to thank the many friends and colleagues from Abbott Laboratories who went above and beyond to see to it that I would have the best possible opportunities in my scientific endeavors. A special thanks to Doctor Rick Yost who originally brought me into his analytical group and helped lead my transition into the Biochemistry division.

I would like to thank the University of Florida Alumni Fellowship program and the University of Florida Startup for funding and the University of Physics department and Doctor Steve Hagan for use and his knowledge on his circular dichroism instrument. This work was supported by NIH R01 GM077232 and NIH 1R01HL076586.

TABLE OF CONTENTS

page

LIST OF TABLES

LIST OF FIGURES

LIST OF ABBREVIATIONS

AAA	Amino acid analysis
AMP	Antimicrobial peptides
ARDS	Adult respiratory distress syndrome
CD	Circular dichroism
CDC	Center for disease control
CrX	Chromium oxylate
CW	Continuous wave
DMSO	Dimethyl sulfoxide
DNA	Deoxyribonucleic acid
DPPC	Dipalmitoylphosphatidylcholine
DTT	Dithiothreitol
EPR	Electron paramagnetic resonance
ER	Endoplasmic reticulum
ESEEM	Electron spin echo envelope modulation
FDA	Food and drug administration
FTIR	Fourier transform infrared
KOH	Potassium hydroxide
LEU	Leucine
LUV	Large unilamellar vesicle
LYS	Lysine
IAP	Iodoacetamido-PROXYL
IASL	4-(2-Iodoacetamido)-TEMPO
ICBR	Interdisciplinary center for biotechnology
IRDS	Infant respiratory distress syndrome

MeOH	Methanol
MLV	Multilamellar vesicles
MSL	4-Maleimido-TEMPO
MTSL	(1-oxyl-2,2,5,5-tetramethyl-Δ3-pyrroline-3-methyl)methanethiosulfonate
NaCl	Sodium chloride
NiAA	Nickel (II) acetylacetonate
NiEDDA	Nickel (II) ethylene-N,N'-diamine diacetate
NMR	Nuclear magnetic resonance
PAP	Pulmonary alveolar proteinosis
PC	Phosphocholine
PG	Phosphoglycerol
POPC	1-palmitoyl-2-oleoyl-*sn*-glycero-3-phosphocholine
POPG	1-palmitoyl-2-oleoyl-*sn*-glycero-3-phosphoglycerol
PSPC	1-palmitoyl-2-steroyl-3-phosphocholine RDS Respiratory distress syndrome
RP-HPLC	Reverse-phase high performance liquid chromatography
SDSL	Site-directed spin labeling
SP	Surfactant protein
ssNMR	Solid-state nuclear magnetic resonance
TCEP	Tris(2-carboxyethyl)phosphine
TEM	Transmission electron microscopy
TFA	Trifluoroacetic acid
TFE	Tetrafluoroethylene
UV	Ultra-violet

Abstract of Dissertation Presented to the Graduate School
of the University of Florida in Partial Fulfillment of the
Requirements for the Degree of Doctor of Philosophy

AN ELECTRON PARAMAGNETIC RESONANCE STUDY OF SURFACTANT PROTEIN B MIMIC KL_4

By

Austin Lisle Turner

May 2012

Chair: Gail Fanucci
Major: Chemistry

KL_4 is a 21 amino acid peptide used to mimic the C-terminus of lung surfactant protein B, a protein known to lower the surface tension in the highly dynamic alveoli. Understanding how KL_4 interacts with lipid vesicles of varying composition will provide insight into potential treatment for diseases such as respiratory distress syndrome. Recent ^{31}P and ^{2}H NMR studies have shown that KL_4 binds differently to POPC:POPG and DPPC:POPG multilamellar vesicles, with the latter being found at elevated levels in lung surfactants. The current study uses electron paramagnetic resonance spectroscopy (EPR) and a technique called power saturation to study the effects of KL_4 binding to lipid bilayers both at the lipid and peptide level. Power saturation can be used to determine a change in the accessibility of the spin label to molecular oxygen in the bilayer interior and to NiAA, an aqueous soluble nickel complex. Using information gathered from these experiments we will provide insights into the depth and orientation of the peptide within different bilayer systems.

CHAPTER 1
INTRODUCTION TO PULMONARY SURFACTANTS

Surfactants

Surfactants are defined as compounds that lower the surface tension of a liquid, and the term is an acronym of *surface active agents*. Usually amphiphilic compounds such as lipids, surfactants are able to interact both with hydrophilic and hydrophobic molecules, giving them a wide variety of functions. Surfactant molecules typically migrate to the air/water surface, as this is an interface between hydrophilic and hydrophobic environments. Typically thought of as detergents, wetting agents, dispersants, foaming agents, or emulsifiers, their function is to lower the interfacial tension between two states in contact whether it be liquid-liquid, liquid-solid, or liquid-gas. Self-assembly into a wide variety of aggregate forms such as micelles, bilayers, or multilamellar vesicles, give surfactants of interest well defined properties and functions. Self-aggregation is controlled by the hydrophobic effect; in particular, lipids assemble into bilayers to minimize exposure of the hydrophobic tails to aqueous environments resulting in vesicular structures. The type of vesicle formed is dictated by the shape and chemical structure of the lipids themselves. Lipids with large head-group cross sections compared to their acyl chain cross section allow for a higher degree of curvature, ultimately resulting in micelle formation. Lipids such as phospholipids, in which the cross section from top to bottom of the lipid is relatively constant, are commonly seen in more planar bilayers like those that allow for compartmentalization of the many organelles within cells. The tremendous importance of surfactants in life cannot be overstated as they allow for life as people know it to exist. Greater detail as

to their behavior will be given in the sections that follow, giving particular focus to a specialized group of surfactants termed pulmonary surfactants.

Properties of Surfactants

Surfactants are found throughout living organisms including some of the most complex, dynamic systems of the human body such as mammalian lungs and are also used in a variety of simple household products such as laundry detergent. Many classes of surfactants exist, but they share one common feature which is their ability to reduce surface tension between immiscible states. To better understand this, a look at how surface tension arises needs to be understood, and an example of this is to look at a droplet of water upon a table and the curvature of the water droplet instead of a flat, evenly-dispersed appearance. This phenomenon occurs because within the droplet each molecule is being pulled equally in all directions resulting in a net zero force. However, at the surface of the droplet there is not a cancellation of forces due to the absence of molecules on one side. Therefore, molecules on the surface are pulled inwards creating an internal pressure, forcing the liquid surface to contract to minimize area – hence, the curvature. In other words, this surface tension characterizes the shape of the droplet and can be altered by introduction of a surfactant. The surfactant adsorbs to the interface (liquid-gas in this scenario) and reduces the interfacial tension between these two states, therefore, reducing the curvature seen in the droplet. This is a very basic description, but it can be used when looking at more complex systems such as pulmonary surfactant. Surfactants are of utmost importance and a further look into how they function at a physical level and at a biological level will follow.

General Mechanism of Surfactant Function

To get a better understanding of surfactant function, consideration of the forces via Laplace's law must be considered. Laplace's law relates the pressure difference at the interfacial regions to the shape of the surface or wall. Visually, a closed sphere of gas is contained within a uniform solution of water. Figure 1-1 illustrates this and can be described by LaPlace's law in Equation 1-1, where ΔP is the pressure difference across the interface, γ is the surface tension, and r is the radius of the sphere and the wall thickness is presumed to be negligible.

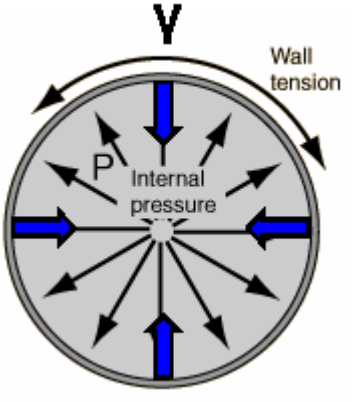

Figure 1-1. An illustration of Laplace's law in a model closed sphere of gas surrounded by a uniform aqueous environment.

$$\Delta P = \frac{2\gamma}{r} \qquad (1\text{-}1)$$

In this scenario, the surface tension, which is perpendicular to the pressure, carries a value depending on the internal pressure and the external pressure pushing in on the sphere. This system is, therefore, in equilibrium and will remain so until a change is exerted upon it, which is the case in many dynamic systems. If this model system was used to interpret a relevant biological system, (e.g. the alveoli in the lung) there would

be changes occurring to the system, for example inhalation and exhalation, in which the variables of the equation must change to keep the system at equilibrium. Figure 1-2 illustrates such a case in which the alveoli are changing in size and are modeled as perfect spheres in which the pressure differential, ΔP, is pushing in on the surface.

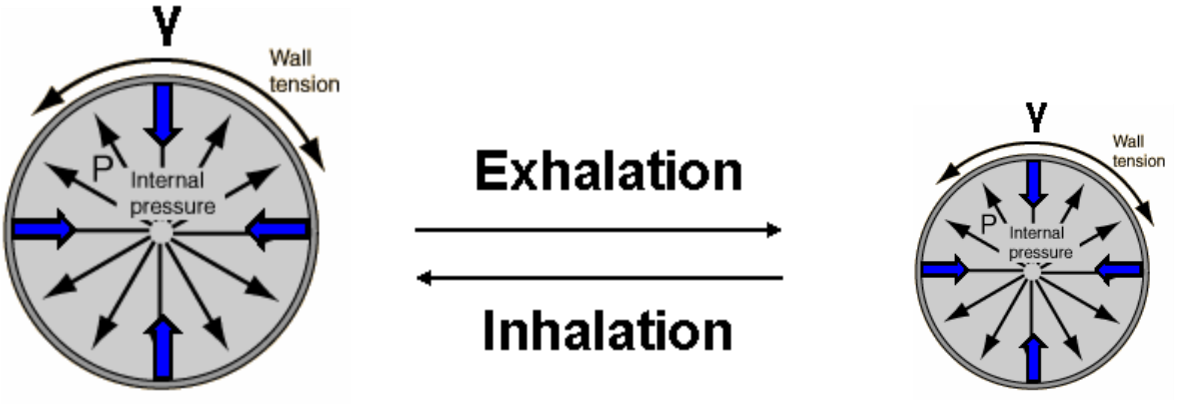

Figure 1-2. LaPlace's law extended to a closed system in which the size of the sphere varies, such as the alveoli in the lung.

From Equation 1-1 there is an inverse relationship between the radius of the alveolus and the surface tension. If the two differing size radii were to have the same surface tension, the alveoli with the smaller radius would experience a greater force inward, expelling its contents to larger alveoli eventually leading to collapse. This is the physics behind the need for surfactant in reducing the surface tension upon exhalation in the pulmonary system to prevent alveolar collapse.

Introduction to Pulmonary Surfactants

Pulmonary surfactant is a vital, lipid-rich fluid found throughout the air-fluid interface of alveoli. It is comprised largely of surface-active lipids, mainly phospholipids and in particular dipalmitoylphosphatidylcholine (DPPC), along with a small mole percentage of hydrophilic and hydrophobic proteins. Pulmonary surfactant is produced

in type II epithelium cells lining the alveoli beginning towards the end of gestation. It facilitates air expansion, prevents collapse, and allows for easy re-expansion of the lungs by drastically reducing alveolar surface tension in a highly dynamic, organized process [1-5]. In addition, it is believed to play a critical role in providing host defense against infection [5-9]. Relative lipid and protein percentages collected via bronchial lavage are shown in Table 1-1 [10-14].

Table 1-1. Pulmonary surfactant make-up by weight %.

Lipid / Protein	Relative weight %
1,2-dipalmitoyl-*sn*-glycero-3-phosphocholine (DPPC)	40
Phosphoglycerols (PG)	8
Unsaturated phosphocholines (PC)	25
Cholesterol	4
Surfactant Proteins (SP-A, B, C, D)	7
Plasma Proteins	3
Other Lipids	7
Fatty Acids	6

These values can vary greatly due to age, environmental factors, disease, and whether in exhalation or inhalation [7, 8, 15, 16]. For example, surfactant production increases drastically at birth when the alveoli transition from fluid-filled with negligible surface tension, to gas-filled with substantial surface tension [9]. This is one of the underlying issues with preterm infant survival rates, as the lung has not had adequate time to develop and produce appropriate amounts of surfactant [17, 18]. Many factors go into producing sufficient amounts of surfactant including the secretion from Type II alveolar cells. This process is not fully understood but is believed to occur in both a continuous manner and via regulated pathways [7, 9, 19-22]. Packaging of the surfactant is done within Type II cells in large concentric bilayers called lamellar bodies. From here the lamellar bodies are secreted into the fluid phase surrounding the alveoli and unravel into highly structured tubular myelin. Although not required, the tubular myelin assists in the

rapid adsorption of a monolayer of surfactant at the air-fluid interface [1, 2, 18-26]. Furthermore, since the system is in continuous flux, the surfactant lipids have a turnover rate with a half-life of just five to ten hours, emphasizing the need for proper surfactant catabolism and recycling [9, 27, 28]. This is performed by alveolar macrophages and the type II cells which secrete the surfactant [28]. Figure 1-3 illustrates the process occurring near the alveoli air-fluid interface. In the following sections a closer look will be given to the individual components that make up pulmonary surfactant in addition to problems that may arise from deficiencies.

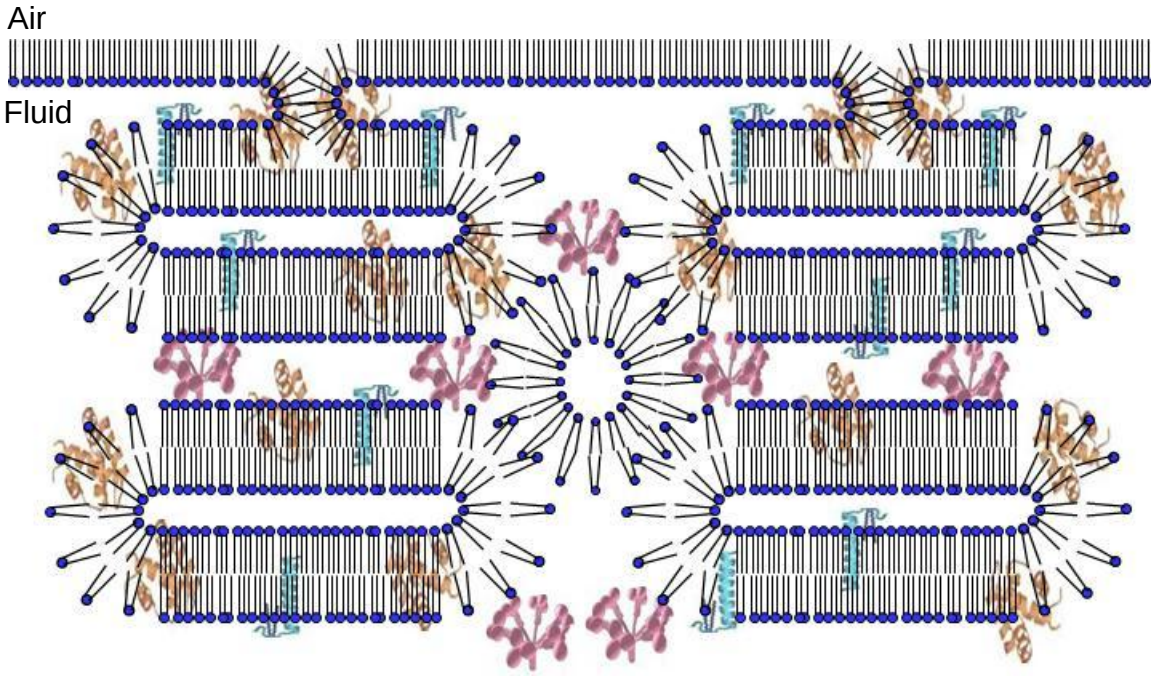

Figure 1-3. Schematic of the processes occurring at the highly dynamic fluid interface in the alveolus, which includes a high rate of lipid turnover (every 5 to 10 hours). Surfactant proteins are shown interacting with lipids in an arbitrary placement.

Pulmonary Surfactant Deficiency Diseases

Pulmonary surfactant plays such a vital role in proper lung function that any disturbance in production can drastically alter breathing capabilities. This leads to a wide range of diseases as illustrated in Table 1-2 [18, 29, 30].

Table 1-2. Several diseases related to improperly functioning pulmonary surfactant [18, 29, 30]

Disease	Possible Cause
Adult Respiratory Distress Syndrome (ARDS)	Infection is most common
Infant Respiratory Distress Syndrome (IRDS)	Insufficient surfactant production
Pulmonary Alveolar Proteinosis (PAP)	Surfactant accumulation
Congenital Surfactant Deficiency	Genetic defects
Pneumonia	Inactivation / deficiencies
Asthma	Inactivation / deficiencies

Unfortunately, due to the complexity and highly dynamic nature of the alveoli, treatment for many lung diseases is difficult and can last a lifetime. Also, since the lung is the singular source of oxygen required by human cellular processes, affliction with some of these disorders can be fatal. This was the case with infant respiratory distress syndrome (IRDS) until the first successful trial of surfactant replacement therapy was developed by Fujiwara et al. in 1980 [31, 32]. In the past thirty years since this landmark trial, RDS treatment has expanded from exogenous surfactant treatments to entirely synthetic options and will be discussed in more detail in the following section [32-42].

Respiratory Distress Syndrome

Respiratory distress syndrome affects people of all ages, is caused by a wide range of factors, and leads to life-threatening illness. Typically classified into two categories, acute respiratory distress syndrome (ARDS) and infant respiratory distress syndrome (IRDS), each is marked with an increase in alveolar surface tension resulting in a disturbance in the lungs' ability to expand, termed compliance [29]. In the case of ARDS this is caused by factors such as: lack of surface-active compounds, changes in lipid composition, altering of surfactant protein composition, and inhibition of proper surfactant function by plasma protein leakage, among others. These factors can be

brought on by infection, massive trauma, pneumonia, pancreatitis, and multiple blood transfusions, in addition to environmental factors like toxic gas inhalation [43-46]. In the case of IRDS, the most common factor leading to the disorder is lack of surface-active compounds. This occurs because the lung is not needed during gestation; therefore, it is one of the last organs to fully develop. When an infant is born preterm, the lungs have not had enough time to produce sufficient levels of pulmonary surfactant and require treatment to allow for normal lung function [1, 18, 32, 47]. In both ARDS and IRDS, the treatment of choice is administering either extracted lung surfactant from an exogenous source or, preferably, a synthetic version in which the immunogenic response is reduces. The surfactant is introduced via a breathing tube directly into the lungs [18, 31, 45, 47]. Since the start of this type of treatment in the early 1980s, a significant reduction in infant mortality rates has been shown [48-51]. Increasing interest has been generated in the study of RDS due to the statistics illustrated in Figure 1-4.

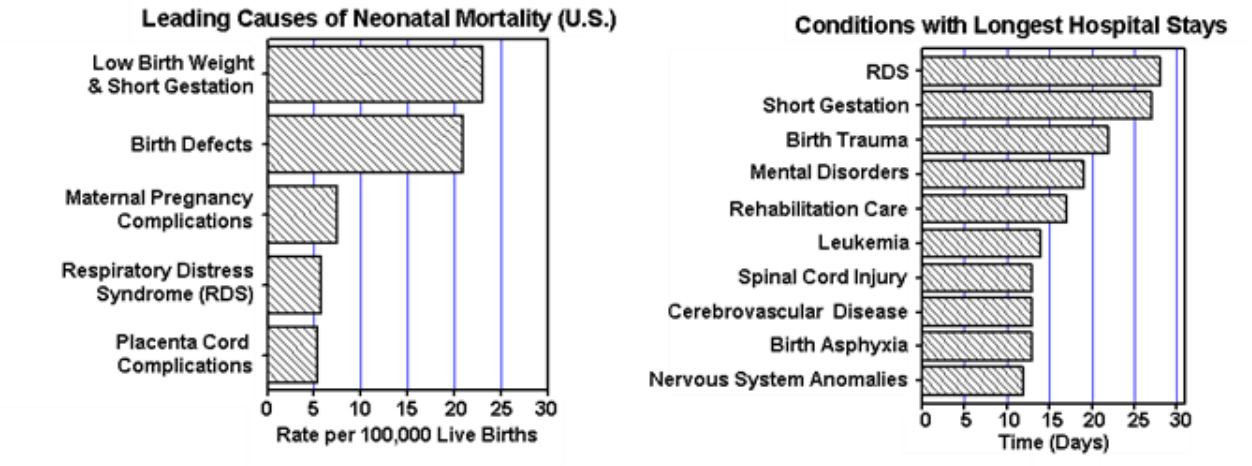

Figure 1-4. Five leading causes of neonatal mortality, with RDS coming in fourth (left) and resulting in longest average hospital stay (right).

Surfactant Lipids

There are multiple components that make up functioning lung surfactant as shown in Table 1-1 and they can be grouped into two categories, surfactant lipids and surfactant proteins [10, 18]. The latter will be discussed in the following section as they play a vital role interacting with the lipids to allow proper lung function. Of the lipids found in lung extract, the high content of DPPC is especially unique when compared to other biological systems. This is because DPPC has two fully saturated acyl chains, giving it a high melting temperature of 41 °C. This places it above a physiological temperature of 37 °C, making it rather unique among the lipid family. Having DPPC at the air-fluid interface in alveoli makes sense though, as its fully saturated acyl chains allows it to be tightly packed or highly compressed and give it the ability to drastically reduce surface tension. When Clements et al. began looking at lung surfactant extracts back in 1961; they compared them with pure DPPC to understand its importance [52]. It was determined by Langmuir-Blodgett trough measurements, and later confirmed by a captive bubble surface tensiometer, that the reduction of surface tension seen in lung surfactant extract was nearly identical to that of pure DPPC [52-55]. This is unusual given the composition shown in Table 1-1 where DPPC only makes up about 40 % of lung surfactant. Current theories, however, hypothesize that there is an enrichment process occurring at the air-fluid monolayer in which DPPC is preferentially adsorbed [1]. This is very plausible as the average lipid composition is determined by lavage procedures involving a saline solution administered into the lungs [10, 18]. This process reveals an average concentration of lipids present; however, there are many concerns with obtaining surfactant in such a manner. The introduction may disrupt the proper biophysical organization of the lipids, therefore generating surfactant form that may not

exist in vivo. In addition, the composition obtained cannot discriminate from the microenvironment of the surfactant at the air-fluid interface and the bulk lipid composition found in lamellar bodies or other large scale structures. Therefore, these numbers give a starting point to use for model studies but should be taken with skepticism as to the exact air-fluid interface lipid composition. Another notable observation was by Hallman et al. in 1975 when elevated levels of phosphatidylglycerol (PG) in healthy lung extract were seen when compared to premature lung extract [56-58]. It was determined that PG contributed to surfactant spreading and along with DPPC were two key lipids involved in proper lung function [59]. These two lipids will go on to play critical roles in the advancement of RDS treatments and will be extensively studied in later Chapters 3-5 of this work. Interactions with surfactant proteins are the next big step in understanding the molecular mechanisms underlying the function of surfactant at the dynamic air-fluid interface.

Surfactant Proteins

Surfactant proteins make up about 10 % by weight of the bronchoalveolar lavage extract and play critical roles in proper lung function and the body's initial defense system [1, 6, 60-64]. Surfactant proteins are divided into two categories, hydrophilic surfactant proteins A and D and hydrophobic surfactant proteins B and C. The hydrophobic proteins B and C have been shown to promote rapid adsorption of lipids to the air-fluid interface and are critical in proper lung function [65-69]. The hydrophilic proteins A and D aid SP-B and SP-C in promoting adsorption and play an important role in lung defense [60-64, 70].

Surfactant proteins B and C are small, hydrophobic proteins with a highly conserved primary sequence and are necessary for surfactant function *in vivo* [32, 71].

An important function of both SP-B and SP-C is their ability to form monolayers by themselves or as mixtures with DPPC, in addition to promoting re-adsorption of materials from collapsed, DPPC-containing monolayers [65, 67]. Their ability to perform these functions leads to their critical importance as shown in SP-B knockout studies in which animals either had significantly decreased lung compliance or did not survive after delivery [72-74]. An important finding from these studies is that SP-A, SP-C, SP-D, and phosphatidylcholine concentrations remained normal, leading to a conclusion of the critical importance of SP-B [75]. Further detail on SP-B will be discussed in the following section. SP-C gene knockout mice were generated and had normal lung function with only minor abnormalities [76].

Surfactant protein A is the most abundant protein in pulmonary surfactant and, like SP-D, is related to a family of water-soluble proteins called collectins, which contain both collagenous regions and C-type lectin domains [77]. The C-type lectin domains, also called a carbohydrate recognition domain (CRD), bind to specific complex carbohydrates of microbes allowing for the innate immune response and elimination [78]. In addition, SP-A binds to DPPC, while SP-D has been shown to bind to phosphatidylinositol (PI). Both are present in lung surfactant [77]. SP-A also interacts with alveolar Type II cells, implicating it in proper formation of the highly structure tubular myelin [77, 79]. SP-A and SP-D play key roles in the innate immune system of the lung by allowing for immediate antibody-independent host defense [32, 60-64, 70]. Knockout studies of SP-A and SP-D genes have shown retention of normal lung function, in addition to achieving adequate minimal surface tensions of compressed films when compared to wild type [79]. However, due to their role in host defense,

infections such as streptococci and pseudomonas commonly occurred in the knockout mice and they were more prone to die [80, 81].

Findings from these studies leads to an understanding of the importance of surfactant proteins to uptake and release of surfactant lipids from Type II epithelial cell; they however, do not provide a detailed understanding of their role in lowering surface tension [1, 82].

Surfactant Protein B and Analogs

Lung surfactant protein B is an extremely hydrophobic homodimer with two 79-81 amino acid disulfide-linked subunits. Each monomer contains an additional six cysteines used in intramolecular disulfide bonding [24]. These disulfide bonds, along with its high hydrophobicity, make protein purification difficult. Synthetic, peptide-based lung surfactant replacements for treatment of RDS have shown promise and would reduce the purification difficulties and immunologic risks associated with exogenous animal derived lung surfactant [83, 84].

Chemically synthesizing the entire dimerized SP-B is a daunting task so efforts have focused on producing truncated proteins and synthetic analogs of the N- and C-termini (SP-B_{1-25}, SP-B_{59-80}, and KL_4) as well as a fusion construct of the N- and C-termini of SP-B, termed Mini-B, which are less hydrophobic and lack the disulfide bridges of SP-B [42, 83-86]. This has proven successful since much of the activity of SP-B in lipid organization and dynamics have been attributed to the 20-25 amino acids on the N- and C- termini [83, 84, 87]. As with SP-B, the N- and C- termini form helices when exposed to a lipid environment; however, their individual roles are not well understood. Although both ends of SP-B have shown considerable surface activity by themselves, similar activity to native SP-B has only been achieved by a construct of

both the N- and C- termini [88-93]. A fully synthetic mimic of SP-B has achieved great interest due to its ease of synthesis, low cost, and elimination of exogenous immunological drawbacks. Cochrane and Revak began much of the synthetic mimic research in the early 1990s with KL_4, which has achieved great success in FDA trials [94]. A more detailed look at KL_4 follows in the next section.

Introduction to KL_4

Discovery of KL_4

KL_4 is an entirely synthetic mimic of the SP-B C-terminus which, much like SP-B and its analogs, forms helices in lipid environments, but its role in lipid trafficking is often unclear [42, 95]. It was developed by Cochrane and Revak, along with several other synthetic peptides to resemble the hydrophobic and hydrophilic domains of the SP-B C-terminus [94]. The 21-mer KL_4 peptide, KLLLLKLLLLKLLLLKLLLLK, demonstrates great clinical success in treatment of RDS and is currently available on the pharmaceutical market as one of the active components in the first-generation, completely synthetic, lung surfactant replacement product Surfactant® (Lucinactant). [92, 96-103]. Table 1-3 compares the amino acid sequence of SP-B C-terminus, KL_4, and Mini-B (construct of N- and C-termini). Although KL_4 is a promising treatment for RDS, molecular level information on how it modulates surface tension in alveolar compartments is lacking. The increased effectiveness of KL_4 when compared to other commercially available formulations in addition to its vast difference in amino acid sequence suggest that understanding the way it affects the molecular and biophysical properties of the lipids is of great importance [104].

Table 1-3. Amino acid sequence of SP-B termini and SP-B analogs.

Peptide	Peptide Sequence
SP-B $_{1-25}$	FPIPLPYCWLCRALIKRIQAMIPK
SP-B$_{59-80}$	DTLLGRLMPQLVCRLVLRCSMD
KL_4	KLLLLKLLLLKLLLLKLLLLK
Mini-B	CWLCRALIKRIQAMIPKGGRMLPQLVCRLVLRCS

Structure and Function of KL_4

As with the terminal ends of SP-B, KL_4 has been found to adopt a helical conformation in a lipid environment, as shown with circular dichroism and Fourier transform infrared spectroscopy (FTIR) [42, 95, 105]. There have, however, been competing theories as to whether the helix partitions into the bilayer, either in the plane of the bilayer or in a transmembrane orientation.

To further elucidate the structure, function, and orientation of KL_4 in lipid bilayers, the following lipid systems are typically used: fully monounsaturated POPC:POPG (3:1) and DPPC:POPG (4:1). The latter contains the fully saturated DPPC lipid and is being used in the therapeutic formulation, Lucinactant. Models for KL_4 partitioning into lipid bilayers have fallen into two categories; a transmembrane helix and a helix lying in the plane of the bilayers. The 21-residue length of KL_4 allows it to adopt a transmembrane helix; however, it would bury 2-3 charged lysine side chains in the hydrophobic interior. A high percentage of leucine side chains and secondary structure could overcome this barrier, but previous studies using similar amino acid ratios suggest that a transmembrane orientation is only likely when the lysines are positioned closer to the N- and C-termini [106]. Nonetheless, recent studies have shown contradicting evidence in which a transcription-translation assay found KL_4 capable of overcoming the energetic barrier and crossing the membrane [107], and another ^2H solid-state NMR study in which KL_4 was shown to adopt a helix lying in the plane of the bilayer [86]. The former

studies compared the ΔG_{app} values (calculated using ΔG_{app} Prediction Server v1.0, http://www.cbr.su.se/Dgpred/) for insertion in endoplasmic reticulum (ER) membranes of KL_4 and the naturally occurring sequences, SP-B_{59-79} and SP-C_{13-35}, which KL_4 is most closely mimicking. These studies predict that SP-C_{13-35} is transmembrane (-4.35 kcal/mol), an transmembrane orientation of SP-B_{59-79} would be unfavorable (+3.12 kcal/mol), and KL_4 has a ΔG_{app} closer to SP-C_{13-35} (-2.14 kcal/mol) [25, 107-109]. Their experiments to assay insertion used a transcription-translation assay with integration of KL_4 into *Escherichia coli* inner membrane protein leader peptidase (Lep), which is translated in ER-derived microsomal membranes and assayed for glycosylation using proteinase K to determine whether the peptide is transmembrane. This assay, however, has two major drawbacks when used with KL_4. First, the addition of the Lep protein may influence the secondary structure of KL_4 in the lipid bilayer. Secondly, KL_4 is known to alter lipid dynamics and trafficking, therefore, altering the overall integrity of the microsomal membranes. In addition, the ΔG_{app} calculated assumes a typical α–helix conformation which may not be the case, as other studies using ssNMR have suggested KL_4 adopts a structure with a lower helical pitch in DPPC:POPG and POPC:POPG membranes [42]. With these structures its hydrophobic moment would be increased 3-4 kcal/mol, making transmembrane insertion much less favorable [86]. The latter study involving ^2H solid-state NMR suggests that KL_4 adopts a helix lying in the plane of the bilayers due to difference seen in the dynamics of leucine side chains which, if transmembrane, would have similar dynamics [86]. These studies, however, looked only at two sides of the helix instead of a complete turn around the predicted helix. Studies using FTIR have also led to conflicting models of the structure and

orientation of KL_4. In early work using DPPC:DPPG (7:3), KL_4 was found to be helical and spanning the bilayer in a transmembrane confirmation [95]. Later FTIR work in either DPPC or DPPC:DPPG (7:3) mixtures have shown that KL_4 lies along the surface of the lipids as a mixture of β–sheet and α–helix [110]. However, once again these assays assume that KL_4 adopts a classic β–sheet or α–helix which may not be the case. To further complicate this system, it has been suggested that KL_4 adopts a helix in the plane of the bilayer while also penetrating the bilayer to different extents depending on whether the fully saturated DPPC lipid is used. This was shown indirectly with ^{2}H and ^{31}P NMR studies of deuterated lipids and suggested that KL_4 partitions further into DPPC:POPG (4:1) than POPC:POPG (3:1) vesicles [86].

Understanding the orientation within the lipid bilayer will provide insights into its functional properties and assist in further development in effective respiratory distress syndrome treatments. In Chapters 4-6 we will optimize the lipid mixture compositions, power saturation parameters, and buffer pH. In addition, we will determine the orientation of KL_4 and depth profiles in two lipid systems, DPPC:POPG (4:1) and POPC:POPG (4:1) vesicles.

CHAPTER 2
BACKGROUND FOR TECHNIQUES AND METHODOLOGIES

Introduction

Methods such as automated solid-phase peptide synthesis, site-directed spin labeling (SDSL), circular dichroism spectroscopy (CD), continuous-wave electron paramagnetic spectroscopy (CW-EPR), and CW power saturation were utilized in the work of this dissertation. General overviews for each of these methods are given in the following sections. Specific details related to my studies are also provided in subsequent material and methods sections of each Chapter.

Peptide Synthesis

The relatively small size of KL_4, KLLLLKLLLLKLLLLKLLLLK, containing 21 amino acids, rendered it easily amendable to peptide synthesis. KL_4 was synthesized via automated solid-phase peptide synthesis on a Wang resin at the Interdisciplinary Center for Biotechnology Research (ICBR) at the University of Florida, using an Applied Biosystems ABI 430 peptide synthesizer operated by Dr. Alfred Chung [92, 111, 112]. The peptide was cleaved from the resin with 90% trifluoroacetic acid (TFA)/ 5% triisopropylsilane/ 5% water and ether precipitated. Purification of the cleaved product was carried out by reverse-phase high performance liquid chromatography (RP-HPLC) using an acetonitrile/ water gradient containing 0.3 % TFA. Fractions corresponding to KL_4 were collected and purity and concentration was verified by amino acid analysis (AAA) at the Molecular Structure Facility at the University of California, Davis. This technique allows for a high level of accuracy in concentration and purity by using Edman degradation, fluorescent labeling, and analytical HPLC to determine the amino acid concentrations from the N- to C-terminus direction of small peptides (<30 amino

acids) [113, 114]. In addition to native KL_4, cysteine variants were synthesized. In that process, individual leucines were replaced by cysteine (C7-C10, C12-C15) purified and mass verified (m/z=2459) in the same manner as stated above. Figure 2-1 shows one of the amino acid analysis results for KL_4.

Amino Acid	nmoles	nms/50 ul	mole %	N (data)	N (exp)
Asx	0.000	0.000	0.00	0.0	
Thr	0.000	0.000	0.00	0.0	
Ser	0.000	0.000	0.00	0.0	
Glx	0.000	0.000	0.00	0.0	
Pro	0.000	0.000	0.00	0.0	
Gly	0.000	0.000	0.00	0.0	
Ala	0.000	0.000	0.00	0.0	
Val	0.000	0.000	0.00	0.0	
Ile	0.000	0.000	0.00	0.0	
Leu	19.835	20.640	73.77	15.5	16
Tyr	0.000	0.000	0.00	0.0	
Phe	0.000	0.000	0.00	0.0	
His	0.000	0.000	0.00	0.0	
Lys	7.054	7.340	26.23	5.5	5
Arg	0.000	0.000	0.00	0.0	
Cysteic	0.000	0.000	0.00	0.0	
Methionine	0.000	0.000	0.00	0.0	
Trp	0.000	0.000	0.00	0.0	
Totals:		27.980	100.00		21
nmol peptide/50 ul:		1.332	Total nmol:	13.323919	

Figure 2-1. Typical amino acid analysis (AAA) mass spectrometry used to determine the relative number of amino acids per peptide (right). A result of 16 leucines for every 5 lysines verifies native KL_4.

Site-directed Spin Labeling

Site-directed spin labeling (SDSL) is a technique that introduces a paramagnetic species at a specific site in a protein or other biological molecule, typically by chemical modification of a cysteine residue, and renders the molecule EPR active [115]. When used with EPR, conformations, conformational changes, solvent accessibility, and bilayer depth profiles are among a few of the details that can be extracted from the specific labeled site making it a well-suited technique to study membrane bound protein or peptides [116-123].

Site-directed spin labeling exploits the chemical reactivity of the cysteine residue to allow for attachment of various spin-labels [117, 119, 124]. Typically a cysteine residue is introduced via site-directed mutagenesis, in which the DNA is manipulated such that a codon for cysteine is positioned at a chosen point within the sequence [115, 119]. As KL_4 is readily available by automated solid-phase peptide synthesis, changing a desired leucine to a cysteine is well suited for this technique. After KL_4 has been modified to include the cysteine, the peptide construct is further modified with a spin label. The label of choice for these studies is iodoacetamido-PROXYL, (IAP) because it forms a non-reducible carbon sulfur bond and is shown in Figure 2-2.

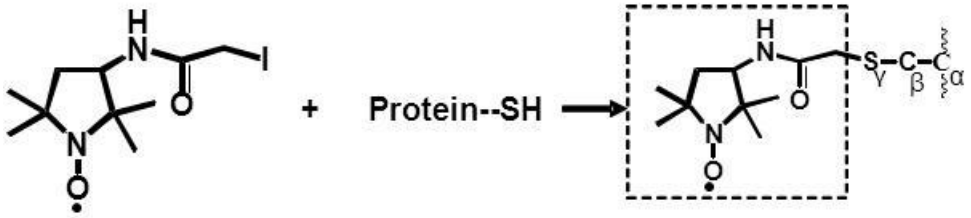

Figure 2-2. The site-directed spin-labeling scheme of a cysteine residue's free thiol with iodoacetamido-PROXYL (IAP) used to form the non-reversible carbon-sulfur bond. The resulting modified cysteine residue is referred to as R1 and will be used in KL_4 studies described in this dissertation.

The sensitivity of the EPR nitroxide spectral line shapes resulting from these various spin labels to local dynamics, conformational changes, and local secondary structural elements allows researchers to monitor the spin label environment using CW EPR spectrometers (Figure 2-3) [117, 118, 125-127]. To better elucidate information from the spectral line shape the types of motion that are being detected by the SDSL-EPR technique need to be understood. There are three types of motion to consider in interpreting SDSL results: the intrinsic motion of the nitroxide spin label, the backbone motion due to the flexibility with the region of the protein the label is attached, and the

overall tumbling of the peptide or protein. Each of these can be altered experimentally by changing the spin label of choice, temperature, viscosity, or altering the overall size of the tumbling system [119]. A variety of semi-quantitative line-shape parameters will be used and discussed in the subsequent EPR section.

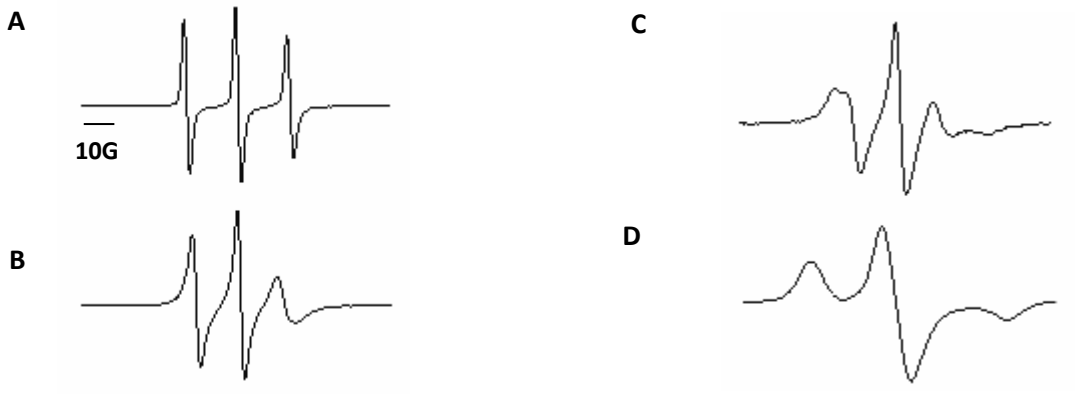

Figure 2-3. CW-EPR spectra for various scenarios: unrestricted motion on the EPR timescale (A), gradually more restricted motion (B & C), and a powder-like spectra in which the spin label is almost static (D).

In addition to studying the EPR spectra of SDSL proteins, another useful CW-EPR technique that assists in elucidating information about membrane-bound proteins is to introduce a spin label onto a lipid, either on the acyl chain as a doxyl nitroxide at varying positions or on the polar head group in the form of a TEMPO nitroxide (Figure 2-4) [117, 120, 128-130]. Spin-labeled lipids compliment well with SDSL protein for EPR studies as an understanding of both the protein and lipid membrane environments can be determined. Addition of a small amount of spin-labeled lipid (1 mol %) to a lipid system of choice gives excellent sensitivity for CW-EPR line shape analysis. In addition, it allows for additional techniques such as power saturation to be performed to determine a relative depth profile which will be discussed later. Using a low concentration of doxyl lipid minimizes perturbation of the lipid system and limits interaction between neighboring spins. Spin-labeled lipids are also widely commercially available at purities

of >99% with doxyl labels at positions 5, 7, 10, 12, 14, and 16 along the acyl chain of PSPC as well as a Tempo label attached directly to the head group of DPPC or POPC (Figure 2-4). In addition to these commercially available, several groups have synthesized additional spin-labeled lipids [131, 132].

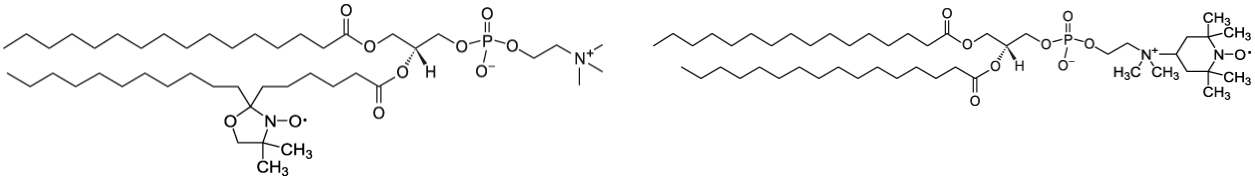

Figure 2-4. Structure of 1-palmitoyl-2-stearoyl-(7-doxyl)-*sn*-glycero-3-phosphocholine (left) and 1,2-dipalmitoyl-*sn*-glycero-3-phospho(tempo)choline (right).

Circular Dichroism Spectroscopy

Circular dichroism (CD) is a technique that observes differences in absorption between left and right-handed circularly polarized light as a function of wavelength. Most notably, this technique is used to study optically active molecules such as biological molecules [133, 134]. The secondary structures of such molecules impart distinct CD spectra which allow for determination of α–helical, β-sheet, and random coil content [135-137]. To understand the technique, circularly polarized light must be defined as $\theta = 45°$ with E_R and E_L being the magnitudes of the electric field vectors of right and left-circularly polarized light, respectively (Figure 2-5). Having $\theta = 45°$ means that there is complete absorbance of the circularly polarized light in one direction; hence, the light is circularly polarized and by definition, chiral. This contrasts with linearly polarized light in which there is no difference between E_R and E_L, where $\theta = 0°$. The chiral property of circularly polarized light allows it to interact with chiral molecules in a distinct way which in turn gives rise to its importance in studying biological molecules. When circularly polarized light passes through a protein sample, the

difference in absorption of left and right-circularly polarized light gives rise to an ellipticity which can be measured to generate a wavelength-dependent plot of differential absorption of circularly polarized light.

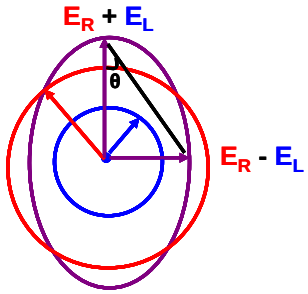

Figure 2-5. Elliptical polarized light (purple) is composed of unequal contributions from right (red) and left (blue) circular polarized light. Figure adapted from Wikipedia.

When circular dichroism is used to determine secondary structural elements in proteins or peptides, the far ultraviolet (UV) region monitored is 180-250 nm, where the peptide bond is absorbing the left and right-handed circularly polarized light to different extents. Depending on the structure of the protein backbone; albeit α-helical, β-sheet, or random coil, a distinct CD spectrum will be obtained (Figure 2-6). In the case of membrane bound proteins in which lipid vesicles are used, scattering from the lipids occur in the region below 200 nm, so CD spectra are typically truncated to the 200 – 250 nm region [136, 138-140]. Changes in secondary structure can be elucidated by comparing CD spectra as a function of sequence and environment and used to determine perturbations in the peptide or protein secondary structure.

Circular dichroism instrumentation, however, does not account for important experimental factors in recording the raw data spectra, so calculations are needed to unify reported CD spectra.

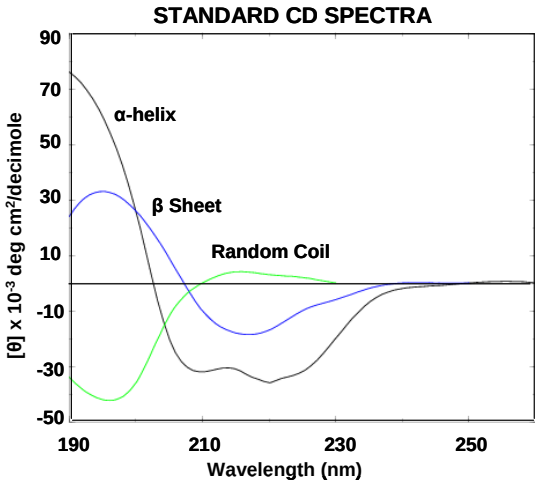

Figure 2-6. Sample circular dichroism spectra for α-helix (grey), β-sheet (blue), and random coil (green). Figure adapted from Chapman.

Raw data is typically expressed in units of millidegrees (θ) and converted to the reported mean residue ellipticity [θ] (deg $cm^{-2}dmol^{-1}residue^{-1}$), as shown in Equation 2-1, where [θ] is the mean residue ellipticity, θ is the ellipticity, M_r is the protein molecular weight, c is the protein concentration (mg/mL), *l* is the cell path length, and N_A is the number of amino acids.

$$[\theta] = \frac{(\theta \, x \, 100 \, x \, M_r)}{c \, x \, l \, x \, N_A} \qquad (2\text{-}1)$$

Further factors during sample preparation must also be considered when accurately measuring secondary structure of the protein sample. Purity of sample is of high importance as any non-target proteins will alter the overall secondary structure ensemble leading to misinterpretation of data. In addition, with a focus on secondary structure, the protein must be properly folded in an ideal buffer of low concentration (< 5 mM) while maintaining structural integrity. Typical protein concentrations should be maintained around 0.5 mg/mL. Any additive to the sample should not absorb in the far-UV region, with the exception of lipid vesicles mentioned earlier. When lipid vesicles

are introduced they need to be accounted for in the background subtraction and extruded through nanoporous membrane to reduce the size of the vesicles and reduce light scattering.

The ease of CD spectroscopy makes it a popular tool when studying proteins and when altering proteins to enable other techniques such as SDSL-EPR. There are drawbacks, however, to the interpretation of CD spectra as they give an overall view of the secondary structure rather than information on a specific region of interest. This means that although secondary structure is revealed, actual determination of a properly folded protein is not possible. Keeping this in mind, CD spectroscopy should be used strictly to show if a protein is changing its structure and never to determine if the protein is indeed properly folded into its functional form. When using SDSL it is always recommended to do CD on the samples because it can show small changes in secondary structure due to the spin label perturbing the protein structure. In addition, CD is a non-destructive technique so hard to obtain samples aren't wasted.

Continuous-Wave Electron Paramagnetic Resonance Spectroscopy

Introduction

Electron paramagnetic resonance spectroscopy (EPR), also known as electron spin resonance (ESR), is a technique for studying chemical species that contain one or more unpaired electron. These paramagnetic species include organic free radicals and inorganic transition metal complexes. Similarities exist between EPR and nuclear magnetic resonance (NMR); however, EPR looks at electronic spin transition while NMR looks at nuclear spin transitions. Although not as widely used as NMR, EPR has increased in use due to the introduction of SDSL which allows for its use in systems which are not naturally EPR active. In its simplest form, a free radical in solution, the

electron has a magnetic moment and spin quantum number s = ½ with spin states m_s = ±1/2. In the absence of an external magnetic field, these spin states are degenerate, simply meaning the energy of the two spin states, m_s = +1/2 (antiparallel) and m_s = -1/2 (parallel) are equal. When an external magnetic field is applied these states have different energies leading to transition energy between them known as the Zeeman Effect. The difference between these two energy levels is described by the Zeeman equation (Equation 2-2), where g_e is the electron's g-factor, μ_B is the Bohr magneton, and β is the strength of the applied magnetic field. The Bohr magneton (9.274 x 10^{-24} J T^{-1}), is a physical constant and is expressed using Equation 2-3, where e is the elementary charge, ħ is the reduced Planck constant which puts it in terms of radians (1.054 x 10^{-34} J s / 2π), and m_e is the electron's resting mass (9.109 x 10^{-31} kg).

$$\Delta E = h\nu = g\beta_e B \tag{2-2}$$

$$\beta_e = \frac{e\hbar}{2m_e} \tag{2-3}$$

In practice, CW-EPR is performed by keeping the frequency fixed as the magnetic field is swept with field modulation, therefore, this means the energy gap between m_s = +1/2 and m_s = -1/2 is changed until it matches the frequency of the microwave or resonance condition, at which point the unpaired electron can transition between the two spin states. Due to the Maxwell-Boltzmann distribution there are typically more electrons in the lower energy state, which leads to a net absorption of energy. It is this absorption which is monitored and converted into an EPR spectrum. The energy diagram describing this is shown in Figure 2-7A, while the simplest form of an EPR spectrum is shown in Figure 2-7B. While this is the case for the simplest free electron, more complicated systems are typically observed with more complex resulting spectra.

For EPR being performed in conjunction with SDSL, in which a nitroxide spin label is used, the spin of the electron, s = ½, interacts with the nuclear spin of the nearby nitrogen (I = 1) via the hyperfine interaction. In this case, both the m_s = +1/2 and m_s = -1/2 energy levels are split into three hyperfine energy levels dues to the 2I+1 splitting rule. The energy diagram for this case is shown in Figure 2-8A, in addition to a corresponding derivative of the absorption spectrum in Figure 2-8B.

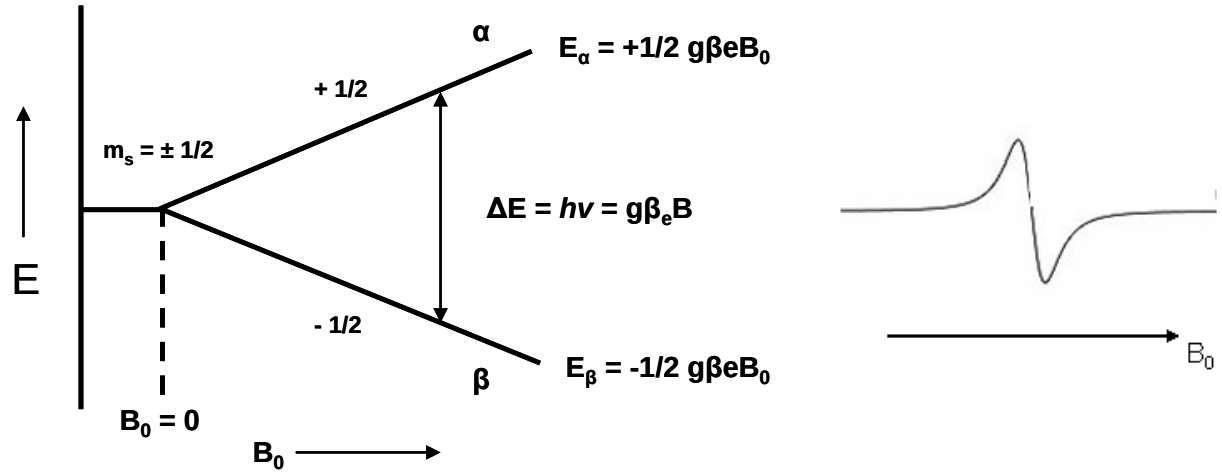

Figure 2-7. (A) An energy diagram for a free electron in an applied magnetic field. (B) A corresponding first derivative spectrum.

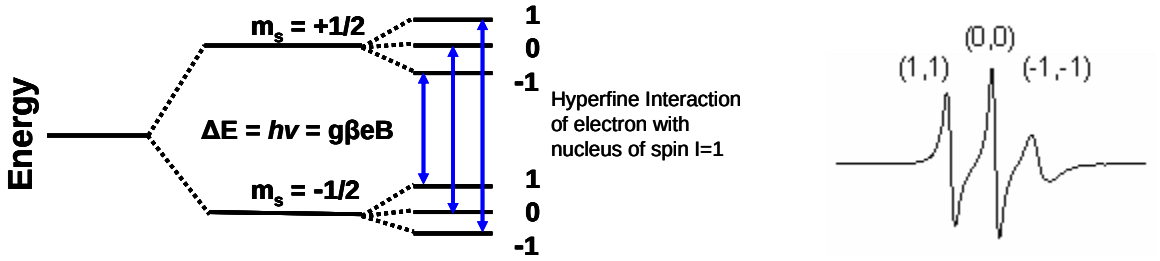

Figure 2-8. (A) An energy diagram for a system with a free electron (ms = ½) being split into three allowed energy transitions due to the hyperfine interaction with a nitrogen nucleus (mI = 1). (B) A derivative spectrum of a nitroxide spin label with the following energy diagram.

As mention previously, in conventional CW-EPR the frequency is held constant throughout the experiment while the magnetic field is swept; however, spectra can be collected at different frequencies depending on the sample of interest. For most

studies, including those presented in this dissertation, collection is done in the X-band range where resonances occur at magnetic fields around 3480 Gauss (0.35 T) and frequencies of about 9.75 GHz. Other common EPR frequencies can be found in Table 2-1.

Table 2-1. Common microwave bands and frequencies used in CW-EPR.

Band	Frequency (GHz)	$B_{resonance}$ (Gauss)
X	9.75	3480
Q	34.0	12000
W	94.0	34000

Nitroxide Spectral Line Shapes

As previously stated and shown in Figure 2-4 the nitroxide EPR spectral line shape is highly sensitive to motion of the spin label environment and changes dramatically with correlation time, or the time it takes for a molecule to rotate one radian on average. To reiterate this, Figure 2-9 shows EPR spectra, which span a range from low correlation times (top) to much higher correlation times (bottom).

The dependence of correlation time on the mobility of the spin label can be broken down into three modes of motion [127, 142, 143]. The first is the internal correlation time (τ_i) is determined by the intrinsic local mobility of the spin label which varies with type of spin label. To an extent this is experimentally distinguished by choosing a wide variety of spin labels with different bulky head groups as well as connectivity differences. Several common spin-labels are shown in Figure 2-10 with R1 corresponding to the boxes. The second mode is a rotational correlation time (τ_R) and is determined by the overall rotation of the protein. Rotational correlation time is dependent on the size of the protein if it is solubilized or the size of the system if it is membrane bound in a lipid vesicle. Sample conditions play an important role in determining τ_R such as temperature, viscosity, and buffer make-up.

Figure 2-9. Dependence of EPR line shape on motion

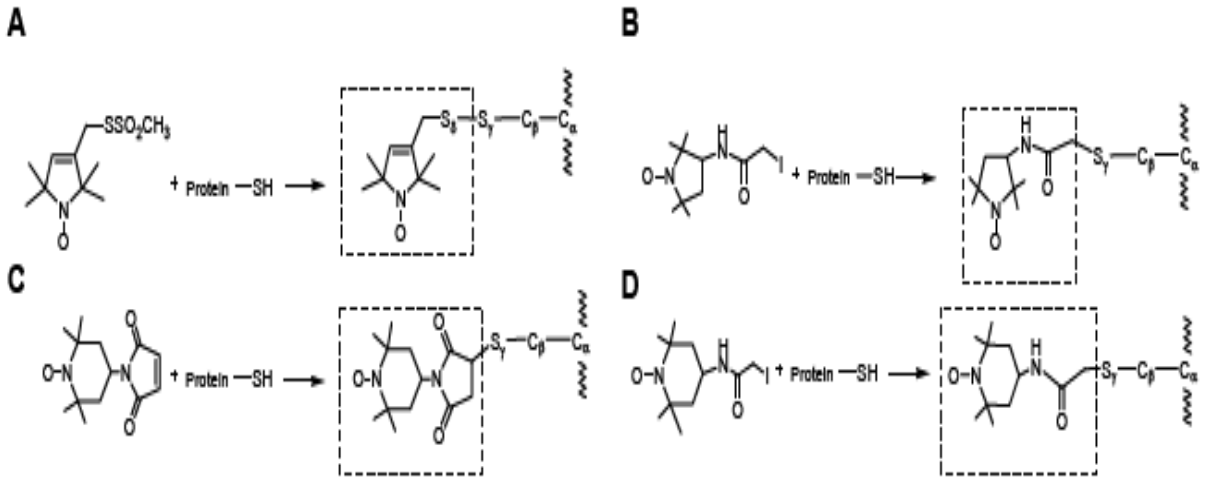

Figure 2-10. Common spin-labels utilized in SDSL. (A) (1-oxyl-2,2,5,5-tetramethyl-Δ3-pyrroline-3-methyl) methanethiosulfonate (MTSL), (B) 3-(2-iodoacetamido)-PROXYL (IAP), (C) 4-maleimido-tempo (MSL), and (D) 4-(2-iodoacetamido)-tempo (IASL). Figure modified from Luis Galiano's dissertation.

The third mode of mobility (τ_B) is determined by backbone fluctuations in the protein and local dynamics affected by neighboring molecules. This mode changes when the spin label is located at different secondary and tertiary structure locations on a protein or when a protein undergoes a conformational change.

Line Shape Data Analysis

CW-EPR line shapes can be analyzed in qualitative, semi-quantitative, and quantitative manners. This is due to the mobility allowed for a given spin label reflects greatly on the overall breadth of a spectrum as well as specific spectral features. In terms of qualitative analysis, a look at a spectrum's overall characteristics help to describe it in terms of breadth. Examples are shown in Figure 2-3 in which the spectrum goes from very narrow in Figure 2-3A to very broad in Figure 2-3D. A semi-quantitative analysis of spectra can be done by measuring spectral parameters such as; peak to peak line width of the central resonance line (ΔH_{pp}); ratios between normalized intensities of the three resonance lines, most notably the central resonance line h(0) over the low field line h(1); the second moment ($<H^2>$); and an order parameter (S) which compares the spectrum to that of a completely static and completely mobile spectrum, giving a value between 0 and 1. There are other mobility parameters used throughout the EPR community, but the focus of this dissertation will be on using these more commonly measured ones. Figure 2-11 shows a graphical representation of the first three parameters and a more detailed explanation follows. The fourth parameter (S) involves a little more detail so it is shown in Figure 2-12.

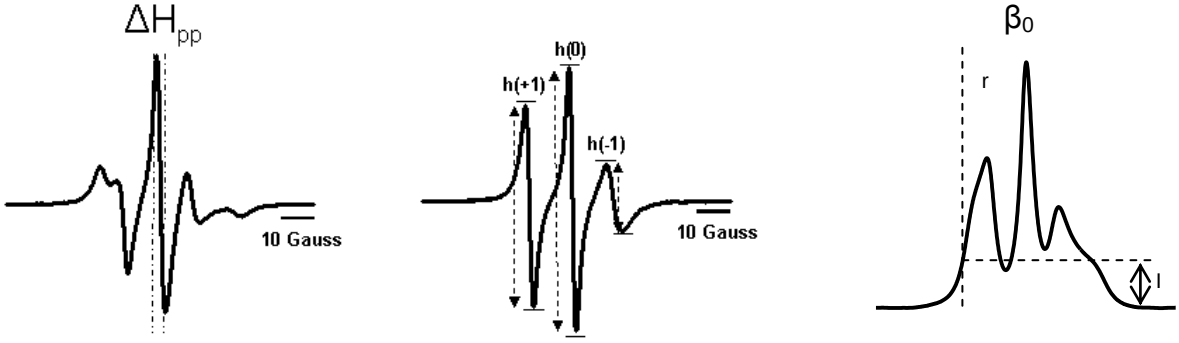

Figure 2-11. Spectral representation of determining three common mobility parameters (A) ΔH_{pp} (B) normalized intensities and (C) second moment ($<H^2>$).

Figure 2-12. Two spectra indicating the parameters used to calculate an order parameter (S) as typically used in doxyl lipid mobility calculations.

The first parameter mentioned, ΔH_{pp}, is defined as the distance, in Gauss, between the maximum and minimum of the central resonance in a first derivative spectrum. When mobility, and therefore correlation time, is affected, ΔH_{pp} will experience either a narrowing or broadening which can easily be seen in Figure 2-9. A short correlation time (high mobility) gives a narrow ΔH_{pp}, while a longer correlation time (restricted mobility) gives a much broader ΔH_{pp}. In addition to looking directly at the ΔH_{pp}, a scaled mobility, M_s, can be used by normalizing the ΔH_{pp} measured by the spectral line widths of the most mobile and immobile proteins to compare data collected on different instruments. Equation 2-4 gives the formula for calculating M_s, where δ_i, δ_m, and δ_{exp} are the ΔH_{pp} from the most immobile, most mobile, and experimental EPR spectra, respectively.

$$M_s = \frac{\delta^{-1}{}_{exp} - \delta^{-1}{}_{i}}{\delta^{-1}{}_{m} - \delta^{-1}{}_{i}} \qquad (2\text{-}4)$$

Comparison of normalized resonance peak intensities is another way of quantitatively comparing mobility of spin labels between two or more samples. This involves normalizing all derivative spectra to the same number of spins via double integration and comparing two of the three normalized EPR resonance intensities, low

field I_{LF}, center field I_{CF}, or I_{HF}. Most commonly, the ratio of the center field and low field intensities (I_{CF}/I_{LF}) is used to compare spin-labeled samples. In the case of highly anisotropic motion, the line shapes become broadened as shown in Figure 2-1, which in turn leads to a decrease in the normalized intensities of each resonance. On the other hand, a fast isotropic motion generates an EPR line shape with narrow peaks of high intensities and therefore an increase in I_{CF}/I_{LF}. This is a useful tool to use in conjunction with ΔH_{pp} since the combination of multiple semi-quantitative parameters gives a better overall understanding of the spectra.

Spectral second moment calculations are different from the other parameters mentioned because they analyze the absorption spectra rather than the derivative spectra to determine an overall spectral breadth. Calculating second moments can be challenging as it involves a precise baseline correction and a need to account for any asymmetry contained within each spectrum. Typically, second moments are the common moment found in literature, but in theory further moments can be calculated as shown in Equation 2-5, where H_0 is the center field, H_j-H_{j-1} is the step size, H_j is the field value for any point j, and y_j is the intensity at point j.

$$\langle H^n \rangle = \frac{H_j - H_{j-1}}{A} \sum_{j=1}^{m} |H_j - H_0|^n \, y_j \qquad (2\text{-}5)$$

The last parameter shown is the order parameter, S, which is used when determining mobility around a doxyl spin label of interest and is determined using Equation 2-6. In determining S, the parameters $T_{\parallel}$ and $T_{\perp}$ are evaluated for spectra with reduced mobility of the doxyl spin label. This being the case, S is usually not used for spin labeled acyl chains deeper in bilayers since the mobility is high in the fluid hydrophobic interior of membranes. In evaluating S, the experimental calculations

(Figure 2-12) are compared with the case of zero mobility provided by simulations as shown in Equation 2-6 [144]. The order parameter ranges between zero to one for isotropic mobility to zero mobility, respectively. This gives another useful tool in comparing data between instruments and different sample preparations.

$$S = \frac{T_{\parallel} - T_{\perp}}{T_{zz} - T_{xx}} \left(\frac{a}{a'}\right) \qquad T_{zz} = 30.8\ G \qquad T_{xx} = T_{yy} = 5.8\ G$$

$$a = {}^{1}/_{3}\ (T_{xx} + T_{yy} + T_{zz}) \qquad a' = {}^{1}/_{3}\ (T_{\parallel} + 2T_{\perp}) \qquad (2\text{-}6)$$

Equation 2-6. Order parameter (S) calculations use the $T_{\parallel}$ and $T_{\perp}$ measured from experimental data and compare them to those calculated for the rigid limit spectrum of a doxyl spin label, T_{zz} and T_{xx}. In addition, polarity differences are taken into account for each spectrum via a and a'.

Power Saturation CW-EPR Spectroscopy

Introduction

Power saturation is a CW-EPR technique that introduces a secondary paramagnetic collider into the sample to look at the distance between the collider and the spin-label via Heisenberg exchange interactions [116]. Power saturation allows for an indirect measure of a relative depth parameter in the lipid environment for doxyl spin labels on lipids as well as nitroxide spin labels on proteins within a membrane. This technique exploits the polarity gradient within lipid bilayers and the resulting partitioning of hydrophobic and hydrophilic molecules to the lipid and aqueous phases, respectively. In lipid bilayers there is a hydrophobic region, made up of lipid acyl chains, and a hydrophilic region, comprised of the polar head groups and the surrounding aqueous environment. The bilayer interior, however, is non-uniform, and consists of gradients of both fluidity and polarity along the bilayer normal [120, 145, 146]. Small molecules can diffuse into the bilayer with a gradient depending on both concentration and polarity [116]. According to Hubbell, the concentration gradient can be defined by "a distance-

dependent standard chemical potential in the bilayer, where $C_{i,m}(x)$ is the concentration of species I in the bilayer at a distance x from the interface, $C_{i,w}$ is the uniform concentration of neutral species I in the aqueous phase, $\mu_{i,m}$ and $\mu_{i,w}$ are the corresponding Henry's law standard state chemical potentials, T is the temperature, and R is the Boltzman constant" (Equation 2-7) [116].

$$C_{i,m}(x) = C_{i,w}\, e^{\frac{\mu^{\circ}_{i,w}}{RT}}\, e^{\frac{\mu^{\circ}_{i,m}(x)}{RT}} \tag{2-7}$$

Introduction of another paramagnetic species, other than the spin label, either in the aqueous phase, such as a soluble transition metal complex, or in the hydrophobic interior, such as molecular oxygen, allows EPR to benefit from this gradient. The paramagnetic collider that has been introduced into the membrane system of interest is allowed to interact, via Heisenberg exchange, with other paramagnetic species around it, such as the spin label. The rate at which the Heisenberg exchange occurs is proportional to the collision rate and is expressed by Equation 2-8, where W_{ex} is the Heisenberg exchange rate, *p* is the exchange probability, *g* is a steric factor, *d* is the collision diameter, $D_m(x)$ is the position-dependent relative diffusion coefficient, and $C_m(x)$ is the position dependent concentration given in Equation 2-8 [116].

$$W_{ex} = 4\pi p g D_m(x) C_m(x) \tag{2-8}$$

The collision rate is, therefore, dependent upon the depth in the bilayer in addition to many other factors such as steric hindrance, diffusion constants, and concentrations along the bilayer normal. However, by using two different paramagnetic colliders with relatively similar sizes and opposite partitioning gradients, i.e. a transition metal complex and oxygen, and by taking the ratio of their exchange rates with a given spin label, many of these factors cancel and the ratio solely depends on the distance through

the concentration gradient. Studying the exchange rates between the colliders and the spin label allow determination of a depth profile within the bilayer. The paramagnetic colliders chosen are fast-relaxing so their effect on nitroxide spin labels is dominated by Heisenberg exchange, as previously stated, and produces changes in the spin-lattice relaxation time (T_1) of the spin label proportional to the collision rate, W_{ex} [147]. The experimental quantity calculated, $\Delta P_{1/2}$, which will be described in detail shortly, is related to this exchange rate according to Equation 2-9, where T^*_{2e} is the electron spin-spin relaxation time.

$$\Delta P_{1/2} \propto {W_{ex}}/{T^*_{2e}} \tag{2-9}$$

Equations 2-7, 2-8, and 2-9 suggest that the logarithm of the experimental quantities $\Delta P_{1/2}$, Φ, follow Equation 2-10.

$$\Phi = ln\frac{\Delta P_{1/2}(1)}{\Delta P_{1/2}(2)} = \frac{[\mu^{\circ}_1(x) - \mu^{\circ}_2(x)]}{RT} + constant \tag{2-10}$$

Meaning Φ is directly related to the difference in chemical potentials of the two paramagnetic colliders regardless of depth, with no consequence of viscosity or steric constraints caused by the system in study. In addition, using a ratio of the two colliders, T^*_2 cancels out leaving Φ independent of EPR line-shape and, therefore, useful over many systems. An assumption to this technique is that the chemical potentials have simple monotonic depth dependence, which is typically the case when two similar sized colliders are used.

Statistical Analysis

Power saturation was developed and tested on the protein system bacteriorhodopsin by Dr. Hubbell and has since been used on many other systems

[116]. The technique is performed by collecting EPR spectra of samples placed in gas-permeable TPX capillary tubes so they can be purged with either air or nitrogen depending on the study of interest. The first derivative peak-to-peak amplitude, A, of the central resonance (m_I=0) is measured and plotted as a function of microwave power, P, over an incident power range of 0.2-63 mW. The resultant curves are fit to Equation 2-11.

$$A = I \cdot P^{1/2} \cdot \left[1 + \left(2^{1/\varepsilon} - 1\right) P \Big/ P_{1/2}\right]^{-\varepsilon} \tag{2-11}$$

Where *I* is a scaling factor, $P_{1/2}$ is the power at which the resonance amplitude is one-half its unsaturated value, and ε is a measure of homogeneity of the saturation of the resonance spin [148]. $P_{1/2}$ values are obtained under three conditions for all peptide/lipid samples: hydrated vesicles equilibrated under nitrogen gas, hydrated vesicles equilibrated under air (20% oxygen), and hydrated vesicles equilibrated with aqueous, soluble 10 mM NiAA (or other aqueous soluble collider such as NiEDDA) under nitrogen gas. $\Delta P_{1/2}$ values for oxygen and NiAA are obtained by subtracting the $P_{1/2}$ value for nitrogen from the $P_{1/2}$ values of oxygen and NiAA. The depth parameter, Φ, is calculated by Equation 2-12.

$$\Phi = \ln \frac{\Delta P_{1/2}(Oxygen)}{\Delta P_{1/2}(NiAA)} \tag{2-12}$$

In addition, collision parameters, π, for oxygen and NiAA can be calculated according to Equation 2-13.

$$\pi\,(Oxygen) = \frac{\left[\frac{P_{1/2}(Oxygen)}{\Delta H_{pp}(Oxygen)} - \frac{P_{1/2}(Nitrogen)}{\Delta H_{pp}(Nitrogen)}\right]}{\left[\frac{P_{1/2}(DPPH)}{\Delta H_{pp}(DPPH)}\right]} \tag{2-13}$$

The π-values for NiAA were calculated by substituting $P_{1/2}$(NiAA) for $P_{1/2}$ (Oxygen) in the equation above. This π value is normalized so that it can be compared between different laboratories regardless of the instrument or resonator used.

Applications

As previously mentioned, a depth profile to determine partitioning depth within the bilayer can be achieved via power saturation [116]. This allows a wide range of applications such as; conformational changes of a membrane protein upon substrate binding, relative location of specific amino acids within a bilayer, and orientation of a protein in a bilayer (transmembrane, tilted, or in the plane of the bilayer) [116-119, 121-123, 126, 149]. A common practice is to experimentally measure Φ for doxyl labeled lipids at different depths along the acyl chain. These values can then be compared to Φ values experimentally determined at different SDSL positions along a membrane bound protein of interest [116]. A relative depth of amino acids can then be used to determine orientation and partitioning depth in the bilayer. This makes it a powerful tool for membrane bound proteins, which are notorious for being difficult to structurally characterize in lipid bilayer environments [116, 131].

CHAPTER 3
OPTIMIZATION FOR CONTINUOUS WAVE ELECTRON PARAMAGNETIC RESONANCE STUDIES

Introduction

As described in Chapter 1, studies of surfactant protein B and its analogs are commonly done in DPPC:POPG (4:1) and POPC:POPG (3:1) lipid mixtures. DPPC:POPG (4:1) is commonly used in FDA approved treatments such as Survanta® while POPC:POPG (3:1) is a lipid system mimicking cell membranes which is commonly employed to probe cationic, amphipathic protein interactions such as antimicrobial peptides (AMPs) with lipids [150-152]. Lipid phases of these compositions can likely be found in localized areas of alveoli during normal breathing cycles [153]. In Chapter3, the content of POPG between POPC:POPG (3:1) and POPC:POPG (4:1) and its effect on CW-EPR will be discussed and explained. In addition, optimization of parameters such as temperature and choice of power saturation paramagnetic colliders for use in Chapters 4 and 5 will be discussed.

Materials and Methods

Materials

POPC, DPPC, POPG, and *n*-doxyl-PSPC were purchased as chloroform solutions from Avanti Polar Lipids (Alabaster, AL) and quantified by phosphate analysis (Bioassay Systems, Hayward, CA). Iodoacetamido-PROXYL spin label (IAP) was purchased from Sigma and used as received. Unless otherwise stated, all other reagents were purchased from Fisher Scientific (Hampton, NH) and used as received.

KL_4, KLLLLKLLLLKLLLLKLLLLK, was synthesized via solid-phase peptide synthesis (ICBR Facility, UF), purified by RP-HPLC, and verified by mass spectrometry

(m/z=2469). Peptide was dissolved in methanol and analyzed by amino acid analysis to determine concentration (Molecular Structure Facility, UC Davis).

Methods

Preparation of lipid/peptide samples

Lipid mixtures were prepared by mixing appropriate volumes of stock lipid chloroform solutions. For samples containing peptide, the peptide was added as a methanol solution to the lipid mixture in chloroform. Organic solvents were evaporated using dry nitrogen; the lipid films were re-suspended in warm cyclohexane (~45 °C), flash frozen and lyophilized. For each combination of lipids and peptide, two separate samples were prepared. The first was rehydrated with 140 mM NaCl, 10 mM Bis-Tris buffer, pH 6.5, and the second was rehydrated with 140 mM NaCl, 10 mM Bis-Tris buffer, pH 6.5, containing 10 mM NiAA or 20 mM NiEDDA. The hydrated dispersions were subjected to 5 freeze-thaw cycles to form MLVs and had a final 10 mM lipid concentration. Samples containing spin-labeled lipid had 1 mol% of either doxyl-PC or tempo-PC added relative to the unlabeled lipids.

CW-EPR spectroscopy

CW-EPR spectra were collected on a modified Bruker ER200 spectrometer (Billerica, MA) with an ER023M signal channel, an ER032M field control unit, and a loop gap resonator (Medical Advances, Milwaukee, WI). Spectra of samples containing spin-labeled were recorded at 45 °C using a 2 mW power level. Temperature was regulated by passing either air or nitrogen gas through a copper coil in a recirculating bath (Thermo Scientific) containing 40% ethylene glycol. This setup is shown in Figure 3-1.

Figure 3-1. Temperature control set-up; A) thermocouple thermometer, B) quartz Dewar around the sample in the loop gap resonator, C) copper coil submerged in recirculating bath, D) gas connected to quartz Dewar.

Samples are stored in a -20 °C freezer and allowed to thaw before use on the EPR. Lipid samples are then heated to above their melting temperatures and placed in the loop gap resonator with the preheated quartz Dewar and allowed to equilibrate at least 20 minutes prior to sample collection. CW EPR spectra were collected with one Gauss modulation amplitude and 100 or 125 Gauss sweep widths; the latter was used for spin-labeled peptide. Additional spectra were collected at 20 Gauss sweep widths for more accurate determination of ΔH_{pp}. Each spectrum contains 1024 points with an approximate center field of 3460 Gauss. Spectra were collected and averaged between 2 – 75 scans with a frequency of 9.6 – 9.7 GHz. Table 3-1 shows a complete list of the typical parameters used in CW-EPR experiments.

Table 3-1. Standard CW-EPR parameters used in this dissertation.

Parameter	Value
Number of points	1024
Center field	3455 - 3465 G
Number of scans	5-75
Sweep width	20-125 G
Acquisition time	40.63 sec
Frequency	9.5 - 9.7 GHz
Power	0.25mW-20mW (29dB-10dB)
Receiver gain	$1x10^4$ – $1x10^5$
Modulation amplitude	~1 G
Time constant	0.164 sec
Receiver phase	100 – 105 deg

Power saturation experiments

Power saturation experiments were collected on the same modified Bruker ER200 spectrometer using gas permeable TPX capillary tubes as developed by Hubbell et al. [116]. Saturation experiments were collected at 25 °C and 45 ºC for POPC:POPG and DPPC:POPG samples, respectively, with a sample volume of 5 µL. Two samples for each experiment were made, one with and one without both 10 mM NiAA or 20 mM NiEDDA, and samples were purged for at least 20 minutes with air or nitrogen gas before collecting power saturation data. To ensure the samples were entirely purged with the gas, the intensity of the central resonance line was plotted as a function of time until no change in intensity was observed. For each sample this was approximately 20 minutes. As mentioned in the previous section, intensity of the central resonance line using a 20 Gauss scan width was plotted as a function of microwave power in the range of 0.25 mW – 20 mW. LabVIEW™ software (National Instruments, Austin, TX) generously provided by Christian Altenbach and Wayne Hubbell (UCLA, Los Angeles, CA) was used for data recording and processing. Resultant power saturation curves were fit using Equation 2-11 and membrane depth was analyzed using Equation 2-12.

Lipid Composition

As previously mentioned, studies of surfactant proteins and their analogs are commonly done in DPPC:POPG (4:1) and POPC:POPG (3:1) systems [42, 85, 86, 105, 107, 153]. The latter lipid composition allows for comparison to previous studies of cationic, amphipathic helix peptides which share similar characteristics to surfactant protein B [150-152]. While this allows for a reference to previously studied lipid/peptide systems, it does raise the question of how differences in negatively charged POPG content in DPPC:POPG (4:1) and POPC:POPG (3:1) mixtures may lead to changes in the interactions of the lipid mixtures with positively charged lysines in KL_4. It has been postulated that the negatively charged POPG plays a critical role in SP-B pulmonary lipid interaction and DPPC enrichment, and if this is true the positively charged KL_4 peptide should be no exception [153-159]. To better understand if EPR can detect differences in interactions of KL_4 with POPC:POPG at a 3:1 versus a 4:1 ratio, CW-EPR power saturation experiments using both ratios were performed.

Results & Discussion

Effect of Negatively Charged Phosphatidylglycerol Lipids

The observation that pulmonary surfactant contains elevated levels of negatively charged lipids when compared to most other biological systems, PG and PI, suggests they play a specific role in surfactant function. This has been demonstrated in multiple studies showing that mixing POPG or DPPG with DPPC enhances adsorption at the air/water interface during film formation while allowing for selective squeeze out of PG during lipid film compression [154, 156, 159]. In addition, these affects are not observed in the absence of SP-B and SP-C and show a much greater effect with SP-B compared to SP-C [155]. The ability of KL_4 to mimic SP-B functions suggest that it too

will be affected by PG content. The extent of its effect is not presently known so studies using lipid systems containing varying amounts of PG, like DPPC:POPG (4:1) and POPC:POPG (3:1), have been of recent concern. In Chapter 3, we use CW-EPR mobility and power saturation studies to determine whether or not differences in POPG content affect the changes in lipid dynamics observed on addition of KL_4.

Initial CW-EPR spectra were collected for both 3:1 and 4:1 POPC:POPG spin-labeled lipids samples at varying concentrations of KL_4 to study the effects of binding on the lipid environment. All spectra collected for the two lipid systems, at concentrations of KL_4 varying from 0 to 3 mol percent, using lipids spin-labeled at 5-, 7-, 12-doxyl positions, are shown in Figure 3-2 through 3-7.

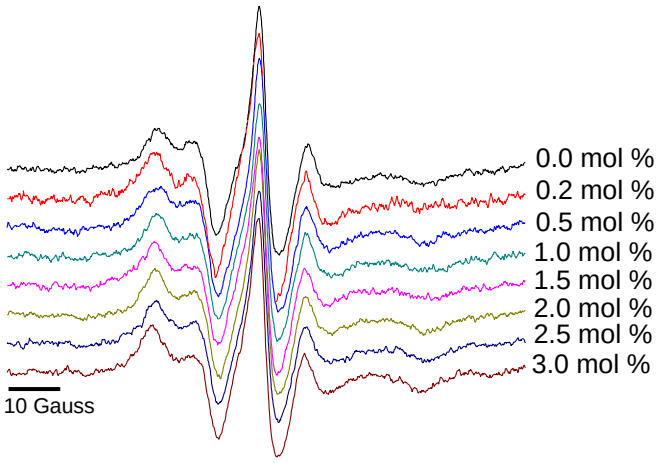

Figure 3-2. CW-EPR spectra collected at 45 ºC under nitrogen for 5-doxyl PC incorporated in 3:1 POPC:POPG lipid vesicles.

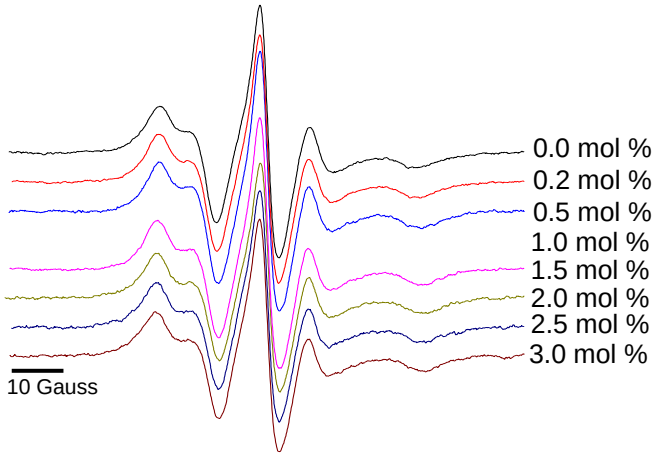

Figure 3-3. CW-EPR spectra collected at 45 ºC under nitrogen for 7-doxyl PC incorporated in 3:1 POPC:POPG lipid vesicles.

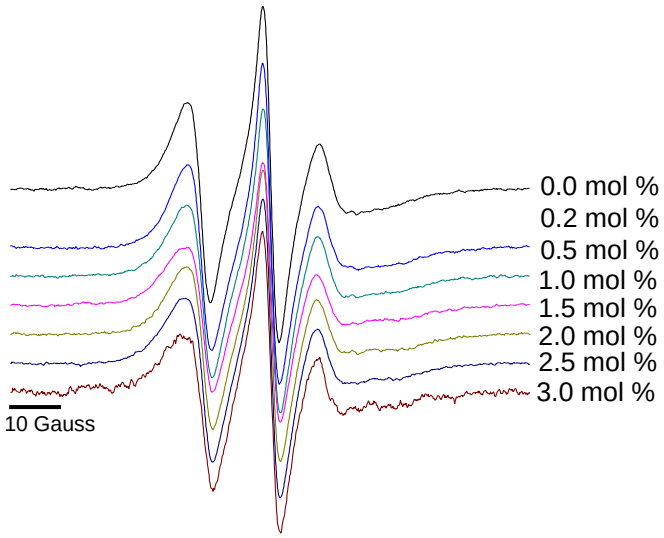

Figure 3-4. CW-EPR spectra collected at 45 ºC under nitrogen for 12-doxyl PC incorporated in 3:1 POPC:POPG lipid vesicles.

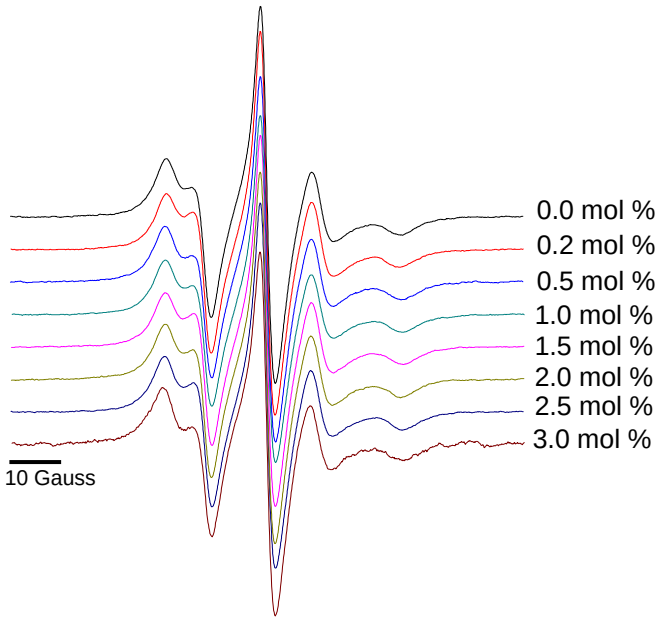

Figure 3-5. CW-EPR spectra collected at 45 ºC under nitrogen for 5-doxyl PC incorporated in 4:1 POPC:POPG lipid vesicles.

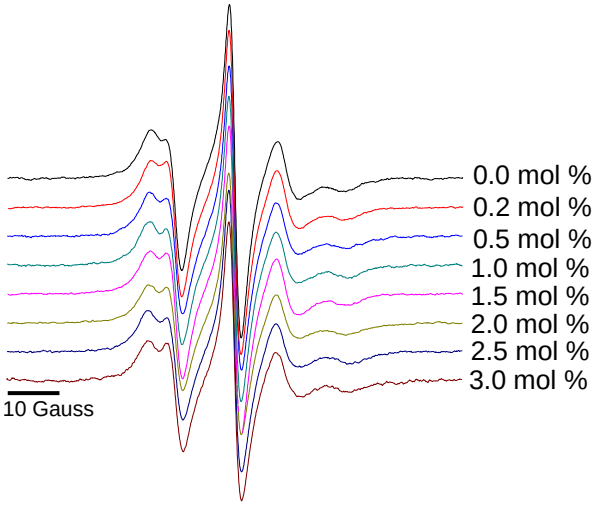

Figure 3-6. CW-EPR spectra collected at 45 ºC under nitrogen for 7-doxyl PC incorporated in 4:1 POPC:POPG lipid vesicles.

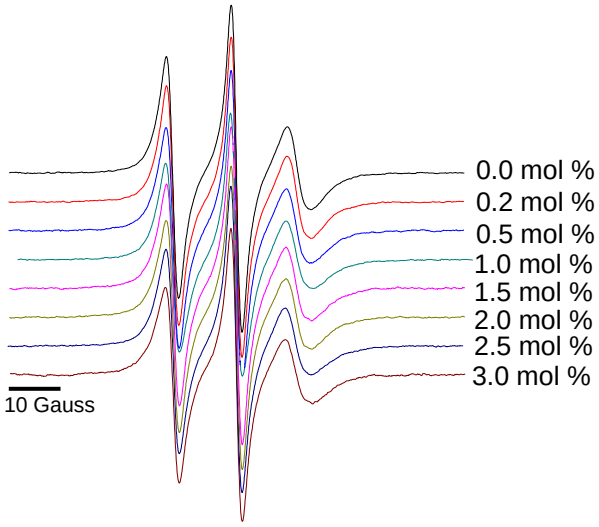

Figure 3-7. CW-EPR spectra collected at 45 ºC under nitrogen for 12-doxyl PC incorporated in 4:1 POPC:POPG lipid vesicles.

To further analyze the spectra, semi-quantitative measurements of ΔH_{pp} and order parameter (S) were used to compare the two lipid systems. These parameters are described in Chapter 2 Figure 2-11 and Equation 2-6. In Figures 3-8 and 3-9 order parameters are compared for 3:1 and 4:1 POPC:POPG lipid mixtures containing 5- and 7-doxyl spin labels with varying KL_4 concentrations.

The order parameter (S) increases upon addition of KL_4 at both the 5- and 7-doxyl position in both lipid systems. This is indicative of KL_4 interacting with the spin label at both positions within the bilayer and decreasing its mobility. This is expected because it is known that KL_4 binds to lipid bilayers containing PG [42, 86, 107]. Interestingly the rate of increase in order parameter is within error between 3:1 and 4:1 POPC:POPG samples, suggesting the small difference in PG content does not alter the results seen by CW-EPR at the 5- and 7-positions along the lipid acyl chain.

As previously stated, order parameters can only be used for more immobilized spin labels and cannot be used for spin labels closer to the bilayer interior. To compare spin labels placed further along the acyl chain, ΔH_{pp} was calculated for spectra of lipids

spin-labeled at the 5-, 7-, and 12-doxyl positions. Figures 3-10 through 3-12 compare the results at all three positions, in both lipid systems, and at varying KL_4 concentrations.

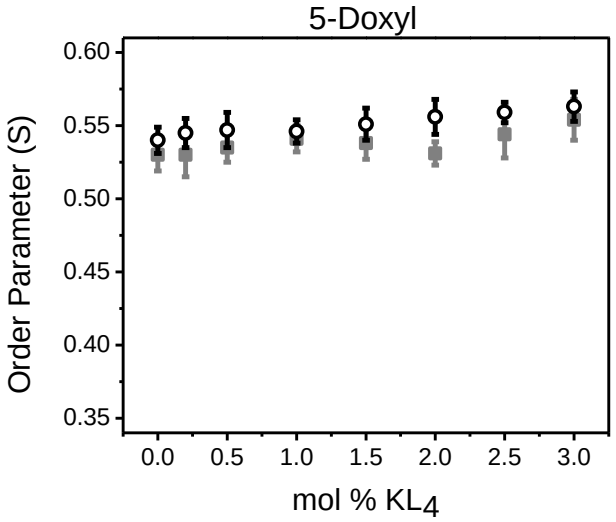

Figure 3-8. Order parameter calculations for 5-doxyl spin-label incorporated into 4:1 POPC:POPG (grey squares) and 3:1 POPC:POPG (open circles) lipid mixtures.

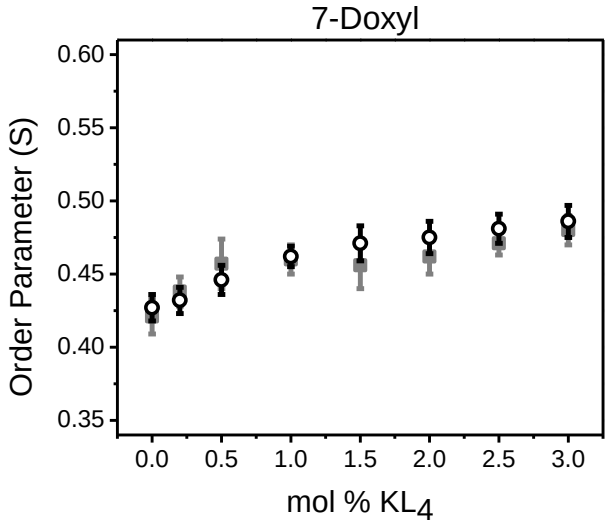

Figure 3-9. Order parameter calculations for 7-doxyl spin-label incorporated into 4:1 POPC:POPG (grey squares) and 3:1 POPC:POPG (open circles) lipid mixtures.

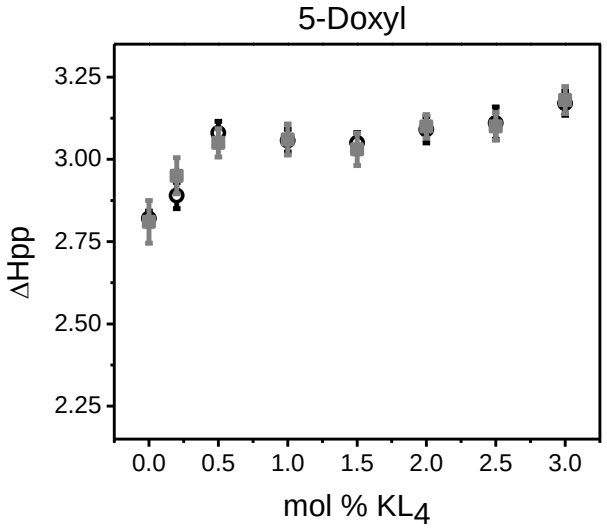

Figure 3-10. ΔH_{pp} calculations for 5-doxyl incorporated into 4:1 POPC:POPG (grey squares) and 3:1 POPC:POPG (open circles) lipid mixtures.

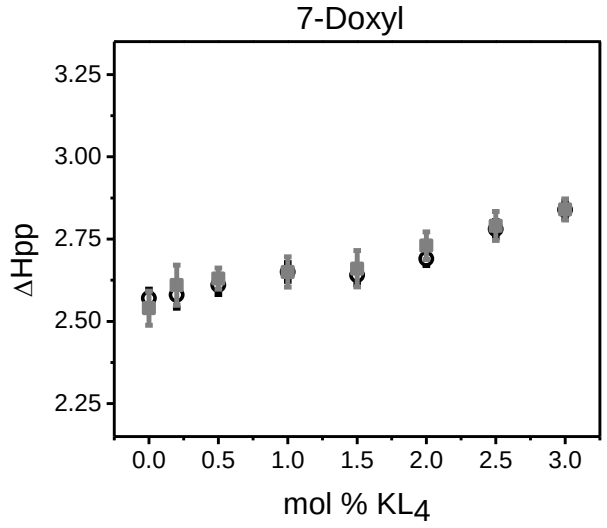

Figure 3-11. ΔH_{pp} calculations for 7-doxyl incorporated into 4:1 POPC:POPG (grey squares) and 3:1 POPC:POPG (open circles) lipid mixtures.

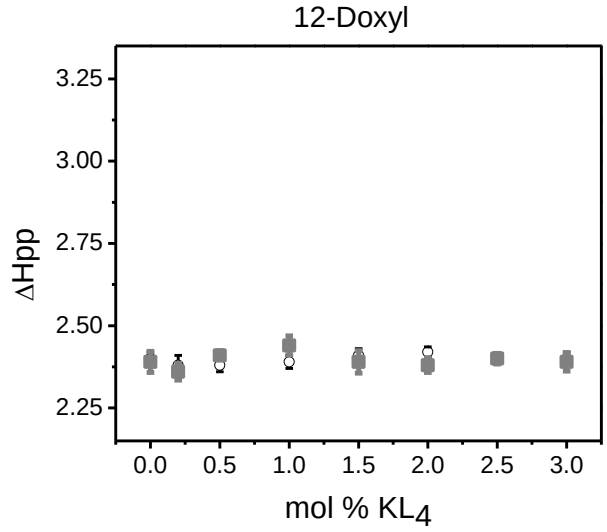

Figure 3-12. ΔH_{pp} calculations for 12-doxyl incorporated into 4:1 POPC:POPG (grey squares) and 3:1 POPC:POPG (open circles) lipid mixtures.

As seen with the order parameter plots in Figures 3-8 and 3-9, ΔH_{pp} increases at the 5- and 7-doxyl positions upon addition of KL_4, indicating a restriction of motion due to the peptide interacting at that depth in the bilayer. A nearly identical increase in ΔH_{pp} is seen for 3:1 and 4:1 POPC:POPG, giving further evidence that the small discrepancy in PG content does not affect the CW-EPR line-shape upon KL_4 addition. Furthermore, ΔH_{pp} allows lipid acyl chain mobility to be determined semi-quantitatively deeper in the bilayer at position 12. As shown in Figure 3-12, the change in ΔH_{pp} upon peptide addition is negligible, suggesting KL_4 is not penetrating deeply enough in either 3:1 POPC:POPG nor 4:1 POPC:POPG lipid bilayers to effect the mobility at the 12-position. Once again in both lipid systems the mobility parameter is within error of the two lipid systems suggesting the charge difference between the two systems does not alter the doxyl spin-label mobility.

The CW-EPR mobility studies presented in Chapter 3 show that the variability of negatively charged PG concentration between 3:1 and 4:1 POPC:POPG gives no substantial change in EPR spectra, alleviating any concern about studies in which 3:1 POPC:POPG and 4:1 DPPC:POPG are compared. For Chapters 4 and 5, equal ratios

of zwitterionic and anionic (4:1) will be used in POPC:POPG and DPPC:POPG lipid mixtures.

Power Saturation Optimization

As stated in Chapter 2, power saturation is a technique which introduces a paramagnetic collider, either an aqueous soluble metal-complex or hydrophobic oxygen, which interacts with a spin-label by Heisenberg exchange and measures relaxation to determine an accessibility parameter of the spin-label with the collider. Molecular oxygen provides a convenient lipophilic paramagnetic collider as it is readily available from air and can be purged into the sample of interest with ease. As for the aqueous soluble paramagnetic collider there have been many choices that vary in price, aqueous solubility, and lipid solubility. A few choices commonly seen in power saturation studies are nickel (II) acetylacetonate (NiAA), nickel (II) ethylenediamine-N,N'-diacetic acid (NiEDDA), and chromium oxylate (CrX) [116]. For the following studies, NiAA and NiEDDA will be compared in our lipid systems to determine advantages and disadvantages of each for future use in power saturation studies.

The aqueous solubility of NiEDDA is far greater to that of NiAA, allowing for concentrations of over 100 mM versus only 20 mM, respectively. This allows for greater interaction between the collider and a spin-label that is exposed to the aqueous phase, resulting in an increased relaxation enhancement detected by power saturation. However, if for spin label sites buried within the hydrophobic phase, NiAA may be more advantageous because of its higher permeability within lipid bilayers, leading to an increased interaction between the collider and the spin-label. To determine which aqueous collider is best for our studies, CW-EPR power saturation data was collected on spin labeled lipids samples containing either 10 mM NiAA or 20 mM NiEDDA. It

should be noted that a higher concentration of NiEDDA was also tested and gave similar results to 20 mM NiEDDA. Figure 3-13 plots the effect of NiEDDA and NiAA on power saturation $P_{1/2}$ values in 4:1 POPC:POPG vesicles as a function of KL_4 concentration and with varying spin-labeled doxyl positions.

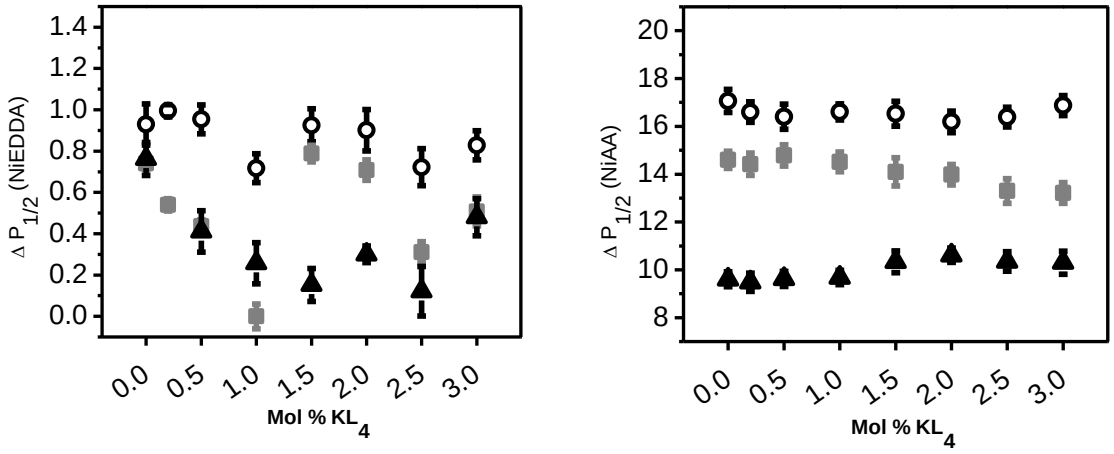

Figure 3-13. Power saturation values ($\Delta P_{1/2}$) for NiEDDA (left) and NiAA (right) as a function of KL_4 concentration with spin label reporters using 5-doxyl (open circles), 7-doxyl (grey squares), and 12-doxyl (black triangles) spin labels.

The solvent accessibility parameter, $\Delta P_{1/2}$, for NiEDDA and NiAA plotted as a function of KL_4 show significant differences in accessibility between the two paramagnetic agents. The NiEDDA samples give $P_{1/2}$ values similar to those of nitrogen, indicating very little collision at each doxyl position with NiEDDA. In addition, the correlation between NiEDDA $\Delta P_{1/2}$ values and the doxyl depths do not show the logical trends seen with the NiAA. The $\Delta P_{1/2}$ values should have a clear change with spin label position, or 5-doxyl > 7-doxyl > 12-doxyl. This is seen when using NiAA but not NiEDDA. For this reason NiAA was selected for future studies of spin label accessibility to an aqueous collider.

NiAA Buffer Optimization

The best suitable aqueous soluble collider for these studies is NiAA due to its favorable permeability into the bilayer allowing for higher rates of collision with all spin-labels used. The next issue to be considered is an optimal buffer to be used in power saturation studies with NiAA. Typically KL_4 is studied using a buffer consisting of 10 mM HEPES, 140 mM NaCl, pH 7.4 [42, 86]. This buffer, however, gave erroneous results for simple NiAA accessibility studies, and therefore other buffers were compared. Results comparing 10 mM HEPES, 140 mM NaCl, pH 7.4 and 10 mM Bis-Tris, 140 mM NaCl, pH 6.5 are shown in Table 3-2. For these studies both POPC:POPG and DPPC:POPG vesicles were used with 10 mM NiAA.

Table 3-2. Comparison of $P_{1/2}$ values measured with NiAA at pH 7.4 and pH 6.5 in two lipid systems.

Spin-label	POPC:POPG (4:1)		DPPC:POPG (4:1)	
	pH 7.4	pH 6.5	pH 7.4	pH 6.5
5-Doxyl	19.0 ± 0.4	19.3 ± 0.2	19.4 ± 0.3	19.6 ± 0.3
7-Doxyl	21.5 ± 0.7	16.8 ± 0.5	22.4 ± 0.5	16.4 ± 0.3
12-Doxyl	15.2 ± 0.2	11.8 ± 0.2	17.1 ± 0.3	14.5 ± 0.3

To focus specifically on the pH of the samples, each sample was made without KL_4 and with 150 mM salt to limit variability. For a buffer to be compatible with NiAA, a trend in $P_{1/2}$ values should match the trend in spin label positions with the $\Delta P_{1/2}$ values for 5-doxyl > 7-doxyl > 12-doxyl. This is clearly not the case at pH 7.4 where a trend of 7-doxyl > 5-doxyl > 12-doxyl is seen. This trend occurs in both POPC:POPG and DPPC:POPG vesicles at pH 7.4, therefore raising the question about whether or not the

charged PG head group is interacting in an unusual manner with the nickel complex or if the charge state of NiAA is being affected by the pH. Ultraviolet-visible spectroscopy (UV-Vis) studies were performed on samples at varying pH to see if a shift in wavelength absorption could be seen indicating the NiAA was undergoing a charge state change. UV-Vis spectroscopy did not indicate any change in absorbance as the pH was varied from 5.5 to 8.5. A future study using transmission electron microscopy (TEM) to study changes in the morphology of the lipid vesicles containing NiAA at varying pH has been considered and could lead to a better understanding of the observed anomalous trend. Lowering the pH to 6.5, however, alleviated this discrepancy in $P_{1/2}$ values for NiAA measured with spin labels at the 5-, 7-, 12-doxyl positions. Table 3-2 shows the expected trend 5-doxyl > 7-doxyl >12-doxyl for both lipid systems at pH 6.5 and is therefore used in all future experiments.

Temperature Selection

When studying peptide partitioning into lipid environments knowing the melting temperature of the lipid system is of importance in order to regulate which phase is being studied. This especially is significant when using fully saturated lipids, like DPPC, because their high melting temperatures can cause them to be in a gel rather than liquid crystalline phase at room temperature. Careful consideration of experimental temperatures and sample preparation protocols should be made when preparing and analyzing saturated lipid systems. The three lipids used in this dissertation, POPC, POPG, and DPPC, have melting transition temperatures of -2 °C, -2 °C, and 41 °C, respectively. This results in a melting temperature for our two systems, POPC:POPG (4:1) and DPPC:POPG (4:1), of -2 ºC and 37 ºC, respectively [85]. In addition, the large discrepancy between DPPC and POPG transition temperatures results in the need for

careful sample preparation to prevent phase separation of the lipid. This can be achieved by mixing in organic solvents at higher temperatures, followed by flash freezing and sublimation of each sample via lyophilization. To further complicate the issue, addition of KL_4 at high concentrations in DPPC:POPG shifts the transition temperature from 37 °C to 39 °C, suggesting a possible peptide induced phase separation [85]. To account for all these factors, 45 ºC was chosen for our studies as it ensures samples are above the melting temperature of all lipids and that any shift in transition temperature due to KL_4 addition will not affect the results. In addition, to allow easy comparison between POPC:POPG and DPPC:POPG, 45 ºC was used for all samples. This eliminates differences in mobility and solvent accessibility studies due to increased motion at higher temperatures.

Conclusions

To accurately study a system of interest, several parameters need to be optimized to give the most sensitive and reproducible results. In Chapter 3, the parameters of lipid composition, power saturation collider, buffer pH, and temperature were all studied to determine the most ideal conditions. These studies allow for an elimination of PG concentration variability, increased accuracy of depth profile measured by power saturation, and comparison of EPR-CW spectra between two different lipid systems. Future data collected and described in this dissertation will use these determined parameters in addition to future work.

CHAPTER 4
CONTINUOUS WAVE ELECTRON PARAMAGNETIC RESONANCE STUDIES OF KL_4/LIPID INTERACTIONS

Introduction

Chapter 3 summarized the optimized conditions for CW-EPR experiments which will be used in this Chapter and Chapters 4 and 5 describing power saturation results. In Chapter 4, results from spin-labeled lipid and KL_4 CW-EPR mobility studies will be reported and discussed. Mobility studies provided a means to understanding the local environment of the lipid spin-label at varying positions along the acyl chain upon addition of KL_4. In addition, changes in mobility around the spin-labeled KL_4 helix were tracked using eight KL_4 variants. Mobility studies can help to elucidate the orientation of KL_4 within the lipid bilayer in addition to helping understand differences between DPPC- and POPC-rich vesicles. By studying changes occurring at different positions within KL_4 and along the acyl chain and by comparing this to the power saturation results in the Chapter 5, a depth profile of KL_4 in DPPC:POPG (4:1) and POPC:POPG (4:1) will be determined.

Materials & Methods

Materials

POPC, DPPC, POPG, *n*-doxyl-PSPC were purchased as chloroform solutions from Avanti Polar Lipids (Alabaster, AL) and quantified by phosphate analysis (Bioassay Systems, Hayward, CA). Iodoacetamido-PROXYL spin label (IAP) was purchased from Sigma and used as received. Unless otherwise stated, all other reagents were purchased from Fisher Scientific (Hampton, NH) and used as received.

KL_4, KLLLLKLLLLKLLLLKLLLLK, was synthesized via solid-phase peptide synthesis (ICBR Facility, UF), purified by RP-HPLC, and verified by mass spectrometry

(m/z=2469). Peptide was dissolved in methanol and analyzed by amino acid analysis for concentration (Molecular Structure Facility, UC Davis). Cysteine variants of KL_4, in which individual leucines were replaced by cysteine, were also synthesized via solid-phase peptide synthesis, purified, and mass verified (m/z=2459).

Methods

Spin-labeling of KL_4 cysteine mutants

Cysteine-containing KL_4 was dissolved at a concentration of ~0.1 mM in MeOH, and the pH was adjusted to >7 with KOH. A five-fold excess of tris(2-carboxyethyl)phosphine (TCEP) was added to keep the cysteine reduced. A solution of 50 mM IAP spin label in DMSO was added to achieve a 20-fold excess of spin label. After 4-5 hours at room temperature, the spin-labeled peptide was purified via HPLC, and lyophilized fractions were brought up in MeOH. The final peptide concentration for each spin-labeled sample was determined by either analytical HPLC or amino acid analysis (AAA).

Preparation of lipid/peptide samples

Lipid mixtures were prepared by mixing appropriate volumes of stock lipid chloroform solutions. For samples containing peptide, the peptide was added as a methanol solution to the lipid mixture in chloroform. Organic solvents were evaporated using dry nitrogen; the lipid films were re-suspended in cyclohexane, flash frozen and lyophilized. For each combination of lipids and peptide, two separate samples were prepared. The first was rehydrated with 140 mM NaCl, 10 mM Bis-Tris buffer, pH 6.5, and the second was rehydrated with 140 mM NaCl, 10 mM Bis-Tris buffer, pH 6.5, containing 10 mM NiAA. The hydrated dispersions were subjected to 5 freeze-thaw cycles to form MLVs and had a final lipid concentration of ~10 mM. Samples

containing spin-labeled lipid had 1 mol% of doxyl-PC added relative to the native lipids during the organic solvent mixing step.

Circular dichroism spectroscopy

CD spectra were acquired at 45 °C on an Aviv Model 202 spectrometer using Hellma CD cuvettes with 1 cm path length, with special thanks to Dr. Steve Hagan in the UF Physics department for assistance. Samples were prepared by hydrating lyophilized peptide-lipid powders in 10 mM Bis-Tris buffer, pH 6.5, with 140 mM NaCl, to achieve a final concentration of ~50 μM KL_4. Samples were extruded through 100 nm filters (Avanti Polar Lipids, Alabaster, AL) to form LUVs. Typical parameters used for CD experiments are summarized in Table 4-1. Background scans of all buffers were collected and subtracted from the final averaged spectra.

Table 4-1. Standard parameters used for circular dichroism experiments.

Parameter	Value
Experiment type	Wavelength
Bandwidth	1 nm
Temperature	45 °C
Wavelength range	260 – 190 nm
Step gradient	1.0 nm
Averaging time	3.0 sec
Settling time	1.0 sec
Multi-scan wait	1.0 sec
Scans	5 – 10

CW-EPR spectroscopy

CW-EPR spectra were collected on a modified Bruker ER200 spectrometer (Billerica, MA) with an ER023M signal channel, an ER032M field control unit, and a loop gap resonator (Medical Advances, Milwaukee, WI). Spectra of samples containing either spin-labeled lipid or spin-labeled KL_4 were recorded at 45 °C using a 2 mW power

level. The temperature was regulated by passing nitrogen gas through a copper coil in a recirculating bath (Thermo Scientific) containing 40% ethylene glycol.

Samples were stored in a -20 °C freezer and allowed to thaw before use on the EPR. Lipid samples were then heated to above their melting temperatures and placed in the loop gap resonator within a preheated quartz Dewar and allowed to equilibrate at least 20 minutes prior to sample collection. CW EPR spectra were collected with one Gauss modulation amplitude and 100 or 125 Gauss sweep widths, the latter used for spin-labeled peptide. Additional spectra were collected at 20 Gauss sweep widths for more accurate determination of ΔH_{pp}. Each spectrum contained 1024 points with an approximate center field of 3460 Gauss. Spectra were collected and averaged for 2 – 75 scans at a frequency of 9.6 – 9.7 GHz. Table 3-1 shows a complete list of the typical parameters used in CW-EPR.

Results & Discussion

Introduction

As discussed in Chapter 1, the orientation and function of SP-B and its analogs in lipid environments is not well understood. In particular, several studies have yielded conflicting results as to how KL_4 is oriented in a lipid bilayer and how it interacts with specific lipids. It is well known that KL_4 adopts a helix upon membrane binding as shown through previous FTIR and CD studies, in addition to CD studies presented in Chapter 4 [42, 95, 105]. The orientation of the helix, however, is believed to either span the bilayer in a transmembrane orientation [107], or lie in the plane of the bilayer [42, 86, 107]. Our CW-EPR mobility studies will help to elucidate the true orientation and relative depth within the two lipid systems, 4:1 DPPC:POPG and 4:1 POPC:POPG, by studying changes in dynamics for both spin labeled lipids and peptides. In addition,

Chapter 5 will use CW power saturation EPR to correlate collision data with the mobility data presented in Chapter 4.

KL_4 Effects on Lipid Dynamics

The first study of CW-EPR mobility was to example the changes in spin label mobility occurring at the 5-, 7-, and 12-doxyl labeled lipid acyl chains upon adding increasing amounts of KL_4 into the two lipid systems of interest. Using the semi-quantitative parameters discussed in Chapter 2 an understanding of the local environment around each doxyl lipid in both lipid systems can be developed. Figure 4-1 through 4-6 displays the CW-EPR spectra at all eight KL_4 concentrations, for all three doxyl positions and in both lipid systems. These spectra along with 20 Gauss spectra were used to determine semi-quantitative parameters of spin-labeled lipid mobility in Chapter 4.

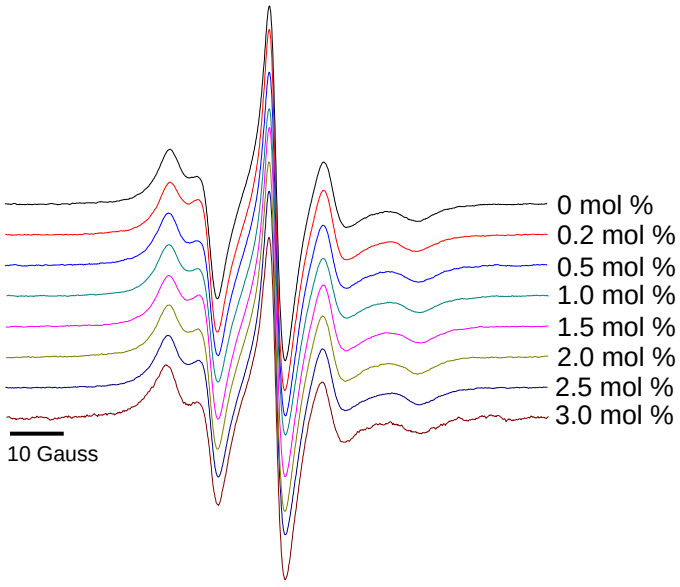

Figure 4-1. CW-EPR spectra collected at 45 ºC under nitrogen for 5-doxyl PC incorporated in 4:1 POPC:POPG lipid vesicles with varying amounts of KL_4.

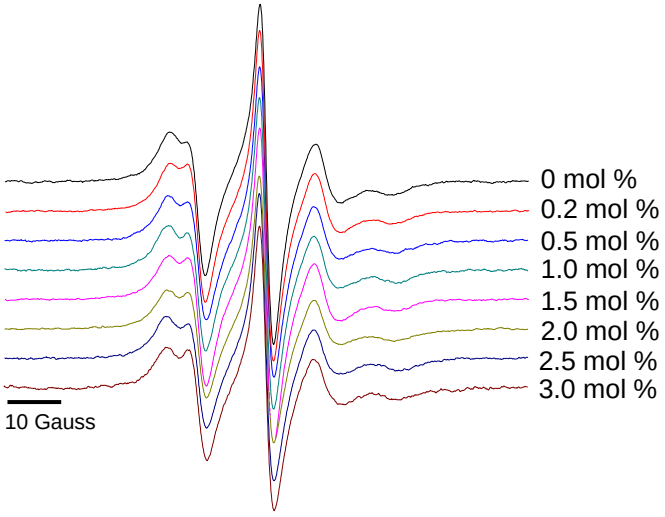

Figure 4-2. CW-EPR spectra collected at 45 ºC under nitrogen for 7-doxyl PC incorporated in 4:1 POPC:POPG lipid vesicles with varying amounts of KL_4.

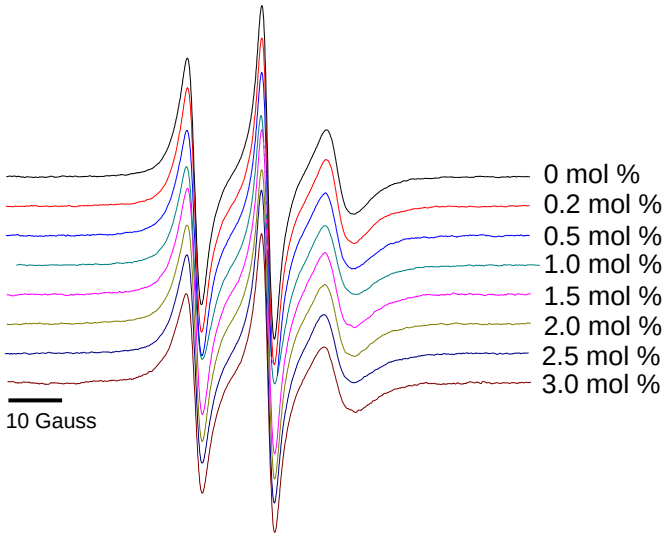

Figure 4-3. CW-EPR spectra collected at 45 ºC under nitrogen for 12-doxyl PC incorporated in 4:1 POPC:POPG lipid vesicles with varying amounts of KL_4.

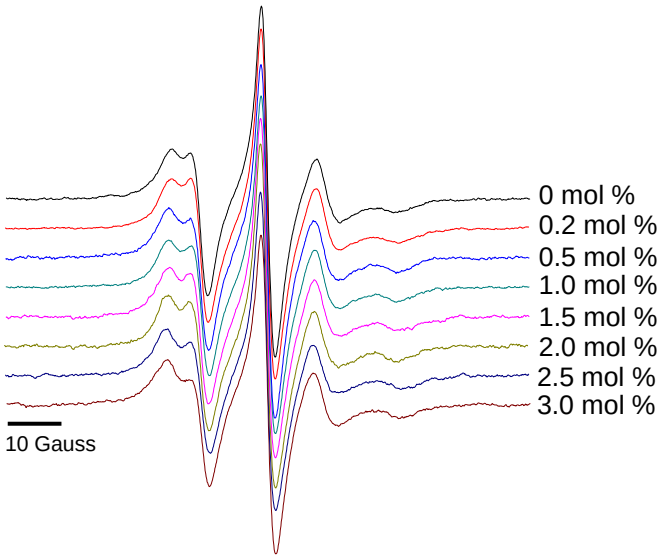

Figure 4-4. CW-EPR spectra collected at 45 ºC under nitrogen for 5-doxyl PC incorporated in 4:1 DPPC:POPG lipid vesicles with varying amounts of KL_4.

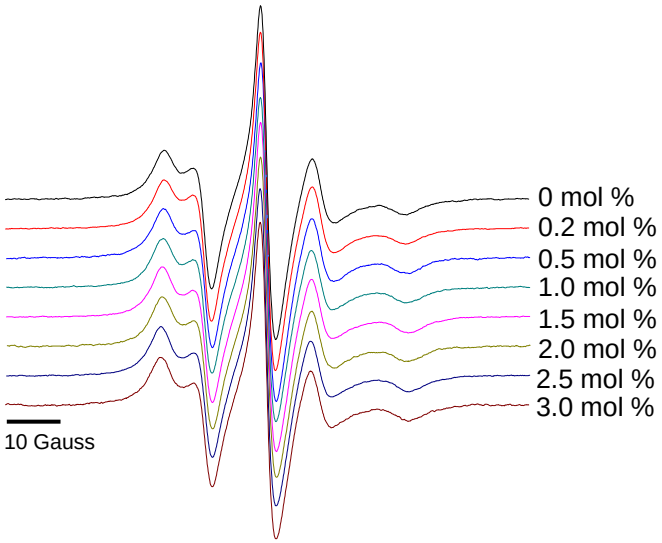

Figure 4-5. CW-EPR spectra collected at 45 ºC under nitrogen for 7-doxyl PC incorporated in 4:1 DPPC:POPG lipid vesicles with varying amounts of KL_4.

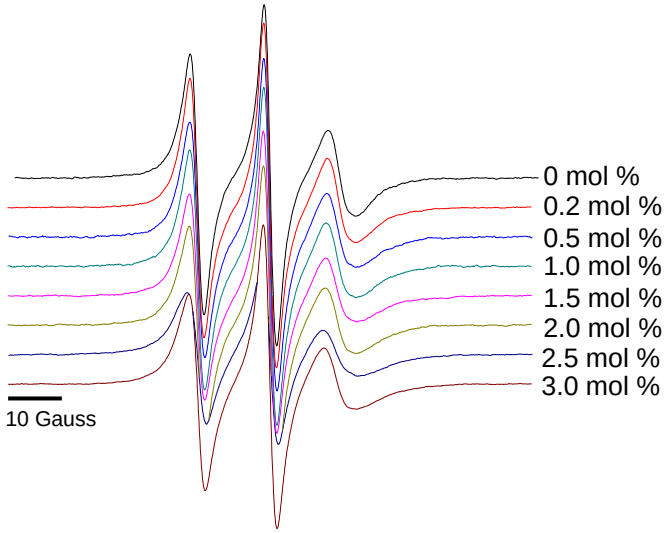

Figure 4-6. CW-EPR spectra collected at 45 ºC under nitrogen for 12-doxyl PC incorporated in 4:1 DPPC:POPG lipid vesicles with varying amounts of KL_4.

Looking qualitatively at the spectra in Figures 4-1 through 4-6, mobility increases as the position of the spin-label increases (from 5-doxyl to 12-doxyl). This is due to the increased fluidity in the bilayer interior when compared to the membrane interface. Qualitative comparison of spectra between the two lipid systems and between spectra of lipids containing varying amounts of KL_4 is difficult, therefore a series of semi-quantitative parameters were determined.

Mobility Parameters

As previously stated, there are several parameters which can be used to describe and quantitate changes in CW-EPR spectra. The first parameter commonly measured is ΔH_{pp}, which is determined as described in Chapter 2. Figures 4-7 through 4-9 compare ΔH_{pp} values for spin-labeled lipids between the two lipid systems at varying concentrations of KL_4 and at varying spin label depths within the bilayer.

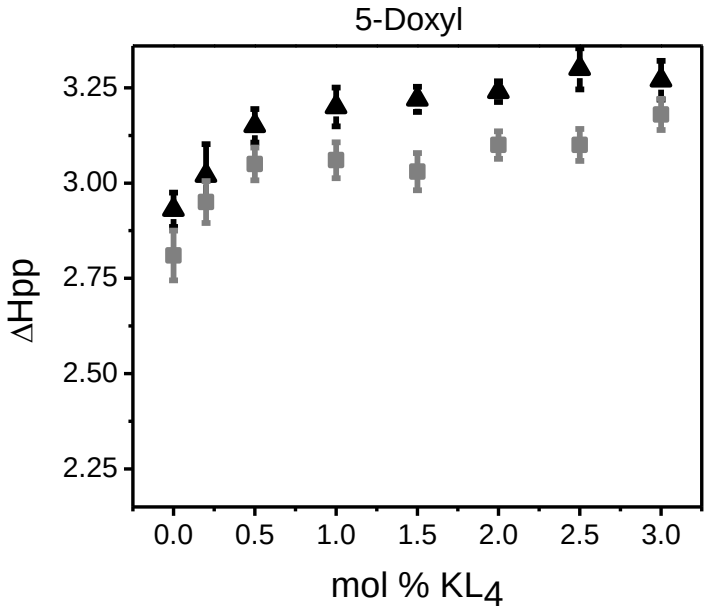

Figure 4-7. ΔH_{pp} plotted as a function of KL_4 concentration for 5-doxyl PC incorporated in 4:1 DPPC:POPG (black triangles) and 4:1 POPC:POPG (grey squares) lipid vesicles.

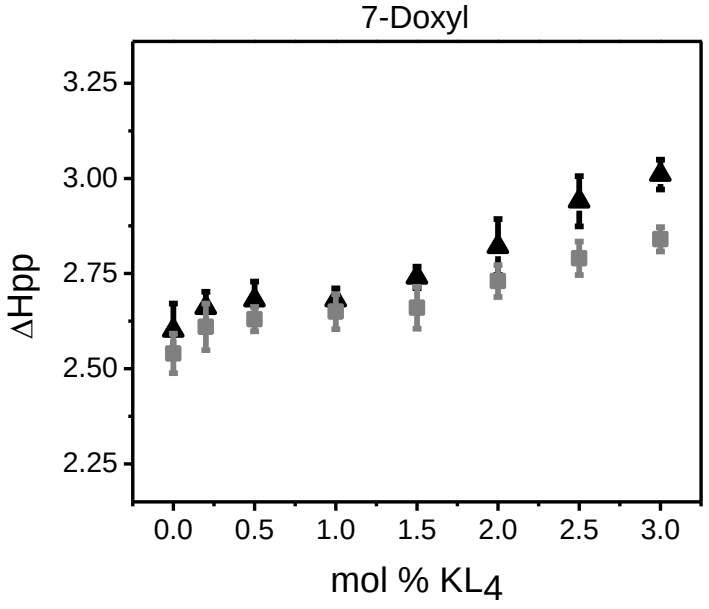

Figure 4-8. ΔH_{pp} plotted as a function of KL_4 concentration for 7-doxyl PC incorporated in 4:1 DPPC:POPG (black triangles) and 4:1 POPC:POPG (grey squares) lipid vesicles.

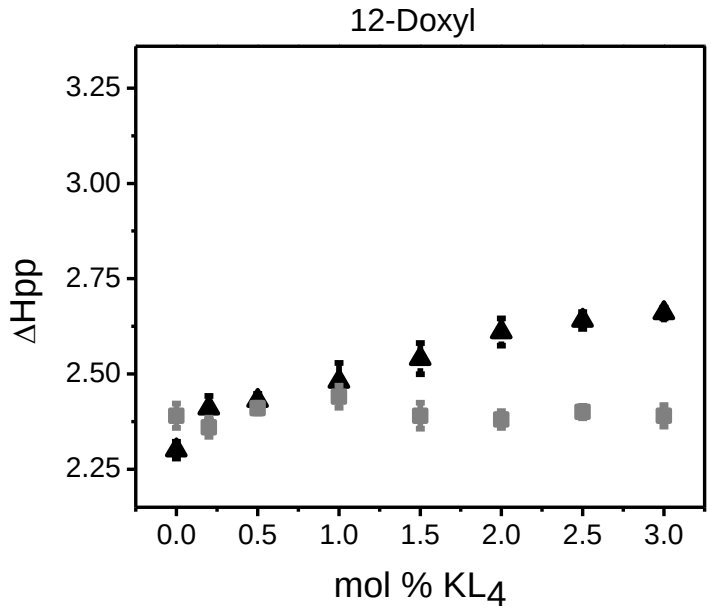

Figure 4-9. ΔH_{pp} plotted as a function of KL_4 concentration for 12-doxyl PC incorporated in 4:1 DPPC:POPG (black triangles) and 4:1 POPC:POPG (grey squares) lipid vesicles.

Figures 4-7 and 4-8 show that as KL_4 concentration is increased, mobility is decreased at about the same rate for 5- and 7-doxyl labeled lipids in both lipid systems. This indicates that KL_4 is interacting with the spin label at these positions along the acyl chain upon membrane binding and doing so in similar manner between the two lipid systems. There is a deviation, however, between the ΔH_{pp} trends for DPPC:POPG and POPC:POPG samples containing 12-doxyl labeled PSPC (Figure 4-9). For DPPC-rich vesicles there is an increase in ΔH_{pp}, indicating an interaction between KL_4 and the 12 position along the acyl chain is restricting the spin label's mobility. This interaction is not seen in 4:1 POPC:POPG MLVs, suggesting the peptide is not interacting as deeply in the bilayer as seen with 4:1 DPPC:POPG. To further illustrate the difference between the two systems, a percentage change in ΔH_{pp} is plotted as a function of KL_4 concentration and shown in Figures 4-10 through 4-12.

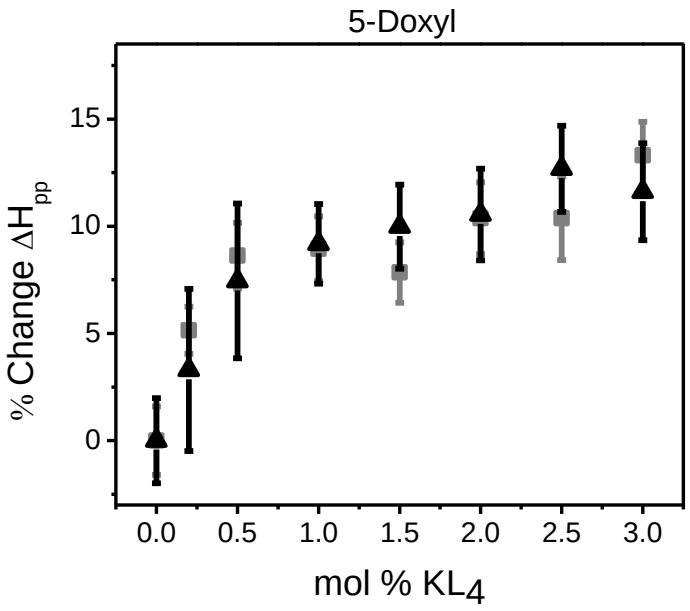

Figure 4-10. The mobility parameter ΔH_{pp} graphed as a percent change to illustrate differences for 5-doxyl PC incorporated in 4:1 DPPC:POPG (black triangles) and 4:1 POPC:POPG (grey squares) lipid vesicles.

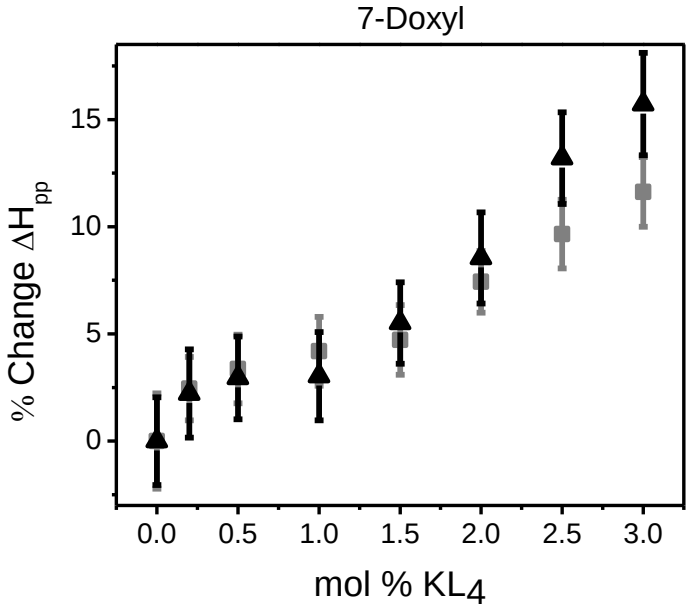

Figure 4-11. The mobility parameter ΔH_{pp} graphed as a percent change to illustrate differences for 7-doxyl PC incorporated in 4:1 DPPC:POPG (black triangles) and 4:1 POPC:POPG (grey squares) lipid vesicles.

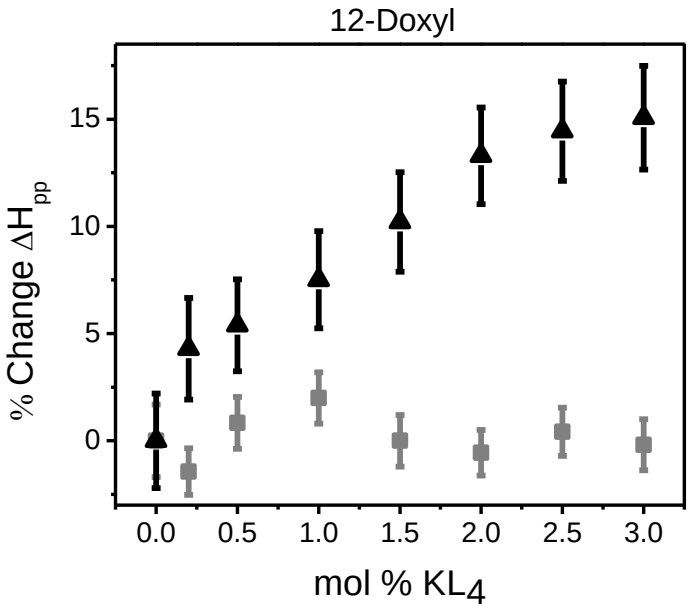

Figure 4-12. The mobility parameter ΔH_{pp} graphed as a percent change to illustrate differences for 12-doxyl PC incorporated in 4:1 DPPC:POPG (black triangles) and 4:1 POPC:POPG (grey squares) lipid vesicles.

As previously stated, ΔH_{pp} is a semi-quantitative parameter which suggests that it alone does not entirely quantitate mobility. For this reason several mobility parameters are typically used to better understand dynamics. For doxyl labeled lipids, another commonly used mobility parameter is the order parameter S, which is described in Chapter 2. To calculate the order parameter, the axial hyperfine anisotropy must be discernible, which is the case for 5- and 7-doxyl labeled lipids but not for the highly isotropic 12-doxyl labeled lipids. Figure 4-13 shows the calculated order parameters for both 5- and 7-doxyl labeled lipids in both lipid systems as a function of peptide concentration.

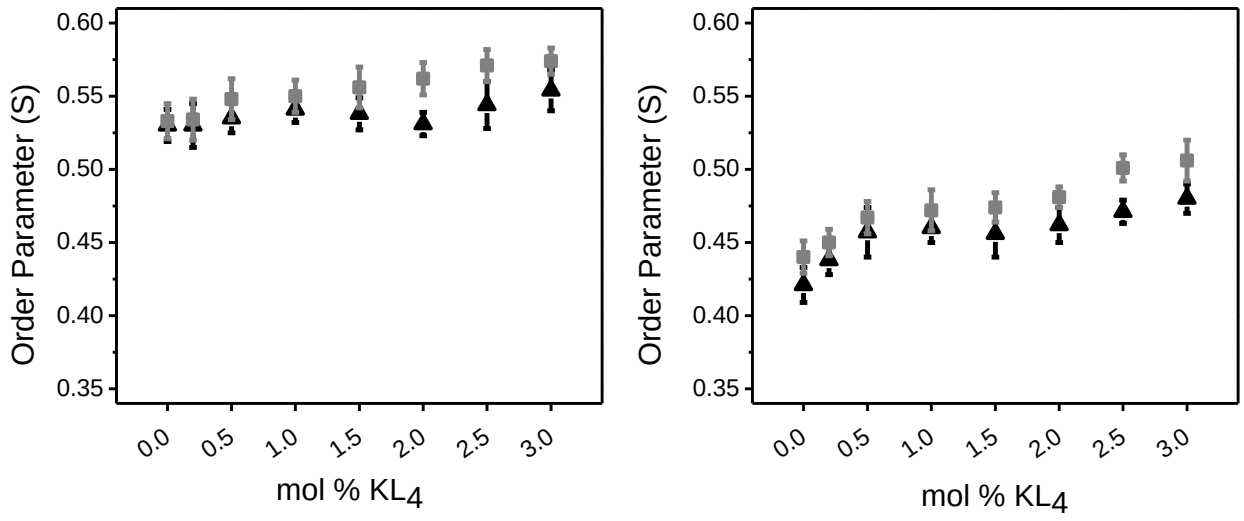

Figure 4-13. Order parameters for 5- & 7-doxyl PC incorporated in 4:1 DPPC:POPG (black) and 4:1 POPC:POPG (blue) lipid vesicles as a function of KL_4 concentration.

As previously seen with ΔH_{pp} measurements, the order parameters for 5- and 7-doxyl in both lipid systems increase with peptide concentration, indicating KL_4 is interacting with the spin labels at these depths. For both DPPC and POPC-rich vesicles, the increase in S is similar upon KL_4 addition. For both semi-quantitative parameters ΔH_{pp} and S, there is a similar trend of decreased mobility at the 5- and 7-doxyl positions in both lipid systems upon KL_4 binding. The fact that a difference was seen at the 12-position between the two systems and the inability to use S as a measure of mobility for 12-doxyl labeled lipid spectra, indicates another parameter needs to be studied to see if indeed there are differences at the 12-doxyl position.

The final mobility parameter looked at is the ratio between the intensity of the first derivative central line with that of the low field line. A detailed description of this parameter is given in Chapter 2 and the results are shown in Figure 4-14. A more substantial increase in h(0)/h(1) is seen in DPPC-rich vesicles when compared to POPC-rich vesicles. To further illustrate this difference, the percent change in h(0)/h(1)

was also graphed as a function of KL_4 concentration. This data correlates well with the trends for ΔH_{pp} in Figures 4-7 through 4-9, which suggest KL_4 penetrating further into DPPC-rich vesicles and interacting with the 12-position of the lipid acyl chain.

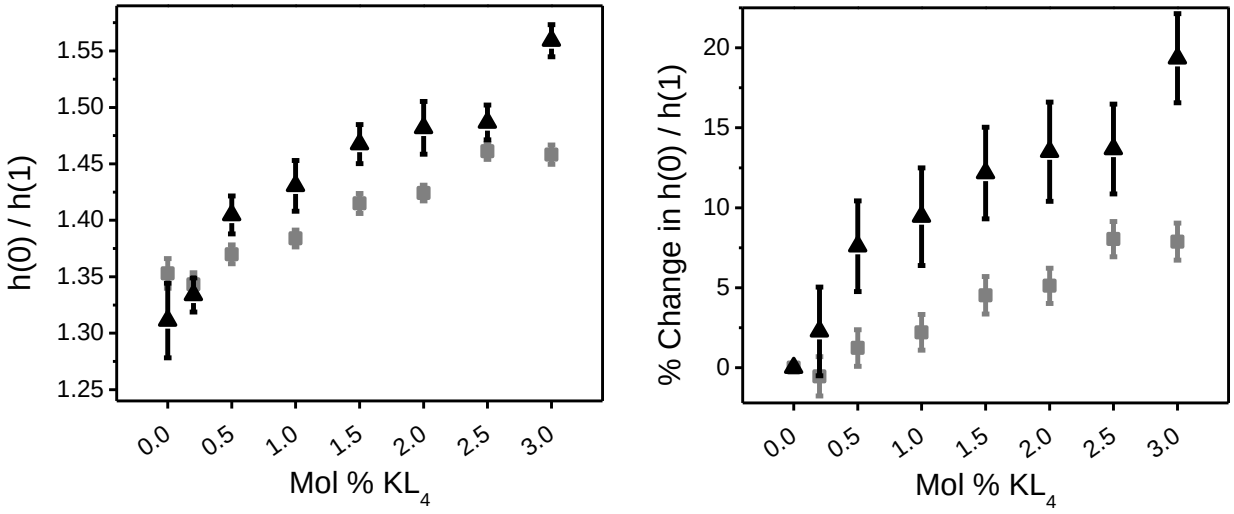

Figure 4-14. This graph shows the ratio of the central resonance line (h0) and the low field line (h1) for 4:1 DPPC:POPG (black triangles) and 4:1 POPC:POPG (grey squares). The left graph shows the raw data and the right as a percentage change to illustrate the discrepancy betweeen DPPC:POPG and POPC:POPG.

Lipid Mobility Conclusions

Studying changes in mobility along the lipid acyl chain gives an understanding of how KL_4 is affecting different regions in the bilayer. The results from ΔH_{pp}, S, and h(0)/h(1) suggest KL_4 displays similar effects on regions closer to the membrane interface in the two lipid systems as reported by 5- and 7-doxyl labeled lipids. However, it appears that KL_4 is interacting further in the bilayer at the 12-doxyl position in 4:1 DPPC:POPG lipids in contrast to 4:1 POPC:POPG lipids. In addition, the lack of an easily detected interaction deep within the bilayer in 4:1 POPC:POPG lipids suggests a transmembrane orientation of KL_4 in this environment is unlikely. These results correlate well with some recently published NMR data [42, 86, 107], specifically ^2H NMR

data which looked at the dynamics of four deuterated leucine positions (3, 10, 12, and 19) [86]. The positions were chosen because two leucines (Leu3 and Leu19) were at the terminal ends while two leucines being in the center of the peptide (Leu10 and Leu12). For a transmembrane orientation, similarities in dynamics between Leu3 and Leu19 would be expected as would similarities between Leu10 and Leu12 because they would lie in the center of the bilayer. The ^{2}H NMR showed that Leu3 and Leu12 exhibited similar dynamics while Leu10 and Leu19 shared similar dynamics. In addition, Leu10 and Leu12 had dynamics that were significantly different which makes a transmembrane orientation highly unlikely. Additionally, further analysis of the leucine side chain dynamics suggested helix-helix packing due to aggregation was unlikely and the differences in dynamics seen are from a helix lying in the plane of the bilayer. The next section will look at changes in the dynamics of KL_4 via EPR to see if correlations can be made with lipid dynamics EPR data and the previously published NMR studies.

KL_4 Dynamics

To properly study membrane bound proteins, analysis of both lipid and protein dynamics are needed. In the previous section, mobility studies were performed to understand changes in dynamics occurring along the lipid acyl chain upon adding increasing amounts of KL_4. In this section the spin-label will be attached to the peptide via site-directed spin-labeling, as described in Chapter 2, and the peptide concentration will be held constant at 2 mole percent. Eight spin-label positions were chosen (C7-C10 and C12-C15) which allow for the study of two complete turns around the KL_4 helix. Helical wheel representations of KL_4 as an α-helix and as calculated by ^{13}C ssNMR peptide torsion angle studies by Dr. Long et al. in POPC:POPG and DPPC:POPG vesicles are shown in Figure 4-15 [42, 86, 107].

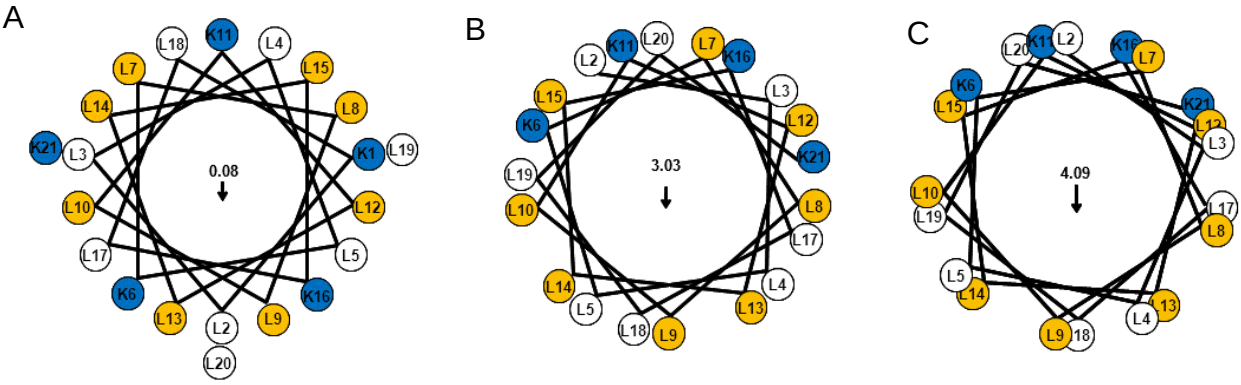

Figure 4-15. The helical wheel representations of KL_4 as a typical α–helix (A), in POPC:POPG vesicles (B), and DPPC:POPG (C) as predicted by NMR studies. Orange amino acids represent positions which were individually spin-labeled and blue amino acids represent positively charged lysines. Lysine at position 1 was left off of the NMR wheels due to its high flexibility. Arrows indicate the net hydrophobic moments resulting from the charged lysine side chains on the helix surface.

Addition of a spin-label to a peptide opens the possibility that the overall structure has been perturbed. A common way to study if a change has occurred in the overall structure is using circular dichroism (CD) as previously described in Chapter 2. Figure 4-16 shows CD for all eight spin-labeled sites (C7-C10 & C12-C15) in both lipid systems in addition to native KL_4 and KL_4 in TFE and MeOH. No change in secondary structure from native KL_4 is seen upon addition of IAP spin label to any of the eight sites used.

To compare differences in mobility at the different peptide positions on partitioning into the two lipid systems, CW-EPR spectra were collected and analyzed. These spectra are shown in Figure 4-17 and were collected at 45 ºC with a 125 Gauss scan width. Each parameter measured is discussed in Chapter 2. To analyze each KL_4-IAP spectrum, ΔH_{pp} was calculated in the same manner as the previous section. Each spectrum was collected using 2 mol percent KL_4 and ΔH_{pp} was plotted as a function of spin-label position. Analysis of ΔH_{pp} is shown in Figure 4-18 along with the projected

helical wheels from KL_4 NMR data [42] for the peptide partitioning into POPC:POPG and DPPC:POPG lipid vesicles as shown in Figure 4-15.

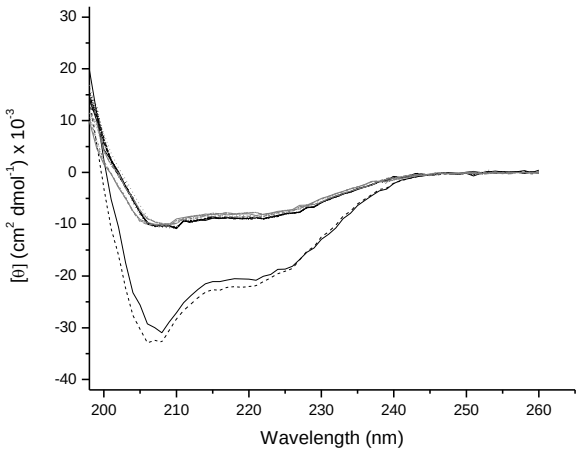

Figure 4-16. CD spectra for KL4 in TFE (----) and KL4 in MeOH (____) used as reference spectra. Overlaid spectra of C7-C10 & C12-C15 spin-labeled KL4-IAP sites and native KL4 in POPC:POPG and DPPC:POPG (grayscale).

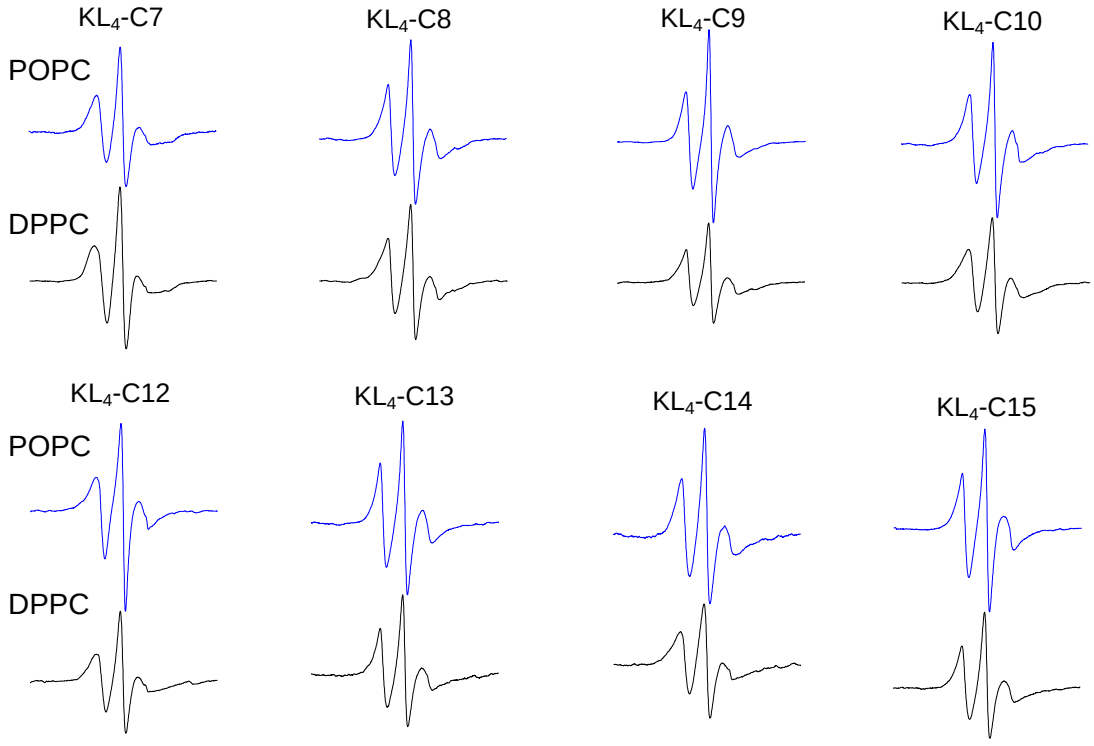

Figure 4-17. Spectra for all eight spin-labeled peptides incorporated in 4:1 POPC:POPG (blue) and 4:1 DPPC:POPG (black) lipid vesicles with 125 Gauss scan widths and 45 ºC are shown.

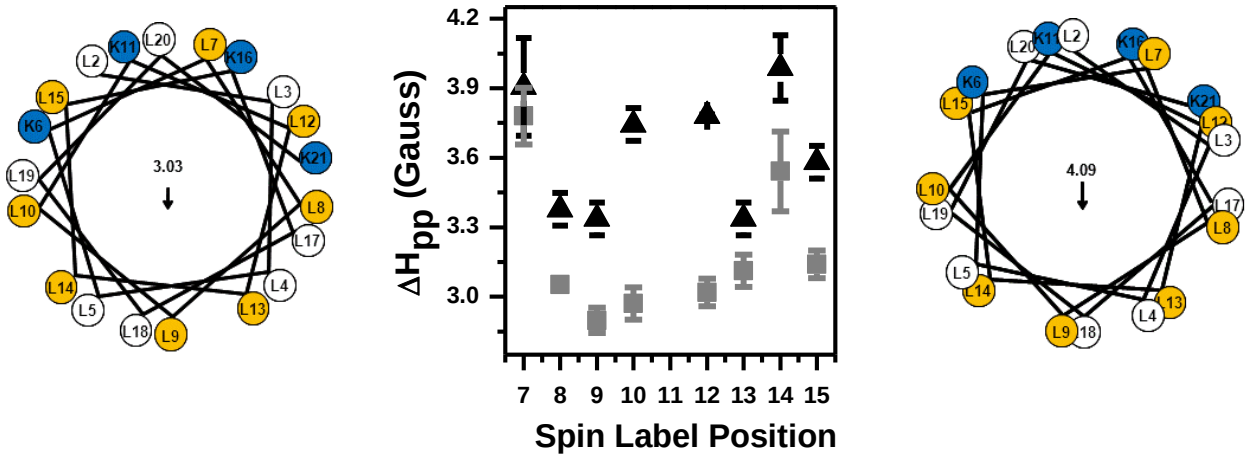

Figure 4-18. ΔH_{pp} measurements (center) for KL_4-IAP individually spin-labeled at positions C7-C10 and C12-C15 and incorporated into 4:1 POPC:POPG (grey squares) and 4:1 DPPC:POPG (black triangles) lipid vesicles. Helical wheel representations for KL_4's predicted structure in POPC:POPG (left) and DPPC:POPG (right) lipid vesicles are shown for positioning reference NMR [42].

Studying the mobility of a spin-label by ΔH_{pp}, allows for an understanding of the local environment at the spin-labeled position. Depending on the orientation of KL_4 in the bilayer, a characteristic pattern of mobility (ΔH_{pp}) would be expected. For example, if KL_4 were to span the bilayer in a transmembrane orientation, the N- and C-termini would be expected to have decreased mobility due to their position in the less mobile interface region of the lipid bilayer. On the other hand, if KL_4 were to lie in the plane of the bilayer an expected mobility pattern would repeat every four amino acids as one proceeds around the helix. This means that one side of the helix would be in a region of high fluidity (bilayer interior), while the opposite side has restricted mobility due to it being at the lipid interface. By choosing two groups of four consecutive amino acids, two full turns around the peptide helix are being studied, as shown in Figure 4-18. The first four sites chosen, C7-C10, were used as they not only make a complete turn around the helix, but they also predicted to lie on opposite sides of KL_4 based on NMR

studies [42, 86], giving the largest possible discrepancy in mobility between each site (see Figure 4-18 helical wheels). In both POPC and DPPC-rich vesicles, position 7 sits closest to the lipid head group while position 9 is deepest in the bilayer interior. In addition, positions 8 and 10 lie at similar depths about half way between positions 7 and 9. This predicted trend is precisely mirrored by the measured mobility parameter ΔH_{pp}. In both POPC and DPPC vesicles the most restricted mobility is seen at position 7 and increases going to position 8 then 9 and finally decreasing slightly at position 10. The overall mobility pattern for this region of KL_4 gives us a trend in which ΔH_{pp} for IAP at C-7 > C-8 ≈ C-10 > C-9. Consistent with a helix lying in the plane of the bilayer the EPR data correlate well with the proposed helical model in Figure 4-18 and rules out the possibility of KL_4 spanning the bilayer. The values measured in POPC- and DPPC-rich environments show similar trends in this region with a DPPC-rich environment yielding ΔH_{pp} values indicating slightly more restricted spin-label mobility. This is to be expected since DPPC, being fully saturated, can more tightly pack allowing for a greater effect on peptide spin-label mobility.

The next set of spin-labels monitored were at positions C12-C15, which are the next set of leucines after the lysine following the first set of labels and they also make a full turn around the helix (Figure 4-18). For this set of spin-labels the discrepancy predicted between where the positions lie in the bilayer is not as great as with the first set, giving similar depth positions for 12 and 15, which are closest to the bilayer interface, and 13 and 14 being similar but deeper in the bilayer. For both POPC and DPPC-rich environments the measured ΔH_{pp} values do not coincide as nicely with the helical wheel predictions as positions C7-C10. For DPPC vesicles (Figure 4-18 black

squares) positions C12, 13, and 15 give ΔH_{pp} values similar to expected from the helical wheel diagram, in which 12 and 15 are similar and 13 is more mobile. However, C14 gives a higher ΔH_{pp} value than any of the other seven positions. This is not to be expected for a helix in the plane of the bilayer with a helix pitch similar to those given in Figure 4-18. This intriguing result is also seen in the POPC-rich environment as well in which C14 gives a ΔH_{pp} similar to that of C7, which is close to the bilayer interface. To better understand if these findings are due to sample preparation, power saturation studies were performed to see if similar results could be seen in solvent accessibility. Chapter 5 will go into the details of the power saturation results, but all indications suggest that these ΔH_{pp} mobility results are indeed real and may be caused by some perturbation of KL_4 around the C14 positions. Two possibilities have been postulated as to the origin of these unexpected values; either KL_4 is slightly tilted in its orientation in the bilayer so as to not lie entirely parallel, to the bilayer planes of KL_4 could have a kink in its structure which might affect the relative mobility at specific spin-labeled positions. Chapter 5 will look at the relative partitioning depth in the bilayer for each spin-labeled position to add further insight into this issue. In addition, power saturation will address the possibility that KL_4 is affecting the bilayer by either thickening or thinning the bilayer.

Conclusions

The CW-EPR mobility studies in this work are consistent with a model in which KL_4 lies in the plane of the lipid bilayer in both 4:1 POPC:POPG and 4:1 DPPC:POPG lipid environments. Spin-labeled KL_4 mobility studies indicate a pattern consistent with a helix in the plane of the bilayer and rule out the possibility of KL_4 spanning the bilayer in a transmembrane orientation. Spin-labeled lipid studies indicate that KL_4 is

partitioning more deeply into DPPC:POPG vesicles compared to POPC:POPG vesicles. This is seen in differences in lipid mobility occurring at the 12 position on the lipid acyl chain upon addition of KL_4. This important difference may play a vital role in lipid trafficking and DPPC enrichment at the air-fluid interface of the alveoli.

CHAPTER 5
POWER SATURATION STUDIES ON KL_4

Introduction

Chapter 4 summarized the mobility experiments performed to understand the local environment around spin-labels attached to specific lipid and peptide positions. Several relative mobility parameters were measured to give an understanding of how KL_4 is oriented in the bilayer and how it partitions differently into 4:1 DPPC:POPG and 4:1 POPC:POPG environments. It was determined that KL_4 does not span the bilayer in a transmembrane orientation, but actually lies in the plane of the bilayer. As shown with previous NMR studies [42, 86], EPR mobility suggests that KL_4 partitions further into DPPC-rich bilayers allowing for a possible mechanism of action in preferentially affecting DPPC dynamics. In Chapter 5, power saturation CW-EPR will be employed to give an understanding of the relative depth of KL_4 in the two lipid systems by looking at the solvent accessibility of spin labels attached at specific lipid and peptide positions. The combination of CW-EPR mobility studies and power saturation experiments gives a better understanding of KL_4 interacts these two lipid systems and allows for the development of a proposed KL_4 binding model.

Materials & Methods

Materials

POPC, DPPC, POPG, *n*-doxyl-PSPC were purchased as chloroform solutions from Avanti Polar Lipids (Alabaster, AL) and quantified by phosphate analysis (Bioassay Systems, Hayward, CA). Iodoacetamido-PROXYL spin label (IAP) was purchased from Sigma and used as received. Unless otherwise stated, all other reagents were purchased from Fisher Scientific (Hampton, NH) and used as received.

KL_4, KLLLLKLLLLKLLLLKLLLLK, was synthesized via solid-phase peptide synthesis (ICBR Facility, UF), purified by RP-HPLC, and verified by mass spectrometry (m/z=2469). Peptide was dissolved in methanol and analyzed by amino acid analysis for concentration (Molecular Structure Facility, UC Davis). Cysteine variants of KL_4, in which individual leucines were replaced by cysteine were also synthesized via solid-phase peptide synthesis, purified and mass verified (m/z=2459).

Methods

Spin-labeling of KL_4 cysteine mutants

Spin-labeling of KL_4 was carried out as described in Chapter 4. The final peptide concentration for each spin-labeled sample was determined by either analytical HPLC or amino acid analysis (AAA).

Preparation of lipid/peptide samples

Power saturation samples were prepared as described in Chapter 4. For power saturation analysis, each sample was made as described previously but in duplicate to allow for one of the samples to contain a final concentration of 10 mM NiAA. One sample contained 140 mM NaCl, 10 mM Bis-Tris buffer, pH 6.5, and the second was rehydrated with 140 mM NaCl, 10 mM Bis-Tris buffer, pH 6.5, containing 10 mM NiAA. This allows for the study of all three power saturation experiments; with nitrogen, oxygen, or NiAA. The hydrated dispersions were subjected to 5 freeze-thaw cycles to form MLVs and had a final lipid concentration of ~10 mM. Samples containing spin-labeled lipid had 1 mol% of doxyl-PC added relative to the native lipids and spin-labeled peptide samples contained a constant 2 mole percent of KL_4-IAP for each experiment.

CW-EPR spectroscopy

Continuous wave EPR experiments were collected as described in Chapter 3. For power saturation curves a microwave power range of 0.25 mW to 25 mW was used to measure peak-to-peak intensities for each sample. Samples were purged and temperature was equilibrated by passing either air or nitrogen gas through a copper coil in a recirculating bath (Thermo Scientific) containing 40% ethylene glycol for 20-30 minutes prior to measurements. Initial spectra of 100 – 125 Gauss sweep width were collected to ensure samples were correctly prepared. Power saturation spectra were collected at 20 Gauss sweep widths centered on the central resonance line to more accurately determine the intensity of the peak.

Power saturation experiments

Power saturation experiments were collected on the same modified Bruker ER200 spectrometer using gas permeable TPX capillary tubes as developed by Hubbell et al. [116]. Saturation experiments were collected at 45 ºC for both POPC:POPG and DPPC:POPG containing samples using a sample volume of 5 µL. Two samples for each experiment were made, with or without 10 mM NiAA and purged for at least 20 minutes with air or nitrogen gas. To ensure the samples were entirely purged with the gas, the intensity of the central resonance line was plotted as a function of time until no change in intensity was observed. For each sample this was approximately 20 minutes. As mentioned in the previous section, intensities of the central resonance line at 20 Gauss scan widths, were plotted as a function of microwave power in the range of 0.25 mW – 25 mW. LabVIEW software (National Instruments, Austin, TX) was used for data recording and generously provided by Christian Altenbach and Wayne Hubbell (UCLA,

Los Angeles, CA). Resultant curves were fit using Equation 2-11 and analyzed using Equation 2-12.

Results & Discussion

Introduction

Power saturation is a technique developed by Hubbell et al. and is used to develop a depth parameter of the system of interest by studying the solvent accessibility of a spin-label with its local environment. The procedure is described in detail in Chapter 2 and will be used here to better understand the partitioning of KL_4 in both 4:1 DPPC:POPG and 4:1 POPC:POPG. The indications from previous experiments [42, 86] and the mobility studies in Chapter 4 which suggest that KL_4 partitions differently in DPPC bilayers, indicates that developing a depth profile for KL_4, using power saturation in these two systems will greatly advance our understanding of the partitioning. In addition, power saturation can aid in the understanding of the mobility studies by differentiating between a decrease in mobility of the spin-label due to interaction with KL_4 or change due to a change in the bilayer thickness. The following sections will discuss the results from the spin-label lipid and spin-label peptide power saturation studies and compare them to results from Chapter 4 and work of other groups/studies.

Effect of KL_4 on Acyl Chain Accessibility

As previously discussed in Chapter 4, CW-EPR mobility studies indicate KL_4 is partitioning deeper in DPPC and interacting with the 12 position on the lipids acyl chain. This interaction was not seen in POPC vesicles, as only a change in mobility was noticed at both the 5- and 7-doxyl positions. Power saturation will show if these mobility changes also correspond to changes in solvent accessibility of the spin-label lipid, albeit aqueous NiAA or hydrophobic oxygen. To determine this, samples were prepared as

mentioned in Chapter 5 methods section with varying amounts of KL_4. The accessibility parameter $\Delta P_{1/2}$ is plotted as a function of KL_4 concentration for oxygen and NiAA and is shown in Figures 5-1 and 5-2. An in-depth description of all power saturation parameters are given in Chapter 2.

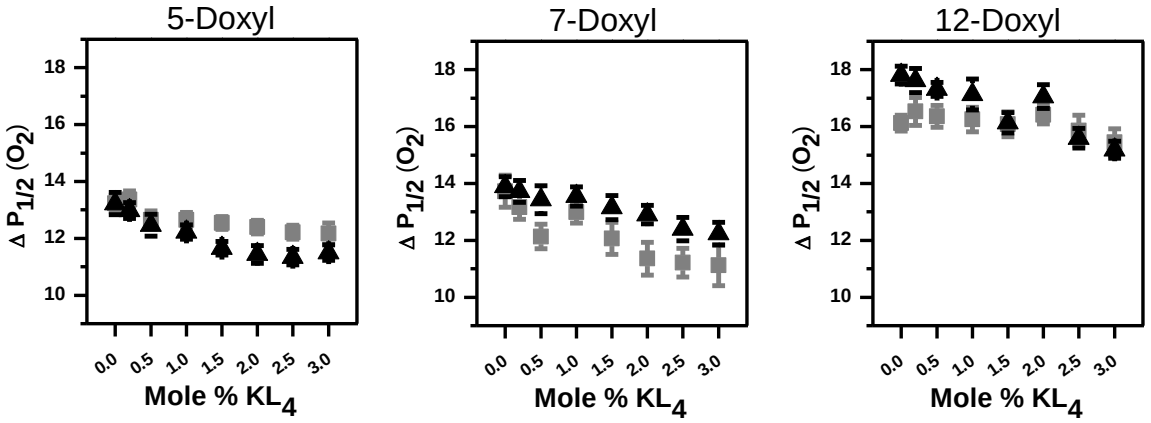

Figure 5-1. Power saturation accessibility parameter $\Delta P_{1/2}$ (oxygen) plotted as a function of KL_4 mole percent. Samples contain either 5-doxyl (left), 7-doxyl (center), or 12-doxyl (right) in 4:1 DPPC:POPG (black triangles) and 4:1 POPC:POPG (grey squares).

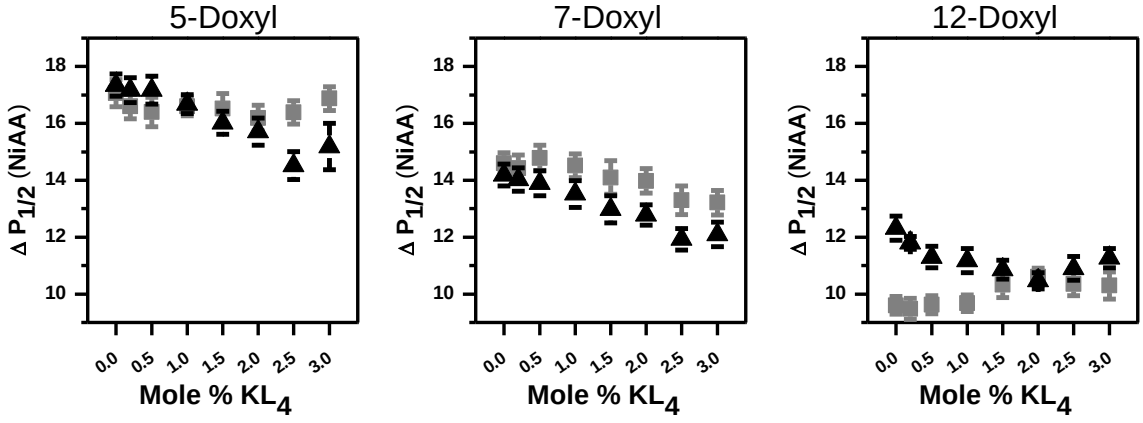

Figure 5-2. Power saturation accessibility parameter $\Delta P_{1/2}$ (NiAA) plotted as a function of KL_4 mole percent. Samples contain either 5-doxyl (left), 7-doxyl (center), or 12-doxyl (right) in 4:1 DPPC:POPG (black triangles) and 4:1 POPC:POPG (grey squares).

The accessibility parameter $\Delta P_{1/2}$ is a measure of the spin-labels interaction via Heisenberg exchange with the paramagnetic collider, either oxygen or NiAA, and

therefore is a measure of the accessibility of the spin-label and that collider. Figure 5-1 shows the $\Delta P_{1/2}$ for oxygen at the 5-, 7-, and 12-doxyl positions in both lipid systems. The $\Delta P_{1/2}$ values increase as the spin-label is moved further down the acyl chain (moving from left to right in Figure 5-1) which is due to oxygen being lipophilic, therefore, having a higher concentration and an increase probability of collision with the doxyl spin-label. The opposite is seen in Figure 5-2 in which NiAA is most concentrated in the aqueous phase, therefore, giving the highest $\Delta P_{1/2}$ value at the 5-doxyl position. Looking at differences in trends upon KL_4 addition at each position between the two lipid systems gives an understanding of changes in the local environment of the spin-label. Figure 5-1 (left) shows a similar decrease in oxygen accessibility between the two lipid systems suggesting both a displacement of oxygen at the 5-doxyl position because of KL_4 binding and a decrease of spin-label and oxygen collisions due to the reduced mobility of the spin-label. The same trend is seen at the 7-doxyl position, Figure 5-1 (center), which correlates well with the previous mobility studies which found similar interactions of KL_4 with both lipid systems at these positions. Deviation once again, occurs at the 12-doxyl position which shows very little change in oxygen accessibility for 4:1 POPC:POPG and a substantial decrease for 4:1 DPPC:POPG. As with the mobility data, $\Delta P_{1/2}$ values for oxygen suggest KL_4 penetrating further and interacting at the 12-doxyl position in DPPC-rich vesicles but not in POPC-rich vesicles.

The aqueous soluble NiAA accessibility data, $\Delta P_{1/2}$ (NiAA), is shown in Figure 5-2 and is plotted in the same manner as Figure 5-1. At the 5-doxyl position there is a decrease in NiAA accessibility upon KL_4 binding suggesting the interaction of KL_4 at that spin-label position. The trend is similar between the two lipid systems, however, there

is a deviation at the higher KL_4 concentrations in which the accessibility of NiAA in POPC-rich vesicles increases slightly whereas DPPC-rich it continues to decrease. This may be caused by KL_4 interacting closer to the bilayer interface in POPC when compared to DPPC and altering the partitioning of NiAA around the lipid head groups in such a manner as to increase the collisions of NiAA and the 5-doxyl spin-label. This deviation, however, is not seen at the 7-doxyl position and the expected similar decrease in $\Delta P_{1/2}$ between the two systems is seen. The $\Delta P_{1/2}$ (NiAA) at the 12-doxyl position again shows the biggest deviation between the two systems. Like all the previous data has suggested, KL_4 interacts further in the bilayer of DPPC vesicles, decreasing the accessibility of 12-doxyl with NiAA.

To better illustrate these trends Figure 5-1 and Figure 5-2 are plotted as a percent change in $\Delta P_{1/2}$ and shown in Figure 5-3 and Figure 5-4. Obvious deviations between the 4:1 POPC:POPG and the 4:1 DPPC:POPG data can be seen at the 12-doxyl position in these graphs.

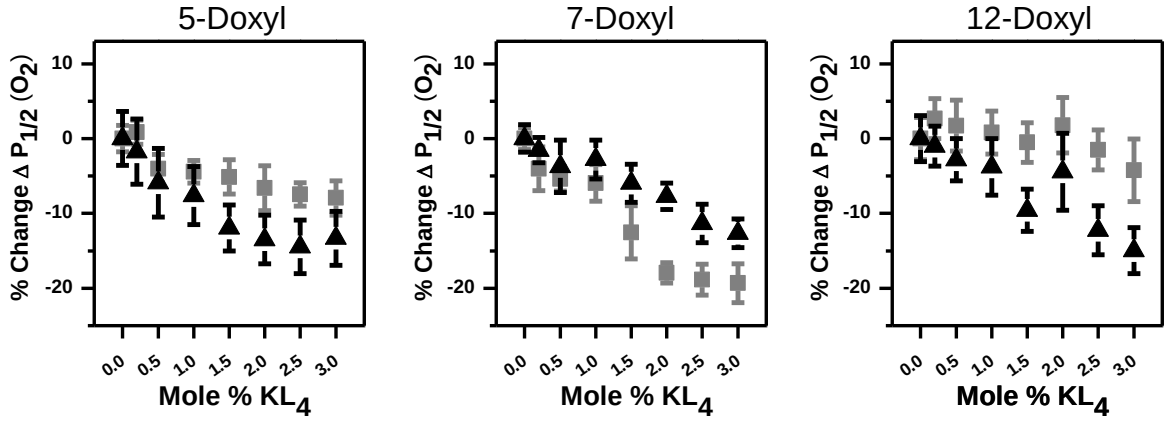

Figure 5-3. Percent change in the accessibility parameter $\Delta P_{1/2}$ (oxygen) plotted as a function of KL_4 mole percent. Samples contain either 5-doxyl (left), 7-doxyl (center), or 12-doxyl (right) in 4:1 DPPC:POPG (black triangles) and 4:1 POPC:POPG (grey squares).

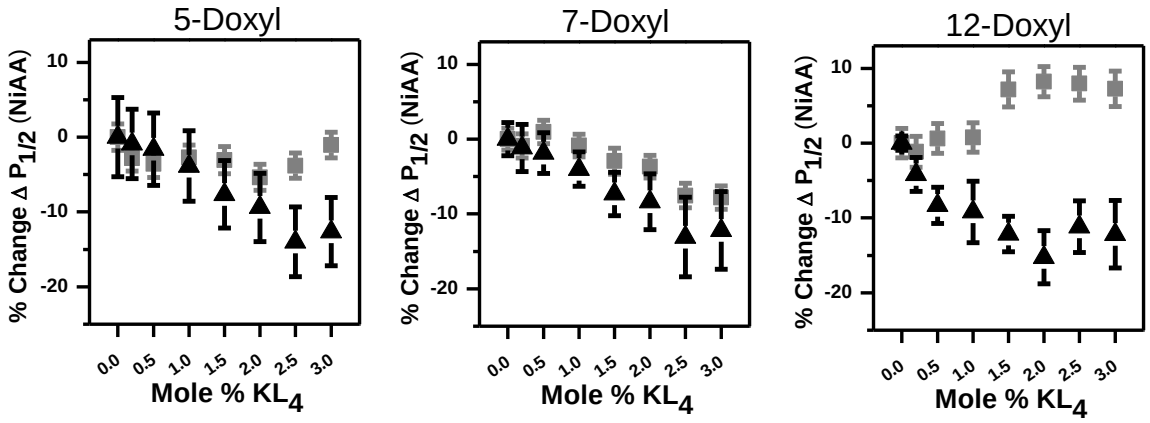

Figure 5-4. Percent change in the accessibility parameter $\Delta P_{1/2}$ (NiAA) plotted as a function of KL_4 mole percent. Samples contain either 5-doxyl (left), 7-doxyl (center), or 12-doxyl (right) in 4:1 DPPC:POPG (black triangles) and 4:1 POPC:POPG (grey squares).

Effect of KL_4 on Spin-label Depth

Power saturation accessibility parameter $\Delta P_{1/2}$ is a good way of looking at changes occurring with a specific paramagnetic collider and a spin-label; however, looking at the ratio of the $\Delta P_{1/2}$ for hydrophilic and lipophilic colliders can give a good understanding of the depth of the spin-label. One issue when looking at the changes in mobility and accessibility is if the peptide is interacting at that spin-label position or if the dynamics of the lipid system have changed, such as a thickening or thinning of the bilayer, which may affect the results. By using the depth parameter Φ, which is discussed extensively in Chapter 2, a depth profile of the doxyl spin-label can be graphed as a function of KL_4 binding. If the accessibility parameter $\Delta P_{1/2}$ is changing because KL_4 is displacing solvent from around the spin-label, as stated previously, the ratio between the two $\Delta P_{1/2}$ values should remain constant. On the other hand, a change in this ratio (defined as Φ) may indicate that the depth of the doxyl spin-label is changing, therefore, a thickening or thinning of the bilayer may be occurring. Figure 5-5 plots Φ as a function of KL_4 concentration for both lipid systems and at three doxyl positions.

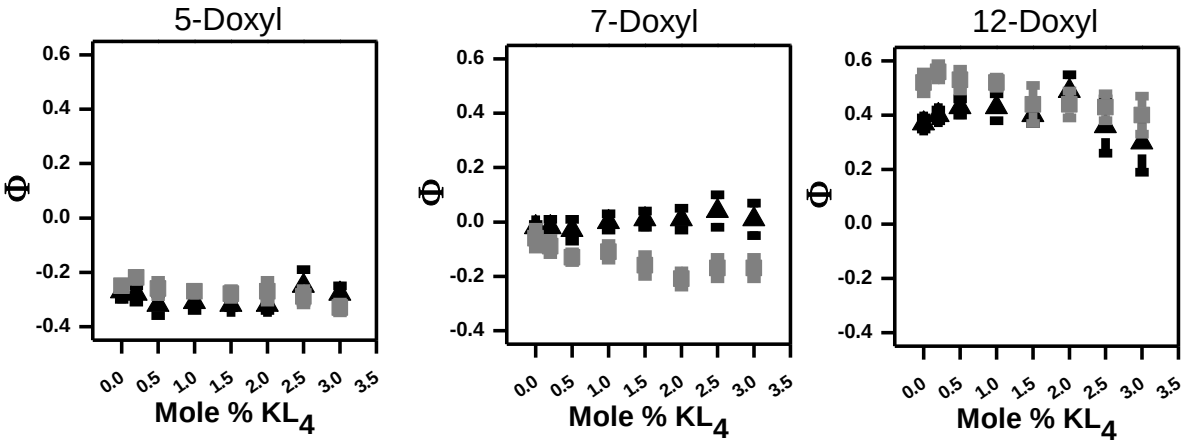

Figure 5-5. Depth parameter Φ plotted as a function of KL_4 concentration at 5-doxyl (left), 7-doxyl (center), and 12-doxyl (right) positions in both 4:1 DPPC:POPG (black triangles) and 4:1 POPC:POPG (grey squares).

From Figure 5-5, the depth parameter Φ increases as the spin-label increases its depth within the bilayer. For the 5 position on the lipid acyl chain Φ is negative because the ration of $\Delta P_{1/2}$ (oxygen) / $\Delta P_{1/2}$ (NiAA) is less than one and the natural log of this will give a negative value. As the $\Delta P_{1/2}$ (Oxygen) increases so does the Φ value which can be seen moving from 5-doxyl to 12-doxyl. Observing the 5-doxyl graph in Figure 5-5 demonstrates that the Φ values do not change upon KL_4 addition in both lipid systems, indicating that the relative depth of the 5-doxyl spin-label does not change as KL_4 binds. The 7-doxyl data suggests the same with a slight deviation in the 4:1 POPC:POPG vesicles in which Φ decreases at higher KL_4 concentrations. This may be due to a slight perturbation in the lipid bilayer but it seems minor as illustrated by Figure 5-6 in which the percent change in Φ is around two. Finally at the 12-doxyl position the trend in Φ upon KL_4 binding remains constant within error of the Φ value with no peptide. Once again showing that the doxyl positions remain at the same relative depth upon KL_4 binding, therefore, suggesting that the bilayer is neither thickening nor thinning and that the trends seen in mobility and accessibility are due to KL_4 interacting directly with

the spin-label. To further illustrate the lack of change in Φ, a percentage change was plotted in Figure 5-6. Overall any change seen in Φ is within 2 percent of the Φ value with no KL_4 suggesting any perturbation in the depth of the doxyl spin-label is minimal.

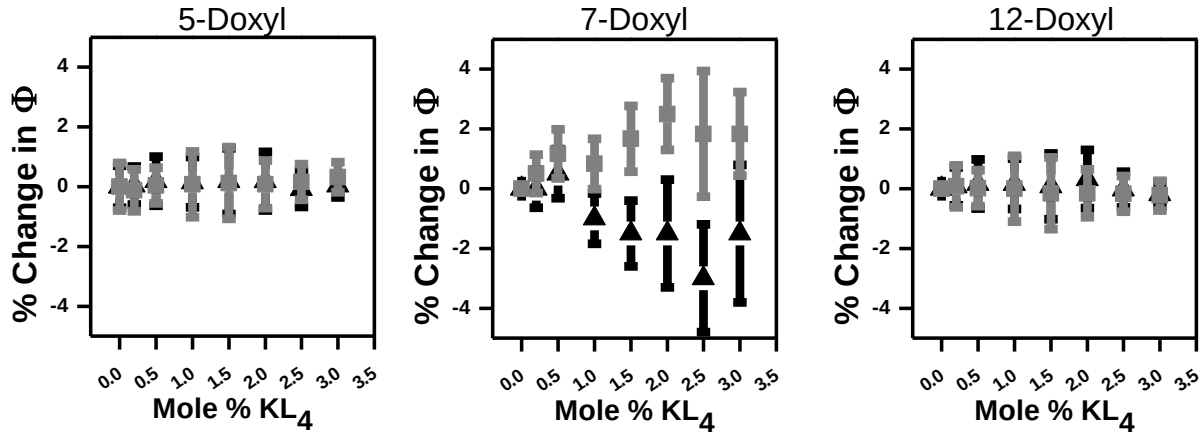

Figure 5-6. Percentage change in depth parameter Φ plotted as a function of KL_4 concentration at 5-doxyl (left), 7-doxyl (center), and 12-doxyl (right) positions in both 4:1 DPPC:POPG (black triangles) and 4:1 POPC:POPG (grey squares).

Insertion Depth of KL_4

The determination of the relative depths of each doxyl spin-label (Φ values from previous section) allows for a "ruler" with which to compare spin-label KL_4 to. This will give a relative depth corresponding to the doxyl spin-labels in the two lipid systems, therefore giving a model of KL_4 penetration depth between POPC- and DPPC-rich vesicles. Power saturation data for all eight KL_4-IAP variants were collected at 2 mol % KL_4-IAP and Φ values were calculated as described in Chapter 2. A plot of Φ as a function of spin-label position is shown in Figure 5-7. For comparison, spin-label lipid Φ values are marked with a line for each doxyl position using the same concentration of KL_4 (2 mol percent).

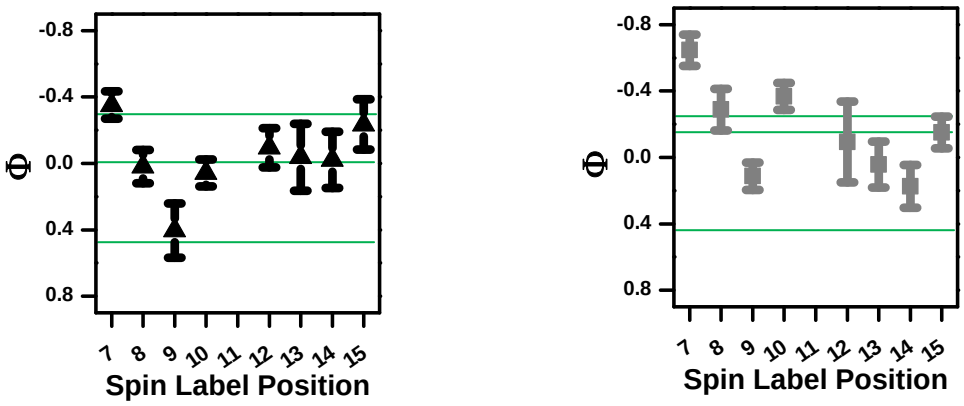

Figure 5-7. Depth parameter Φ for KL_4-IAP plotted as a function of spin-label position for 4:1 DPPC:POPG (left) and 4:1 POPC:POPG (right). Spin-labeled lipid Φ values are given for the 5-, 7-, and 12-doxyl and shown in green lines. These are used as a ruler to determine the relative depth of KL_4 in each bilayer.

As previously stated, the first four spin-labels (C7-C10) make a full turn around the peptide's helix (Figure 4-18) and their results should be compared to one another. Figure 5-7 shows that in both DPPC- and POPC-rich systems, moving from C7 to C9 there is an increase in Φ which corresponds to an increase in depth within the bilayer, followed by a decrease at C10 completing the full turn around a helix in the plane of the bilayer. In addition, the increased values of Φ compared with the spin-label lipid "ruler" for DPPC indicate that KL_4 is penetrating deeper in these vesicles than POPC.

The next set of spin-labeled KL_4-IAP samples are C12-C15 and also make a complete turn around the helix. Figure 5-7 shows a similar trend as seen for C7-C10 however much less pronounced. This is expected after analysis of the mobility results from Chapter 4 which suggests KL_4 may not be lying entirely in the plane of the bilayer but may exhibit a slight tilt causing erratic results at the C12-C15 positions. An important observation is at the C14 position which gave peculiar results in the mobility studies (Figure 4-18). The relative depth as calculated from power saturation shows C14 being deeper in the bilayer when compared to the neighboring amino acid

positions. This correlates well with the proposed helical wheel projections (Figure 4-18) and suggests that the decrease in mobility seen at this position may be due to some hindrance in the helical structure such as a “kink” at this position. Comparing the power saturation depth parameter of spin-labeled lipids with that of spin-labeled peptide allows for the determination of a relative penetration depth between the two lipid systems. Figure 5-7 displays the Φ values for KL_4-IAP at eight positions in addition to the corresponding spin-labeled lipid values (green lines) which are used as a depth “ruler”. A model of KL_4 in the two lipid systems is proposed and is shown in Figure 5-8 using the first four spin-labeled peptide positions (C7-C10). A slight alteration may need to be made for POPC because of the increase depth calculated at positions C12-C15 when compared with C7-C10 from Figure 5-7. The data suggests KL_4 lying at a slight angle in the POPC-rich vesicles with the C12-C15 positions penetrating slightly further into the bilayer when compared to C7-C10. For DPPC vesicles the data in Figure 5-7 suggests KL_4 lies parallel with the bilayer throughout positions C7-C10 and C12-C15. The peptide model is based on the NMR data previously discussed [42, 86] while using the Φ values from Figure 5-7 to determine the side chain penetration depths using the color coded schematic discussed in the Figure 5-8 caption. In 4:1 DPPC:POPG vesicles KL_4 penetrates deeper in the bilayer when compared to 4:1 POPC:POPG allowing for a possible mechanism of DPPC enrichment. In addition, the difference in either lying parallel or being slightly tilted, as suggested from the power saturation data for POPC, may also play a role in KL_4 function by altering its overall binding interaction.

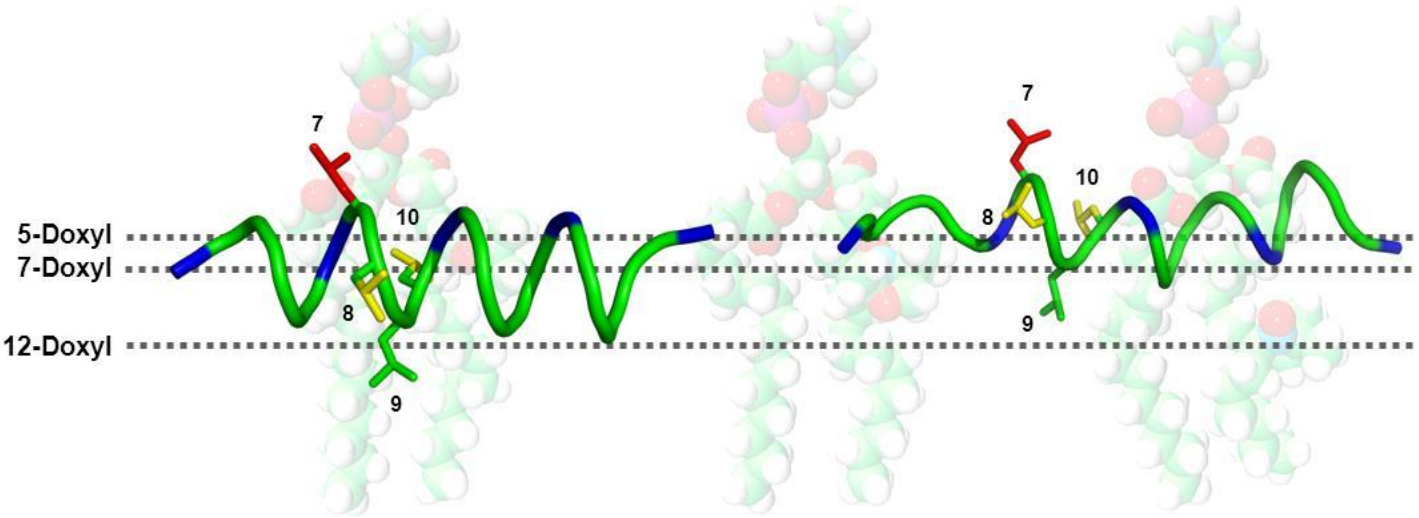

Figure 5-8. Models of KL_4 partitioning into DPPC-rich (left) and POPC-rich (right) regions. Partitioning depths are based on Φ values obtained for the KL_4-C variant (Figure 5-7). The leucines substituted in this study are color-coded with respect to relative partitioning of the IAP spin label at 45 °C with L7R1 (red) < L8R1 ≈ L10R1 (yellow) < L9R1 (green). The structures for KL_4 are based on NMR measurements in DPPC-rich and POPC-rich environments.

Conclusions

In Chapter 4, the mobility studies suggested what was already seen in Dr. Long et al. NMR studies that KL_4 inserted in the plane of the bilayer and at different depths for DPPC- and POPC-rich vesicles. In Chapter 4 power saturation CW-EPR was performed to give a better understanding of the relative depths between the two lipid systems. The proposed model in Figure 5-8 is based on the NMR data and the power saturation data collected for both spin-labeled lipid and spin-labeled KL_4 samples in Chapter 4. It shows that KL_4 inserts deeper in DPPC-rich vesicles with the C9 position reaching deep in the bilayer beyond the 12-doxyl position. This difference in binding may play a critical role in what many believe is an enriching of DPPC at the air-fluid interface in the alveoli. Understanding these differences of KL_4 and lipid interactions allows for further development of more specific and targeted drug development.

CHAPTER 6
CONCLUSIONS AND FUTURE DIRECTIONS

Conclusions

Pulmonary surfactant is a mixture of lipids and proteins that are vital to proper lung function. Deficiencies or mutations in pulmonary surfactant can lead to a wide range of diseases, and one of utmost importance is respiratory distress syndrome (RDS), a condition which commonly occurs in premature infants. According to the center for disease control (CDC), RDS is the fourth leading cause of neonatal mortality and contributes to the longest hospital stay among preterm infants. Current treatment for RDS consists of administering calf lung extract via a breathing tube directly into the lungs of the patient until proper lung function returns. This is of concern because administrating exogenous surfactant to a preterm infant with a compromised immune system can produce undesired effects. Many studies have attempted to remedy this issue by closely studying the make-up of pulmonary surfactant. From these studies it has been shown that the fully saturated DPPC lipid, the negatively charged POPG lipid, and the hydrophobic surfactant protein B (SP-B) are of critical importance. Due to the hydrophobicity of SP-B, it has been difficult to purify, so synthetic constructs mimicking its efficacy are in development. One such mimic is the 21 amino acid peptide KL_4, which is currently in FDA trials. Chapter 1 provides detailed background information relevant to both pulmonary surfactant and KL_4. The techniques used to examine KL_4 include circular dichroism (CD), continuous wave electron paramagnetic resonance spectroscopy (CW-EPR), and power saturation CW-EPR. Detailed descriptions on each of these methodologies are given in Chapter 2.

Chapter 3 describes the optimization of the CW-EPR studies described in Chapters 4 and 5. In order to stay consistent with charge in the lipid studies, determination of differences between 3:1 POPC:POPG and 4:1 POPC:POPG needed to be determined. In addition, proper temperature and pH studies were performed to allow for increased sensitivity for the power saturation studies.

To understand changes occurring at both the lipid and protein's local environment upon KL_4 binding, CW-EPR mobility studies were performed using either a doxyl spin-label on the lipid acyl chain or employing an IAP spin-label to the peptide backbone. Results in Chapter 4 show that KL_4 does not span the bilayer in a transmembrane orientation but lies parallel to the bilayer normal. In addition, differences are seen between DPPC- and POPC-rich vesicle systems. As previously indicated by NMR studies performed by Dr. Long et al., CW-EPR shows KL_4 penetrates deeper into DPPC bilayers interacting at the 12-position on the lipid acyl chain. CW-EPR mobility results analyzed using multiple semi-quantitative parameters each indicate this difference in penetration depth between the two lipid systems.

In addition to the CW-EPR mobility studies, power saturation EPR was used in Chapter 5 to study spin-label solvent accessibility at both the lipid and peptide level and develop a penetration depth profile in the two systems. As with the mobility studies in Chapter 4, power saturation suggests KL_4 penetrates deeper in the DPPC-rich bilayers when compared to POPC-rich. A penetration model was constructed in both lipid systems as determined by comparing power saturation values of the peptide with that of power saturation values of the lipid acyl chain. In addition, the solvent accessibility trend is indicative of a peptide lying in the plane of the bilayer and not of a peptide in a

transmembrane conformation. A slight tilt deviating from an entirely parallel peptide is suggested in the POPC vesicles, providing another possible difference between these two lipid systems.

An important aspect of understanding KL_4's function is in knowing how it interacts with different lipids. As it has been hypothesized that KL_4 preferentially inserts DPPC at the air-fluid interface, understanding how it interacts differently with DPPC than other non-saturated lipids can allow for a fundamental understanding of KL_4 and possible advancements in future drug development.

Future Directions

CW-EPR Studies on SP-B C-terminus

To date, research has focused on the terminal ends of SP-B, a construct of both N- and C-terminus called mini-B, and a few entirely synthetic mimics like KL_4. Our group has performed CW-EPR studies on KL_4 but our collaborator Dr. Long has looked at not only KL_4 but the N- and C-termini of SP-B by a variety of NMR techniques. Since EPR and NMR have complemented each other well in studying KL_4, it is inevitable to expand the group's interest to the N- and C-termini. Collaboration has already begun on CW-EPR mobility and power saturation studies, similar to that presented in this dissertation, on the C-terminus of SP-B. The large discrepancies at the amino acid level between KL_4 and the termini suggest a careful consideration of spin-label placement will be needed, especially due to the presence of prolines and native cysteines.

Pulsed EPR on KL_4 by Electron Spin Echo Envelope Modulation (ESEEM)

CW-EPR power saturation studies allow for an indirect study of the water penetration into the bilayer by use of an aqueous paramagnetic collider such as NiAA.

To directly look at changes in the water penetration profile a pulsed EPR technique called electron spin echo envelop modulation (ESEEM) can be utilized. ESEEM allows for a direct look at D_2O bonded to the N-O group of the nitroxide spin-label. This technique was first established by Dr. Marsh et al. and used on a similar system of DPPC but with cholesterol to affect the water penetration profile within the bilayer [160]. This technique does require cryogenic temperatures; therefore, it works well in tandem with CW-EPR power saturation which can be run at physiological temperatures.

CW-EPR KL_4 Studies in Different Lipid Systems

Surfactant proteins have been studied in a variety of different lipid systems with varying composition. One such composition that has interested our group is a combination of the two systems employed in this dissertation, DPPC:POPC:POPG (2:2:1). Studying a lipid system such as this one may show results that resemble one of the two systems presented in this dissertation, giving further insight into KL_4 interaction. Preliminary results of CW-EPR mobility and power saturation studies have been collected at the 12-doxyl position and C7-C10 KL_4 IAP.

LIST OF REFERENCES

1.Goerke, J., *Pulmonary surfactant: functions and molecular composition.* Biochimica et Biophysica Acta, 1998(1408): p. 79-89.

2.Piknova, B., V. Schram, and S.B. Hall, *Pulmonary surfactant: phase behaivor and function.* Current Opinion in Structural Biology, 2002. **12**: p. 487-494.

3.Serrano, A.G. and J. Perez-Gil, *Protein-lipid interactions and surface activity in the pulmonary surfactant system.* Chemistry and Physics of Lipids, 2006(141): p. 105-118.

4.Whitsett, J.A. and T.E. Weaver, *Hydrophobic surfactant proteins in lung function and disease.* New Englan Journal of Medicine, 2002. **26**(347): p. 2141-2148.

5.Wright, J.R., *Immunoregulatory functions of surfactant proteins.* Nature Reviews Immunolgy, 2004. **5**: p. 58-68.

6.Iwaarden, F.v., et al., *Pulmonary surfactant A enhances the host-defense mechanism of rat alveolar macrophages.* American Journal of Respiratory Cellular Molecular Biology, 1990. **2**: p. 91-98.

7.Ohmer-Schrock, D., et al., *Lung surfactant protein A (SP-A) activates a phospoinositide/calcium signaling pathway in alveolar macrophages.* Journal of Cell Science, 1995. **108**: p. 3695-3702.

8.Thet, L.A., et al., *Changes in the sedimentation of surfactant in ventilated excised rat lungs.* Journal of Clinical Investigations, 1979. **64**: p. 600-608.

9.Wright, J.R., *Regulation of pulmonary surfactant secretion and clearance.* Annual Review of Physiology, 1991. **53**: p. 395-414.

10.Baughman, R.P., *The uncertanties of Bronchoalveolar lavage.* European Respiration Journal, 1999. **10**: p. 1940-1942.

11.Holt, P.G., *A simple technique for the preparation of high numbers of viable alveolar macrophages from laboratory animals.* Journal of Immunology, 1979. **27**: p. 189-198.

12.Medin, N.I., J.W. Osebold, and Y.C. Zee, *A procedure for pulmonary lavage in mice.* American Journal of Veterinarians, 1976. **37**: p. 237-238.

13.Reynolds, H.Y. and H.H. Newball, *Analysis of proteins and respiratory cells obtained from human lungs by bronchial lavage.* Journal of Laboratory Clinical Medicine, 1974. **84**: p. 559-573.

14.Rudent, A., et al., *Enhancement of bronchoalveolar cell recovery and stimulation of alveolar macrophage chemiluminescence and resistance to influenza virus after treatment with RU 41821 aerosol.* Antimicrobial Agents and Chemotherapy, 1987. **31**(6): p. 920-924.

15.Nicholas, T.E., J.H. Power, and H.A. Barr, *Surfactant homeostasis in the rat lung during swimming exercise.* Journal of Applied Physiology, 1982. **53**: p. 1521-1528.

16.Nicholas, T.E., J.H. Power, and H.A. Barr, *The pulmonary consequences of a deep breath.* Respiratory Physiology, 1982. **49**: p. 315-324.

17.Clements, J.A. and M.E. Avery, *Lung surfactant and neonatal respiratory distress syndrome.* American Journal of Respiratory and Critical Care Medicine, 1998. **157**: p. S59-S66.

18.Griese, M., *Pulmonary surfactant in health and human lung disease: state of the art.* European Respiration Journal, 1999. **13**: p. 1455-1476.

19.Burgess, T.L. and R.B. Kelly, *Constitutive and regulated secretion of proteins.* Annual Review of Cell Biology, 1987. **3**: p. 243-293.

20.Dobbs, L.G., et al., *Secretion of surfactant by primary cultures of alveolar type II cells isolated from rats.* Biochimica et Biophysica Acta, 1982. **713**: p. 118-127.

21.Kikkawa, Y., et al., *The type II epithelial cells of the lung: chemical composition and phospholipid synthesis.* Laboratory Investigation, 1975. **32**: p. 295-302.

22.Mason, R.J., et al., *Isolation and propeties of type II alveolar cells from rat lung.* American Review of Respiratory Disease, 1977. **115**: p. 1015-1026.

23.Clements, J.A., *Functions of the alveolar lining.* American Review of Respiratory Disease, 1977. **115**: p. 67-71.

24.Johansson, J. and T. Curstedt, *Molecular structures and interactions of pulmonary surfactant components.* European Journal of Biochemistry, 1997. **3**(244): p. 675-693.

25.Johansson, J., et al., *The NMR structure of pulmonary surfactant-associated polypeptide SP-C in an apolar solvent contain a valyl-rich □□helix.* Biochemistry, 1994. **33**: p. 6015-6023.

26.Postle, A.D., E.L. Heeley, and D.C. Wilton, *A comparison of the molecular species compositions of mammalian lung surfactant phospholipids.* Comparative Biochemistry and Physiology, 2001. **129**: p. 65-73.

27.Wright, J.R. and J.A. Clements, *Metabolism and turnover of lung surfactant.* American Review of Respiratory Disease, 1987. **135**: p. 426-444.

28.Ikegami, M., *Surfactant catabolism.* Respirology, 2006. **11**: p. S24-S27.

29.Gunther, A., et al., *Surfactant alteration and replacement in acute respiratory distress syndrome.* Respiratory Research, 2001. **2**(6): p. 353-364.

30.Wright, J.R., *Pulmonary surfactant: a front line of lung host defense.* Journal of Clinical Investigations, 2003. **111**: p. 1453-1455.

31.Fujiwara, T., et al., *Artificial surfactant therapy in hyaline membrane disease.* Lancet, 1980: p. 55-59.

32.Halliday, H.L., *History of surfactant from 1980.* Biology of the Neonate, 2005. **87**: p. 317-322.

33.Soll, R.F., *Prophylactic natural surfactant extract for preventing morbidity and mortality in preterm infants.* Cochrane Database System Reviews, 1997. **4**.

34.Soll, R.F., *Multiple versus single dose natural surfactant extract for severe neonatal respiratory distress syndrom.* Cochrane Database System Reviews, 1999. **2**.

35.Soll, R.F. and F. Blanco, *Natural surfactant extract versus synthetic surfactant for neonatal respiratory distress syndrome.* Cochrane Database System Reviews, 2001. **2**.

36.Soll, R.F. and P. Dargaville, *Surfactant for meconium aspiration syndrome in full term infants.* Cochrane Database System Reviews, 2000. **2**.

37.Soll, R.F. and C.J. Morley, *Prophylactic versus selective use of surfactant in preventing morbidity and mortality in preterm infants.* Cochrane Database System Reviews, 2001. **2**.

38.Stevens, T.P., M. Blennow, and R.F. Soll, *Early surfactant treatment with brief ventilation versus selective surfactant and continued mechanical ventilation for preterm infants with or at risk of RDS.* Cochrane Database System Reviews, 2004. **3**.

39.Yost, C.C., *Early versus delayed selective surfactant treatment for neonatal respiratory distress syndrome.* Cochrane Database System Reviews, 1999. **4**.

40.Zhu, Y., et al., *KL4-surfactant (Lucinactant) protects human airway epithelium from hyperoxia.* Pediatric Reseach, 2008. **64**(2): p. 154-158.

41.Gunning, P.A., et al., *Effect of surfactant type on surfactant-protein interactions at the air-water interface.* Biomacromolecules, 2004. **5**: p. 984-991.

42.Mills, F.D., et al., *The helical structure of surfactant peptide KL4 when bound to POPC:POPG lipid vesicles.* Biochemistry, 2008. **47**: p. 8292-8300.

43.Artigas, A., et al., *The American-European consensus conference on ARDS, part 2.* American Journal of Respiratory and Critical Care Medicine, 1998. **157**: p. 1332-1347.

44.Hudson, L.D. and K.P. Steinberg, *Epidemiology of acute lung injury and ARDS.* Chest, 1999. **116**: p. 74S-82S.

45.Lewis, J.F. and R. Veldhuizen, *The role of exogenous surfactant in the treatment of acute lung injury.* Annual Review of Physiology, 2003. **65**: p. 613-642.

46.Suchyta, M.R., et al., *The adult resporatory distress syndrome. A report of survival and modifying factors.* Chest, 1992. **101**: p. 1074-1079.

47.Halliday, H.L., *Recent clinical trials of surfactant treatment for neonates.* Biology of the Neonate, 2006. **89**: p. 323-329.

48.Obladen, M., *History of surfactant up to 1980.* Biology of the Neonate, 2005. **87**: p. 308-316.

49.Revak, S.D., et al., *Use of human surfactant low molecular weight apoproteins in the reconstitution of surfactant biologic activity.* Journal of Clinical Investigations, 1988. **81**: p. 826-833.

50.Robertson, B. and H.L. Halliday, *Principles of surfactant replacement.* Biochimica et Biophysica Acta, 1998. **1408**: p. 346-361.

51.*Centers for Disease Control and Prevention Web site*. 2010; Available from: http://www.cdc.gov/nchs.

52.Klaus, M.H., J.A. Clements, and R.J. Havel, *Composition of surface-active material isolated from beef lung.* Proceedings of the National Academy of Sciences, 1961. **47**: p. 1858-1859.

53.Goerke, J. and J.A. Clements, *Alveolar surface tension and lung surfactant.* Handbook of Comprehensive Physiology, 1986: p. 247-261.

54.Malcolm, J.D. and C.D. Elliott, *Interfacial tension from height and diameter of a single sessile drop or captive bubble.* The Canadian Jornal of Chemical Engineering, 1980. **58**(2): p. 151-153.

55.Schurch, S., et al., *Surface properties of rat pulmonary surfactant studied with the captive bubble method: adsorption, hysteresis, stability.* Biochimica et Biophysica Acta, 1992. **1103**: p. 127-136.

56.Engle, M.J., R.L. Sanders, and W.J. Longmore, *Phospholipid composition and acyltransferase activity of lamellar bodies isolated from rat lung.* Biochemistry and Biophysics, 1976. **173**: p. 586-595.

57.Hallman, M. and L. Gluck, *Phosphatidylglycerol in lung surfactant. Possible modifier of surfactant function.* The Journal of Lipid Research, 1976. **17**: p. 257-262.

58.Rooney, S.A., P.M. Canavan, and E.K. Motoyama, *The identification of phosphatidylglycerol in the rat, rabbit, monkey, and human lung.* Biochimica et Biophysica Acta, 1974. **360**: p. 56-67.

59.Hallman, M., B. Feldman, and L. Gluck, *The absence of phospatidylglycerol in surfactant.* Pediatric Reseach, 1975. **9**: p. 396.

60.Brogden, K.A., et al., *Isolation of an ovine pulmonary surfactant-associated anionic peptide bactericidal for Pasteurella haemolytica.* Proceedings of the National Academy of Sciences, 1996. **93**: p. 412-416.

61.Iwaarden, J.F.V., et al., *Rat surfactant protein D enhances the production of oxygen radicals by rat alveolar macrophages.* Biochemical Journal, 1992. **286**: p. 5-8.

62.Manz-Keinke, H., H. Plattner, and J. Schlepper-Schafer, *Lung surfactant protein A (SP-A) enhances serum-independent phagocytosis of bacteria by alveolar macrophages.* European Journal of Cell Biology, 1992. **57**(1): p. 95-100.

63.Tenner, A.J., et al., *Human pulmonary surfactant protein (SP-A), a protein structurally homologous to C1q, can enhance FcR- and CR1-mediated phagocytosis.* The Journal of Biological Chemistry, 1989. **264**(23): p. 13923-13928.

64.Zimmerman, P.E., et al., *120-kD Surface glycoprotein of Pneumocystis carinii is a ligand for surfactant protein A.* Journal of Clinical Investigations, 1992. **89**: p. 143-149.

65.Oosterlaken-Dijksterhuis, M.A., et al., *Characterization of lipid insertion into monomolecular layers mediated by lung surfactant proteins SP-B and SP-C.* Biochemistry, 1991. **30**: p. 10965-10971.

66.Poulain, F.R., S. Nir, and S. Hawgood, *Kinetics of phospholid membrane fusion induced by surfactant apoproteins A and B.* Biochimica et Biophysica Acta, 1996. **1278**: p. 169-175.

67.Taneva, S.G. and K.M.W. Keough, *Dynamic surface properties of pulmonary surfactant proteins SP-B and SP-C and their mixtures with dipalmitoylphosphatidylcholine.* Biochemistry, 1994. **33**: p. 14660-14670.

68.Wang, Z., et al., *Differential activity and lack of synergy of lung surfactant proteins SP-B and SP-C in interactions with phospholipids.* The Journal of Lipid Research, 1996. **37**: p. 1749-1760.

69.Yukitake, K., et al., *Surfactant apoprotein A modifies the inhibitory effect of plasma proteins on surfactant activity in vivo.* Pediatric Reseach, 1995. **37**(1): p. 21-25.

70.Wong, C.J., et al., *Localization and developmental expression of surfactant proteins D and A in the respiratory tract of the mouse.* Pediatric Reseach, 1996. **39**(6): p. 930-937.

71.Hatzis, D., et al., *Human surfactant protein-C: Genetic homogeneity and expression in RDS comparison with other species.* Experimental Lung Research, 1994. **20**(1): p. 57-72.

72.Akinbi, H.T., et al., *Rescue of SP-B knockout mice with a truncated SP-B proprotein.* The Journal of Biological Chemistry, 1997. **272**(15): p. 9640-9647.

73.Clark, J.C., et al., *Decreased lung compliance and air trapping in heterozygous SP-B deficient mice.* American Journal of Respiratory Cell and Molecular Biology, 1997. **16**(1): p. 46-52.

74.Grossman, G., et al., *Pathophysiology of neonatal lung injury induced by monoclonal antibody to surfactant protein B.* Journal of Applied Physiology, 1997. **82**: p. 2003-2010.

75.Tokieda, K., et al., *Pulmonary dysfunction in neonatal SP-B deficient mice.* American Journal of Physiological Lung and Cell Molecular Physiology, 1997. **273**: p. 875-882.

76.Weaver, T.E. and J.J. Conkright, *Functions of Surfactant Proteins B and C.* Annual Review of Physiology, 2001. **63**: p. 555-578.

77.Kuroki, Y. and H. Sano, *Functional roles and structural analysis of lung collectins SP-A and SP-D.* Biology of the Neonate, 1999. **76**: p. 19-21.

78.Wetering, J.K.v.d., L.M.G.v. Golde, and J.J. Batenburg, *Collectins: Players of the innate immune system.* European Journal of Biochemistry, 2004. **271**: p. 1229-1249.

79.Korfhagen, T.R., et al., *Altered surfactant function and structure in SP-A gene targeted mice.* Proceedings of the National Academy of Sciences, 1996. **93**: p. 9594-9599.

80.Korfhagen, T.R., A.M. LeVine, and J.A. Whitsett, *Surfactant protein A (SP-A) gene targeted mice.* Biochimica et Biophysica Acta, 1998. **1408**(2-3): p. 296-302.

81.Korfhagen, T.R., et al., *Surfactant protein-D regulates surfactant phospholipid homeostasis in vivo.* Journal of Biological Chemistry, 1998. **273**: p. 28438-28443.

82.McCormack, F.X., et al., *Alanine mutagenesis of surfactant protein A reveals that lipid binding and pH-dependent liposome aggregation are mediated by the carbohydrate recognition domain.* Biochemistry, 1997. **36**: p. 13963-13971.

83.Robertson, B., J. Johansson, and T. Curstedt, *Synthetic surfactants to treat neonatal lung diesease.* Molecular Medicine Today, 2000. **6**: p. 1-6.

84.Seurynck, S.L., J.A. Patch, and A.E. Barron, *Simple, helical peptoid analogs of lung surfactant protein B.* Chicstry & Biology, 2005. **12**: p. 77-88.

85.Antharam, V.C., et al., *Penetration depth of surfactant peptide KL4 into membranes is determined by fatty acid saturation.* Biophysical Journal, 2009. **96**: p. 4085-4098

86.Long, J.R., et al., *Partitioning, dynamics, and orientation of lung surfactant peptide KL_4 in phospholipid bilayers.* Biochimica et Biophysica Acta, 2010. **1798**: p. 216-222.

87.Lipp, M.M., et al., *Phase and morphology changes in lipid monolayers induced by SP-B protein and its amino-terminal peptide.* Science, 1996. **273**: p. 1196-1199.

88.Baatz, J.E., et al., *Effects of surfactant-associated protein SP-B synthetic analogs on the structure and surface activity of model membrane bilayers.* Chemistry and Physics of Lipids, 1991. **60**: p. 163-178.

89.Bruni, R., H.W. Taeusch, and A.J. Waring, *Sufactant protein B: lipid interactions of synthetic peptides representing the amino-terminal amphipathic domain.* Proceedings of the National Academy of Sciences, 1991. **88**: p. 7451-7455.

90.Lipp, M.M., et al., *Fluorescence, polarized fluorescence, and Brewster angle microscopy of palmitic acid and lung surfactant protein B monolayers.* Biophysical Journal, 1991. **72**: p. 2783-2804.

91.Longo, M.L., et al., *A function of lung surfactant protein SP-B.* Science, 1993. **261**: p. 453-456.

92.Revak, S.D., et al., *The use of synthetic peptides in the formation of biophysically and biologically-active pulmonary surfactants.* Pediatric Reseach, 1991. **29**: p. 460-465.

93.Waring, A., et al., *Synthetic amphipathic sequences of surfactant protein B mimic several physiochemical and in vivo properties of native pulmonary surfactant proteins.* Peptide Research, 1989. **2**: p. 308-313.

94.Cochrane, C.G. and S.D. Revak, *Pulmonary surfactant protein B (SP-B): structure-function relationships.* Science, 1991. **254**: p. 566-568.

95.Gustafsson, M., et al., *The 21-residue surfactant peptide ($LysLeu_4)_4Lys(KL_4$) is a transmembrane □-helix with a mixed nonpolar/polar surface.* Federation of European Biochemical Societies, 1996. **384**: p. 185-188.

96.Cochrane, C.G., et al., *Bronchoalveolar lavage with KL4 surfactant in models of meconium aspiration syndrome.* Pediatric Reseach, 1998. **44**: p. 705-715.

97.Revak, S.D., et al., *Efficacy of KL4 surfactant in premature-infant monkeys.* Pediatric Reseach, 1995. **37**: p. A347-A347.

98.Revak, S.D., et al., *Efficacy of synthetic peptide-containing surfactant in the treatment of respiratory distress syndrome in preterm infant rhesus monkeys.* Pediatric Reseach, 1996. **39**(715-724).

99.Walther, F.J., et al., *Spiking Survanta with synthetic surfactant peptides improves oxygenation in surfactant-deficient rats.* American Journal of Respiratory and Critical Care Medicine, 1997. **156**: p. 855-861.

100.Walther, F.J., et al., *Protein composition of synthetic surfactant affects gas exchange in surfactant-deficient rats.* Pediatric Reseach, 1998. **43**: p. 666-673.

101.Cochrane, C., et al., *The efficacy and safety of KL4-surfactant in preterm infants with respiratory distress syndrome.* Respiratory Critical Care Medicine, 1996. **153**: p. 404-410.

102.Mansour, H.M., S. Damodaran, and G. Zografi, *Characterization of the in situ structural and interfacial properties of the cationic hydrophobic heteropolypeptide, KL4, in lung surfactant bilayer and monolayer models at the air-water interface: Implications for pulmonary surfactant delivery.* Molecular Phamaceutics, 2008. **5**(5): p. 681-695.

103.Wiswell, T.E., et al., *Bronchopulmonary segmental lavage with surfaxin (KL4-surfactant) for acute respiratory distress syndrome.* American Journal of Respiratory and Critical Care Medicine, 1999. **160**: p. 1188-1195.

104.Moya, F.R., et al., *A multicenter, randomized, masked, comparison trial of lucinactant, colfosceril palmitate, and beractant for the prevention of respiratory distress syndrome among very preterm infants.* Pediatrics, 2005. **115**: p. 1018-1029.

105.Saenz, A., et al., *Physical properties and surface activity of surfactant-like membranes containing the cationic and hydrophobic peptide KL_4.* FEBS J., 2006. **273**: p. 2515-2527.

106.Vogt, B., et al., *The topology of lysine-containing amphipathic peptides in bilayers by circular dichroism, solid-state NMR, and molecular modeling.* Biophysical Journal, 2000. **79**: p. 2644-2656.

107.Martinez-Gil, L., J. Perez-Gil, and I. Mingarro, *The surfactant peptide KL_4 sequence is inserted with a transmembrane orientation into the endoplasmic reticulum membrane.* Biophysical Journal, 2008. **95**: p. L-36-L38.

108.Hessa, T., et al., *Recognition of transmembrane helices by the endoplasmic reticulum translocon.* Nature, 2005. **433**: p. 377-381.

109.Hessa, T., et al., *Molecular code for transmembrane-helix recognition by the Sec61 translocon.* Nature, 2007. **450**: p. 1026-1030.

110.Cai, P., C.R. Flach, and R. Mendelsohm, *An infrared reflection-absorption spectroscopy study of the secondary structure in $(KL_4)_4K$, a therapeutic agent for respiratory distress syndrom, in aqueous monolayers with phospholipids.* Biochemistry, 2003. **42**: p. 9446-9452.

111.Houghten, R.A., *General method for the rapid solid-phase synthesis of large numbers of peptides: specificity of antigen-antibody interaction at the level of individual amino acids.* 1985, 1985. **82**: p. 5131-5135.

112.Merrifield, R.B., *Solid phase peptide synthesis. I. The synthesis of a tetrapeptide.* Journal of American Chemical Society, 1963. **85**: p. 2149-2154.

113.Edman, P., *Method for determination of the amino acid sequence in peptides.* Acta Chemica Scandinavica, 1950. **4**: p. 283-293.

114.Niall, H.D., *Automated degradation: The protein sequenator.* Methology of Enzymology, 1973. **27**: p. 942-1010.

115.McConnell, H.M., et al., *Spin-Labeled Biomolecules.* PNAS, 1965. **54**(4): p. 1010-1017.

116.Altenbach, C., et al., *A collision gradient method to determine the immersion depth of nitroxides in lipid bilayers: Application to spin-labeled mutants of bacteriorhodopsin.* Proceedings of the National Academy of Sciences, 1994. **91**: p. 1667-1671.

117.Hubbell, W.L. and C. Altenbach, *Investigation of structure and dynamics in membrane proteins using site-directed spin labeling.* Current Opinion in Structural Biology, 1994. **4**(4): p. 566-573.

118.Hubbell, W.L., D.S. Cafiso, and C. Altenbach, *Identifying conformational changes with site-directed spin labeling.* Nature Structural Biology, 2000. **7**(9): p. 735-739.

119.Hubbell, W.L., et al., *Recent advances in site-directed spin labeling of proteins.* Current Opinion in Structural Biology, 1998. **8**: p. 649-656.

120.Hubbell, W.L. and H.M. McConnell, *Molecular Motion in Spin-Labeled Phospholipids and Membranes.* Journal of the American Chemical Society, 1971. **93**(2): p. 314-326.

121.Klug, C.S., et al., *Ligand-induced conformational change in the ferric enterobactin receptor FepA as studied by site-directed spin labeling and time-domain ESR.* Biochemistry, 1998. **37**: p. 9016-9023.

122.Langen, R., et al., *Crystal structures of spin labeled T4 lysozyme mutants: Implications for the interpretation of EPR spectra in terms of structure.* Biochemistry, 2000. **39**: p. 8396-8405.

123.Voss, J., et al., *A method for distance determination in proteins using a designed metal ion binding site and site-directed spin labeling: Evaluation with T4 lysozyme.* Proceedings of the National Academy of Sciences, 1995. **92**: p. 12295-12299.

124.Hubbell, W.L., et al., *Watching proteins move using site-directed spin labeling.* Structure, 1996. **4**: p. 779-780.

125.Czogalla, A., et al., *Attaching a spin to a protein - site directed spin labeling in structural biology.* Acta Biochimica Polonica, 2007. **54**(2): p. 235-244.

126.Fanucci, G.E. and D.S. Cafiso, *Recent advances and applications of site-directed spin labeling.* Current Opinion in Structural Biology, 2006. **16**: p. 644-653.

127.Mchaourab, H.S., et al., *Motion of spin-labeled side chains in T4 lysozyme: Effect of side chain structure.* Biochemistry, 1999. **38**: p. 2947-2955.

128.Jost, P., et al., *Lipid spin labels in lecithin multilayers. A study of motion along fatty acid chains.* Journal of Molecular Biology, 1971. **59**: p. 77-98.

129.Keana, J.F.W., *Newer aspects of the synthesis and chemistry of nitroxide spin labels.* Chemical Reviews, 1978. **78**(1): p. 37-64.

130.Libertini, L.J., et al., *Orientation of lipid spin labels in lecithin multilayers.* PNAS, 1969. **64**(1): p. 12-19.

131.Marsh, D. and A. Watts, *Lipid-protein interactions.* Wiley-Interscience, 1982. **2**.

132.Snel, M.M.E. and D. Marsh, *Accessibility of spin-labeled phospholipids in anionic and zwitterionic bilayer membranes to paramagnetic relaxation agents. Continuous wave power saturation EPR studies.* Biochimica et Biophysica Acta, 1993. **1150**: p. 155-161.

133.Atkins, P. and J.d. Paula, *Elements of Physical Chemistry, 4th Ed.* 2005: Oxford University Press.

134.Fasman, G.D., *Circular dichroism and the conformational analysis of biomolecules*. 1996: Springer.

135.*Applied Photophysics*. 2003.

136.Greenfield, N. and G.D. Fasman, *Computed circular dichroism spectra for the evaluation of protein conformation.* Biochemistry, 1969. **8**: p. 4108-4116.

137.Sreerama, N. and R.W. Woody, *A self-consistent method for the analysis of protein secondary structure from circular dichroism.* Analytical Biochemistry, 1993. **209**: p. 32-44.

138.Gillard, R.D., *Circular dichroism.* Analyst, 1963. **88**: p. 825-828.

139.Jongh, H.H.J.d., E. Goormaghtigh, and J.A. Killian, *Analysis of circular dichroism spectra of oriented protein-lipid complexes: Toward a general application.* Biochemistry, 1994. **33**: p. 14521-14528.

140.Lenard, J. and S.J. Singer, *Protein conformation in cell membrane preparations as studied by optical rotatory dispersion and circular dichroism.* Biochemistry, 1966. **56**: p. 1828-1835.

141.*Bruker Biospin*. 2011.

142.Columbus, L. and W.L. Hubbell, *A new spin on protein dynamics.* Trends in Biochemical Sciences, 2002. **27**(6): p. 288-295.

143.Mchaourab, H.S., et al., *Motion of spin-labeled side chains in T4 lysozyme. Correlation with protein structure and dynamics.* Biochemistry, 1996. **35**: p. 7692-7704.

144.Schorn, K. and D. Marsh, *Extracting order parameters from powder EPR lineshapes for spin-labelled lipids in membranes.* Spectochimica Acta, 1997. **53**: p. 2235-2240.

145.Brown, M.F., J. Seelig, and U. Haberlen, *Structural dynamics in phospholipid bilayers from deuterium spin-lattice relaxation time measurements.* Journal of Chemical Physics, 1979. **70**(11): p. 5045-5053.

146.Griffith, O.H., P.J. Dehlinger, and S.P. Van, *Shape of the hydrophobic barrier of phospholipid bilayers (Evidence of water penetration in biological membranes).* Journal of Membrane Biology, 1974. **15**: p. 159-192.

147.Hyde, J.S., C.A. Popp, and S. Schreier, Frontier of Biological Engineering, 1978. **2**: p. 1253-1261.

148.Altenbach, C., et al., *A collision gradient method to determine the immersion depth of nitroxides in lipid bilayers: Application to spin-labeled mutants of bacteriorhodopsin.* Biophysics, 1994. **91**: p. 1667-1671.

149.Horie, T. and J. Hildebrandt, *Dynamic compliance, limit cycles, and static equilibria of excised cat lung.* Journal of Applied Physiology, 1971. **31**: p. 423-430.

150.Ramamoorthy, A., et al., *Solid-state NMR investigation of the membrane-disrupting mechanism of antimicrobial peptides MSI-78 and MSI-594 from magainin and melittin.* Biophysical Journal, 2006. **91**: p. 206-216.

151.Terzi, E., G. Holzemann, and J. Seelig, *Interaction of Alzheimer □-amyloid peptide (1-40) with lipid membranes.* Biochemistry, 1997. **36**: p. 14845-14852.

152.Wieprecht, T., et al., *Thermodynamics of the □-helix-coil transition of amphipathic peptides in a membrane environment: implications for the peptide-membrane binding equilibrium.* Journal of Molecular Biology, 1999. **294**(3): p. 785-794.

153.Veldhuizen, R., et al., *The role of lipids in pulmonary surfactant.* Biochimica et Biophysica Acta, 1998. **1408**: p. 90-108.

154.Baatz, J.E., B. Elledge, and J.A. Whitsett, *Surfactant protein SP-B induces ordering at the surface of model membrane bilayers.* Bichemistry, 1990. **29**: p. 6714-6720.

155.Egberts, J., H. Sloot, and A. Mazure, *Minimal surface tension, squeeze-out and transition temperatures of binary mixtures of dipalmitoylphosphatidylcholine and unsaturated phospholipids.* Biochimica et Biophysica Acta, 1989. **1002**: p. 109-113.

156.Meban, C., *Effect of lipids and other substances on the adsorption of dipalmitoyl phosphatidyl choline.* Pediatric Reseach, 1981. **15**: p. 1029-1031.

157.Possmayer, F., *Physichemical aspects of pulmonary surfactant.* Fetal and Neonatal Physiology, 1997. **115**: p. 1259-1275.

158.Qanbar, R., et al., *Role of the palmitoylation of surfactant-associated protein C in surfactant film formation and stability.* American Journal of Physiology, 1996. **271**: p. L572-L580.

159.Yu, S.H. and F. Possmayer, *Effect of pulmonary surfactant protein B (SP-B) and calcium on phospholipid adsorption and squeeze-out of phosphatidylglycerol from binary phospholipid monolayers containing dipalmitoylphosphatidylcholine.* Biochimica et Biophysica Acta, 1992. **1126**: p. 26-34.

160.Erilov, D.A., et al., *Water concentration profiles in membranes measured by ESEEM of spin-labeled lipids.* Journal of Physical Chemistry, 2005. **109**: p. 12003-12013.

BIOGRAPHICAL SKETCH

Austin Lisle Turner was born in Evanston, Illinois. The middle child of three males, he grew up in the Northwest suburbs of Chicago, Illinois, graduating from Adlai E. Stevenson High School in 1999. He earned his B.S. in chemistry from the University of Wisconsin at Whitewater in 2005 after transferring after two year at Bradley University.

Upon graduating with his B.S. in chemistry he entered the pharmaceutical field at Abbott Laboratories in North Chicago. After beginning as an intern he worked his way up in the Department of Drug Metabolism as a research associate. After acquiring a broad area of knowledge in the fields of biochemistry and analytical chemistry he opted to pursue a doctoral degree at the University of Florida.

Upon completion of his Ph.D. program, Austin will be looking to re-enter the pharmaceutical industry as a research associate.